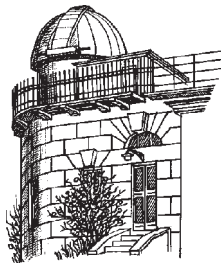


ODESSA ASTRONOMICAL PUBLICATIONS

Volume 25 Issue 1
(2012)



Odessa
«AstroPrint»

FOREWORD

This issue of the Odessa Astronomical Publications (OAP, Volume 25 Issue 1, 2012) has gathered papers from several fields of astronomy. The reader can find here publications devoted to the variable stars (s-Cepheids, first detected super-lithium beat Cepheid, chemical composition of the Cepheid X Sgr, application of the method of statistical parallaxes, photometric variability of the semi-regular pulsating stars, Mira variables, CCD photometric system investigation which is used for pulsating star observations), binary systems and roAp stars (binary systems containing neutron stars, MCP star phenomenon, line properties of the roAp star alpha Cir, properties of the semi-detached binary WZ Cor), Solar system (gravitation field in the external parts of the Solar system), galaxies (angular momenta of galaxies and their environment).

The authors of the papers presented in this issue would like to devote OAP (Volume 25 Issue 1), to the memory of Professor V.P.Tsessevich, who had given almost 40 years of his life to Astronomical observatory in Odessa, and whose 105th anniversary we celebrate this year.

Editor-in-chief

CONTENTS

Foreword.....	2
Contents	3
SPECTRAL LINE PROFILES VARIATIONS IN THE α STAR ALPHA CIRCINI Alentiev D.V.....	4
GRAVITY FIELD IN EXTERNAL PARTS OF THE SOLAR SYSTEM Bazey N.V., Bazey A.A.....	7
THE NATURE OF MAGNETIC CHEMICALLY PECULIAR STARS PHENOMENON AND THE ORIGIN OF LITHIUM Gopka V.F., Shavrina A.V., Yushchenko A.V., Yushchenko V.A.....	9
THE MATHEMATICAL MODEL OF THE PHOTOMETRIC VARIABILITY AND CLASSI- FICATION OF SEMIREGULAR PULSATING ASYMPTOTIC GIANTS BRANCH STARS Kudashkina L.S.....	18
COMMENTS ON ENVIRONMENTAL EFFECTS IN THE ORIGIN OF ANGULAR MOMENTA IN GALAXIES Panko E., Pajowska P., Godłowski W., Flin P.	21
A CURRENT APPLICATION OF THE METHODS OF SECULAR AND STATISTICAL PARALLAX Turner D.G.....	29
INVESTIGATION OF THE PHOTOMETRIC SYSTEM OF CCD-PHOTOMETER AND THE AZT-3 TELESCOPE Udovichenko S.N.....	32
SOME EVOLUTIONARY ASPECTS OF THE BINARY STELLAR SYSTEMS CONTAINING NEUTRON STAR Ulyanov O.O., Andrievsky S.M., Gopka V.F., Shavrina A.V.....	35
FUNDAMENTAL PARAMETERS AND CHEMICAL COMPOSITION OF CEPHEID X SGR Usenko I.A., Knyazev A.Yu., Berdnikov L.N., Kravtsov V.V.	40
MODELLING OF THE SEMI-DETACHED BINARY STAR WZ CORVI Virnina N.A., Zola S., Krajci T.	45
DISCOVERY OF THE FIRST SUPER-LITHIUM RICH BEAT CEPHEID: V371 PER Kovtyukh V.V., Gorlova N.I., Hillen M.....	52
ARE THE s-CEPHEIDS CROSSING THE INSTABILITY STRIP FOR THE FIRST TIME? Andrievsky S.M., Garbuzov G.A., Doikov D.N.....	56
MIRAS OR SRA'S – THE TRANSIENT TYPE VARIABLES Marsakova V.I., Andronov I.L.	60
PRELIMINARY STUDY OF RED SUPERGIANT RM_1-667 IN THE LARGE MAGELLANIC CLOUD Gopka V., Shavrina A., Vasilyeva S., Yushchenko A., Andrievsky S., Yushchenko V.....	64
RESULTS OF OBSERVATIONS OF SELECTED ASTEROIDS AT THE NEW TELESCOPE MOBITEL OF NAO IN 2011-12 A. Ivantsov, A. Pomazan, V. Kryuchkosriy, L. Gudkova	66

SPECTRAL LINE PROFILES VARIATIONS IN THE α CIRCINI STAR ALPHA CIRCINI*

D.V. Alentiev

Department of Physics, Tavrian National University
Vernadskiy's Avenue 4, 95007 Simferopol, Ukraine
sl4m@ukr.net

ABSTRACT. We analyse behavior of the line profile variations of the brightest known α CIRCINI star based on the high-resolution spectra obtained with the HARPS spectrometer. The rapid variations of Nd and Pr line profiles are similar to other α CIRCINI stars.

Key words: line: profiles - stars: chemically peculiar - stars: oscillations - stars: individual: α CIRCINI.

1. Introduction

α CIRCINI (HD 128898, HR 5463, HIP 71908, $V = 3.2$ mag) is the brightest known rapidly oscillating α CIRCINI star. It was for the first time reported as a α CIRCINI variable by Kurtz (1982). The author reports photometric variability with a period of 6.8 min at a few mmag level. More recent photometric studies reveal four additional low amplitude oscillation modes (Kurtz, 1994).

α CIRCINI stars is a class of variable stars pulsating in high-overtone, low-degree p-modes. The oblique pulsator model is used to describe them. The model assumes that pulsation axis aligns with the magnetic axis which in turn is inclined to the rotation axis of the star (e.g., Kurtz, 1982; Kurtz, 1994; Shibahashi & Takata, 1993). An amplitude modulation of the main pulsation mode allowed to estimate rotation period of the star to $P_{rot} = 4.4790$ d (Kurtz, 1994). Several further non-radial modes have been detected by means of the photometric analysis of WIRE satellite data (Bruntt, 2007).

A strong magnetic field suppresses convection in outer layers of atmosphere (Michaud, 1970). The diffusion leads to stratification of some chemical elements (Babel & Lanz, 1992). The first spectroscopic analysis of the star α CIRCINI showing α CIRCINI characteristics was performed by Kupka et al. (1996). Recent spectroscopic analysis performed by Bruntt et al. (2008) confirmed remarkable overabundances of Co, Y, Nd and Eu (Bruntt et al., 2008). Similar to other chem-

ically peculiar (CP) stars, α CIRCINI shows abundance spots on its surface (Kochukhov & Ryabchikova, 2001). Ryabchikova et al. (2007) carried out reconstruction of vertical distribution of pulsation amplitude and phase. The derived effective temperature of 7420 K and surface gravity of 4.1 dex agree with the stratified model (Kochukhov et al., 2009) and with the interferometric measurements (Bruntt et al., 2009). Chemical stratification analysis showed inhomogeneous distribution of some chemical elements. The pulsational variability in α CIRCINI stars is dominated by the lines of rare-earth elements (REE), especially those of Pr and Nd.

In this paper we present analysis of LPVs focusing on a single Nd III spectral line at 6145 Å. The line shows remarkable variations with the rotation phase which is characteristic of α CIRCINI-type stars and is probably linked to the stellar surface inhomogeneities. We adopt the same methodology as used in Kochukhov et al. (2004) for α CIRCINI star HR 3831.

2. Observations and analysis

We base our analysis on high-resolution spectra obtained with the HARPS (High Accuracy Radial velocity Planetary Search) spectrograph attached to the 3.6-m telescope at La Silla. All spectra were downloaded from ESO archive. Principal investigator and co-investigators of the proposal 081.D-0008 were A. Hatzes, D. Mkrtichian and H. Saio. The two HARPS fibres produce a resolving power of 115000. This accuracy is enough to resolve a radial velocity of an order of 1 m s^{-1} . The data have been reduced using dedicated ESO pipeline. Reduced spectra were normalized using accurate calculation of a continuum level.

The two data sets of correspondingly 1600 and 3000 spectra have been obtained in February and April 2008. Typical exposure time was from 15 to 70 sec. We rejected 17 spectra with exposure time over 30 sec because this time range does not correspond with selected

*Based on observations collected at the European Southern Observatory, Chile (program 081.D-0008).

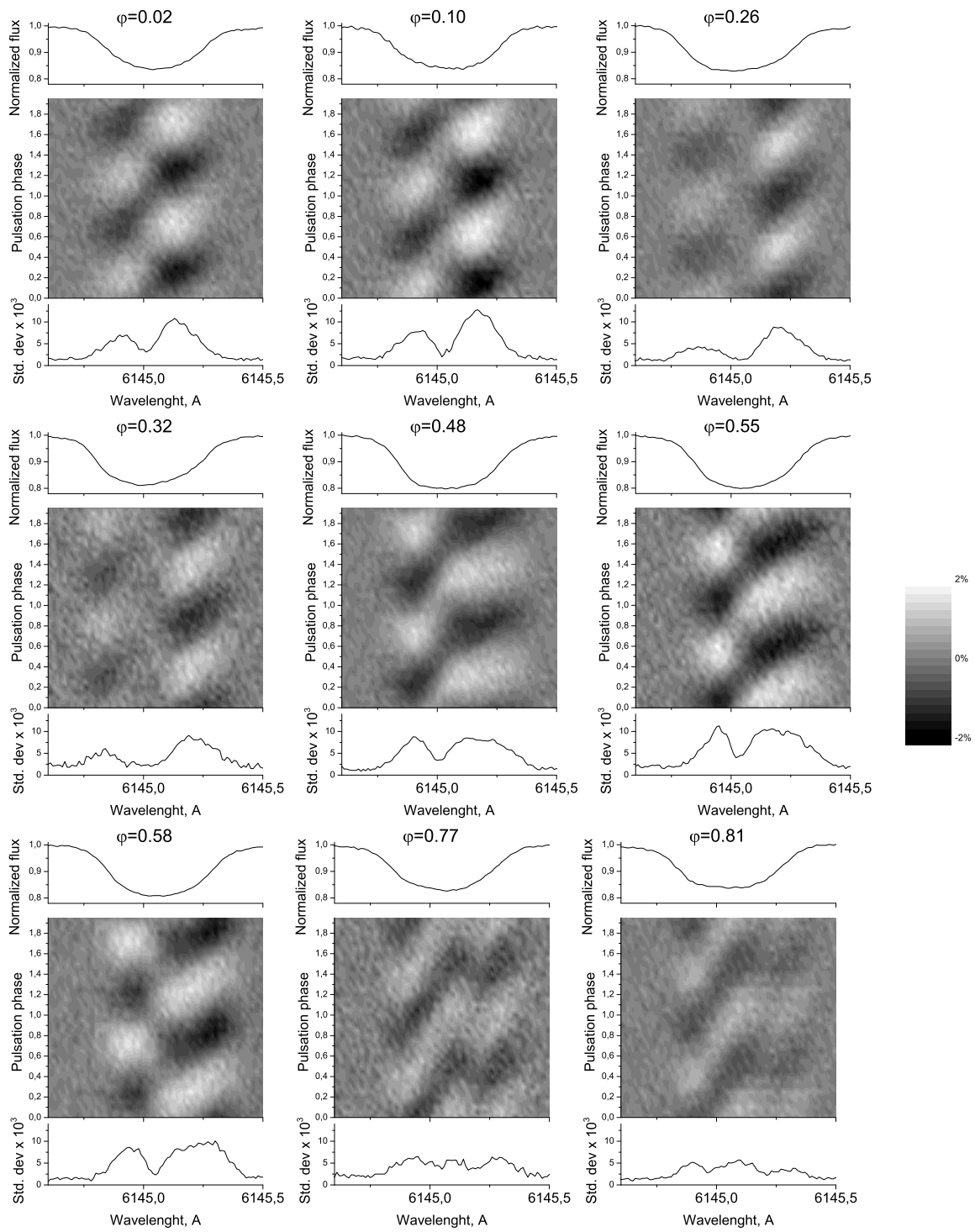


Figure 1: Illustration of the Nd III 6145.07 Å line profile variation at different rotation phases of the star α Circini. Upper panel of each plot show averaged spectra during the night. The middle greyscale plots show time evolution of the difference between averaged spectrum and phased spectra with the main pulsation frequency. The scale for the greyscale 2.5% of the continuum intensity. Bottom panels show standard deviation. All plots sorted by phase.

step of pulsational phase (see below). The rotational phase has been computed using the following equation $\phi = (\text{HJD} - 2400000.0) / 4.4792$, where HJD- Heliocentric Julian Date, 4.4792 - rotational period determined by Bruntt et al. (2009). Following step of reduction was averaging of all spectra from each set of observation during main pulsational phase. For this step we took main frequency $2442\mu\text{Hz}$ determined by Bruntt et al. (2009). Each set was divided by 20 pulsational phases. We could not increase accuracy because maximum exposure time 30 sec occupy 0,07 of pulsational phase.

3. Pulsational behavior of Nd and Pr spectral lines

High precision spectra enable to detect line profile variations in rare earth elements spectral lines. The upper panels in Fig.1 represent the average of all spectra acquired during single night in a small wavelength range centered at Nd III 6145.07 Å spectral line. The line shows obvious modulation with the rotation phase. The difference in the average profile can be explained by magnetic field modulation during rotation. Also it can be explained by inhomogeneous distribution of Nd in the atmosphere of α Circini. The line reaches its maximum depth at $\varphi_{rot} = 0.48$ whereas minimum in equivalent width appears at $\varphi_{rot} = 0.02$. The grayscale plots in Fig.1 illustrate time evolution of the residuals obtained by subtracting the mean profile from phased (according to the main pulsation period) individual spectra in every single night. Maximum deviation does not exceed 2% level relative to the mean spectrum. Obviously, the red wing of the line is more sensitive to the pulsations which is confirmed by the standard deviation shown in the bottom panel of each plot in Fig.1. Amplitude of the standard deviation reaches maxima at $\varphi_{rot} = 0.10$ and $\varphi_{rot} = 0.58$. The two low-resolution figures at $\varphi_{rot} = 0.77$ and $\varphi_{rot} = 0.81$ show nonstandard behavior of the line.

We adopt the same methodology for few other Nd III and Pr III lines. The behavior of LPVs does not show significant difference from the Nd III 6145 Å spectral lines.

4. Conclusions

A clear modulation of the line with rotation phases implies the need of Doppler Imaging (DI) (Kuschnig et al., 1999) and Magnetic Doppler Imaging (MDI) (Kochukhov & Piskunov, 2002) mapping. The detailed analysis of the behavior of the Nd III 6145 Å spectral line is a subject of the future research.

References

- Babel J.; Lanz T.: 1992, *A&A*, **263**, 232
 Bigot L., Dziembowski W. A.: 2002, *A&A*, **391**, 235
 Bruntt H., North J. R., Cunha M., et al.: 2008, *MNRAS*, **358**, 2039
 Bruntt H., Kurtz D. W., Cunha M., et al.: 2009, *MNRAS*, **396**, 1189
 Kochukhov O., Ryabchikova T.: 2001, *A&A*, **377**, L22
 Kochukhov O., Piskunov N.: 2002, *A&A*, **388**, 868
 Kochukhov O.: 2004, *A&A*, **499**, 851
 Kochukhov O.; Shulyak D., Ryabchikova T.: 2009, *A&A*, **499**, 851
 Kuschnig R., Ryabchikova T., Piskunov N.: 1999, *A&A*, **348**, 924
 Kupka F., Ryabchikova T., Weiss W., et al.: 1996, *A&A*, **308**, 886
 Kurtz D. W.: 1982, *MNRAS*, **200**, 807
 Kurtz D. W., Sullivan D. J., Martinez P., et al.: 1994, *MNRAS*, **270**, 674
 Michaud G.: 1970, *ApJ*, **160**, 641
 Ryabchikova T., Sachkov M., Kochukhov O., et al.: 2007, *A&A*, **473**, 907
 Saio H.: 2005, *MNRAS*, **360**, 1022
 Shibahashi H., Takata M.: 1993, *PASJ*, **45**, 617
 Takata M., Shibahashi H.: 1995, *PASJ*, **47**, 219

GRAVITY FIELD IN EXTERNAL PARTS OF THE SOLAR SYSTEM

N.V. Bazey², A.A. Bazey¹

¹Department of Astronomy and ²Astronomical Observatory, Odessa National University, T.G.Shevchenko Park, Odessa. 65014, Ukraine, *ii1966@mail.ru*

ABSTRACT. Taking into account the gravitational perturbations from the center of the galaxy and using the catalogue closest to the Sun, stars modeled surfaces of equal gravitational potential energy fields in the outskirts of the solar system. Constructed three-dimensional model of equipotential surfaces in the vicinity of the solar system. It is shown that for certain values a constant of the energy the Sun is within the common equipotential surface Toliman, Sirius and Procyon.

Key words: nearest stars; attraction; potential energy; galactic center

The solar system is a combination of many celestial bodies, held by gravity. About 99.8% of the mass falls on the Sun. Therefore, almost all of the Sun determines the motions of the solar system. Move around the Sun eight major planets with satellites, dwarf planets, asteroids, comets, Kuiper belt objects, meteoroid and gas-dust complexes. With the sun's surface continuously flows expire plasma – the solar wind. With increasing distance from the Sun, its density and velocity continuously decrease. At some distance the solar wind mixes with the interstellar medium. This boundary is called the heliopause. At present, it is assumed that it is at a distance of 119 AU from the Sun (NASA, 2012).

With increasing distance from the center of the solar system, the attraction of the sun diminishes. To describe the boundaries of the space within which, it is advisable to take the main attraction of the sun, apply the concept of the incidence (Chebotarev, 1965; Balk, 1965). When moving inside the sphere, acceleration, directed towards the Sun is considered the main, all other speed - disturbing. The radius of incidence of the sun relative to the galactic center is estimated at 60 000 AU (Chebotarev, 1965). The area of the circumsolar space that lies beyond this distance is called the outskirts of the solar system. In this region the gravitational acceleration toward the Sun is comparable to the gravitational acceleration to other celestial

bodies surrounding the solar system.

Thus, part of the Kuiper belt objects and comets move in the interstellar medium, but remain deep within the incidence of the Sun. According to (Oort, 1950) exist cloud around the Sun of comet nuclei, called the Oort cloud. This cloud is not available observations. But if it exists, the comet nucleus moving near the outskirts of the solar system.

At the outskirts of the solar system must take into account the attraction of the nearest stars, and the additive effect of our Galaxy.

It is known that our galaxy is a collection of hundreds of billions of stars, gas-dust matter and other objects a length several thousand parsecs. The masses in the galaxy are concentrated toward the center. The Sun is located about 8000 pc from the galactic center (Binney & Merrifield, 1998). The size of the solar space is much smaller than the size of the galaxy. For this reason, gravitational perturbations from the Galaxy in the first approximation can be regarded as a perturbation a centre of the galaxy. Its diameter is small compared with the diameter of the galaxy, and the distance to the Sun. This allows approximately replaced an attraction of the central part of the Galaxy by the attraction of a point mass $1.3 \cdot 10^{11} M_{\odot}$ (Chebotarev, 1965).

Because the diameters of stars are negligible compared to interstellar distances, then the abstraction of "material point" is fully applicable for the description of gravitational fields close to the outskirts of the solar system of stars. To examine the behavior of particles in the interstellar distances is necessary to consider the influence of nearby stars. For this purpose, we used the Zakhzhaj Catalogue of Nearest Stars until 10pc (Zakhzhaj, 1996). This is one of the few catalogues that contain estimates of the masses of nearby stars that are within 10 pc from the Sun.

To describe the gravitational field, we use the concept of potential energy. Relative to an arbitrary material point of the potential energy is given by:

$$U_i = -G \frac{m_i}{r_i} \quad (1)$$

were G – the gravitational constant;
 m_i – mass of the material point;
 r_i – the distance from the material point.

If a material point is isolated, then the surfaces of equal potential energy presented a set of concentric spheres. In the case of set of N material points, the potential energy with respect to each of them, summed up:

$$U = -G \sum_{i=1}^N \frac{m_i}{r_i} \quad (2)$$

View surfaces of equal potential energy depends on the relative positions and masses of all the N material points. Thus, taking into account the gravity 355 nearby stars and the central part of the Galaxy, we have constructed a set of surfaces of equal potential energy. Figure 1 shows the equipotential surfaces surrounding the nearest star, the distance to which does not exceed 3.5 ps. Red dwarfs are not shown. The value a constant of the energy is sufficiently small, therefore a surface deviates from spherical shape. The radius of the equipotential surface that surrounds the sun, close to the radius of the sphere of the sun relative to the center of the galaxy.

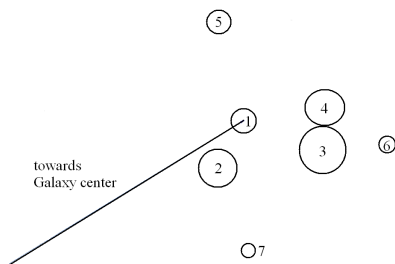


Figure 1: Equipotential surfaces for small values of potential energy, separately covering the Sun and the nearest massive star 1 – The Sun, 2 – Toliman (α Centauri), 3 – Sirius (α Canis Major), 4 – Procyon (α Canis Minor), 5 – 61 Cygni, 6 – ϵ Eridani, 7 – ϵ Indi.

Modelling of the gravitational field in the vicinity of the solar system shows that among the nearest neighbors of the Sun released some of the most massive stars or star systems. First of all, this is the closest star system – α Centauri. Its total mass, taking into account the mass of Proxima Centauri is more than twice the mass of the Sun. In a set of equipotential surfaces exist such that the system includes the Sun and α Centauri. For the same value the constant of the energy surface of a covering Sirius and Procyon neighbors (Fig. 2).

For larger value the constant of the energy surface exist, covering all four relatively massive stars (the

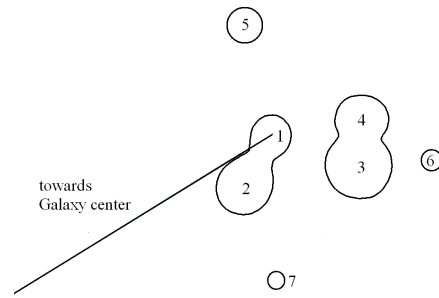


Figure 2: Equipotential surfaces for a larger value of the potential energy, covering a group of stars.

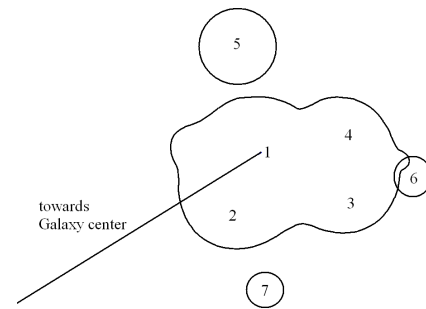


Figure 3: Equipotential surfaces for the maximum value of potential energy, covering a group of stars.

system) – Sun, α Centauri, Sirius and Procyon. Inside of the equipotential surface are also much smaller red dwarfs – Leyte (near Procyon) and Barnard's Star. Since the stars have proper motions, their position in space is continuously changing. Therefore, the outskirts of the solar system gravitational field strength is anisotropic, the anisotropy is variable. Equipotential surfaces deform and move. The interstellar medium and the celestial bodies, is not associated with stars, moving in a variable gravitational field with small gradient.

References

- Balk M.: 1965, *Elements of space flight dynamics*, Moscow, "Science", 338 pp. (in Russian)
 Binney J., Merrifield M.: 1998, *The Galactic Astronomy*, Princeton University Press, 796 pp.
 Oort J.: 1950, *Bull. Astron. Inst. Neth.*, **11**, 91.
 Chebotarev G.: 1965, *Analytic and numerical methods of Celestial Mechanics*, Moscow, "Science", 368 pp. (in Russian)
 Zakhozaj V.: 1979, *Vestnik Khar'kovskogo Universiteta*, **190**, 52.
 NASA, Voyager, http://voyager.jpl.nasa.gov/news/new_region.html

THE NATURE OF MAGNETIC CHEMICALLY PECULIAR STARS PHENOMENON AND THE ORIGIN OF LITHIUM

V.F. Gopka¹, A.V. Shavrina², A.V. Yushchenko³, V.A. Yushchenko¹

¹Astronomical observatory, Odessa National University, T.G. Shevchenko Park, Odessa 65014, Ukraine, *gopkavera@mail.ru*

²Main Astronomical Observatory of NASU, Zabolotnogo str. 27, Kyiv, 03680, Ukraine, *shavrina@mao.kiev.ua*

³Department of Astronomy & Space Sciences, Sejong University, Gunja-dong, Seoul, 143-747, Korea, *yua@sejong.ac.kr*

ABSTRACT. According to the modern theory of the evolution of chemical elements their origin seems understandable for most of the elements, from the lightest up to the heavy ones. For element with atomic number $Z=3$ (lithium) the situation is following: the physical processes and the possible mechanisms of lithium production in stars of different types and ages remain completely unidentified up to now.

This paper is an attempt to explain the observed properties of lithium in the magnetic chemically peculiar (MCP) stars by the existence of a neutron star (NS) companion. It is supposed that MCP stars are binary systems with stable relativistic outflow of charged particles falling on the poles of MCP stars along the magnetic field lines (Gopka et al., 2010). The production of lithium is possible as a result of interaction of highly accelerated charged particle and the photosphere of MCP star. The location of lithium spots on the magnetic poles seems natural.

The problem of lithium formation is directly connected to the problem of origin of MCP stars. The assumption of origin of double systems with pre-supernova is based on the observations of binary population in OB association Sco2 (Brown, 2001) is discussed. The distribution of primordial binary population clearly answers the question about the origin of systems with NS companions. The phenomenon of MCP stars with lithium production can be the key to the understanding of the origin of Li in other stellar objects.

It is assumed that the formation of binaries with a primary star at the evolutionary stage of pre-supernova occurs in the areas of star formation due to the ambient matter accretion and the mass exchange between the stars of intermediate mass in binary systems. The explosion of a more massive companion as a type II supernova results in a qualitative change in binary system when a young star is accompanied by a neutron

star. Such systems can be a lithium producers.

An important aspect of this assumption is a clear understanding of the evolutionary status of young objects at the stage before the main-sequence, the progenitors of MCP stars, such as the Herbig AeBe stars. The observational data for Herbig AeBe stars (and for T Tauri stars with Herbig AeBe properties continuing in the region of stars with masses less than $2 M_{\odot}$) indicate the existence of young stars surrounded by accretion disks with typical outflow along the magnetic field lines of the disk. It was pointed by Grinin & Tambovtseva (2012) and now can be explained in the framework of our model of MCP stars (Gopka et al., 2010). On the other hand, the binary systems containing a NS companion and the detectable lithium, were really identified by Martin et al. (1994) and Rebolo et al. (1995).

Key words: stars, magnetic chemically peculiar stars, evolution, lithium, binary stars, neutron stars.

1. Introduction: lithium in the Universe

The origin of lithium in the atmospheres of some MCP stars is not understood up to now, and the main reason for this seems to be the lack of understanding of the nature of MCP stars. Recall that MCP stars are part of upper main sequence CP stars, these are the slowly rotating stars with anomalous chemical abundances, but unlike other CP (Hg-Mn, Am) stars MCP stars have global, mainly dipole magnetic field up to 30 kilogauss. The spectral types of these objects are B2-F0 and the range of the masses is $1.6-8 M_{\odot}$ (Braithwaite et al., 2010).

MCP stars show the periodical variations of light and (or) spectral features, magnetism, radial velocity, radio, X-ray, and IR-emissions. The modern stellar evolution theory is unable to answer why we can observe the lithium in the atmospheres of some MCP stars,

and why we not always can detect the lithium in the atmospheres of other representatives of this type stars.

Lithium is observed in the areas of magnetic poles in the atmospheres of stars, that was shown and modelled at the first in the works of Polosukhina et al. (1999, 2000), Shavrina et al. (2000, 2001). The lithium abundance in the polar spots can be significantly higher than the "cosmic" values and up to 6 dex exceeds the solar concentrations (Polosukhina et al. 1999, 2000, Shavrina et al. 2000, 2001, Kochukhov et al. 2004, Drake et al., 2005). Note, that the lithium abundance is equal to $\log N(\text{Li})=1.03$ in the atmosphere of the Sun and to $\log N(\text{Li})=3.25$ for meteorites (Spite & Spite, 2010).

The high abundance of lithium in MCP stars reflects the complex physical processes in these stars and requires challenging modeling beyond the standard stellar theory (as the main sequence stars with magnetic field). The phenomenon of MCP stars with lithium production can be the key to the understanding of the origin of Li in other stellar objects.

As a rule, the study of lithium is carried out using the doublet of neutral lithium at 6708 Å. It will be interesting to note that the doublet of Li consists of four lines: 6707.761 Å & 6707.912 Å for ${}^7\text{Li}$ isotope and 6707.921 Å & 6708.072 Å for ${}^6\text{Li}$ one (Meissner et al., 1948). According to Wallerstein & Conti (1968) the intensities of components are in the ratio of 2:1 for both isotopes. Therefore, as we can see, the weaker ${}^7\text{Li}$ component almost exactly overlaps the stronger ${}^6\text{Li}$ component.

In the analysis of high quality spectra one can use a weaker subordinate lithium line at 6103 Å. Note, that there are no significant differences between the LTE and non-LTE abundances extracted from the 6708 Å and 6103 Å lines as it was shown for metal poor dwarf stars by Lambert (2004) and Asplund (1999, 2000). The typical error of LTE abundances is near 0.2-0.5 dex from the difference between $\log N(\text{Li})$ that was found for the 6708 Å and 6103 Å lines as it was shown by Ford et al. (2002), Shavrina et al. (2005b), and Ruchti et al. (2011) for metal poor and MCP stars.

The wavelengths of lines of singly ionized lithium fall in the soft X-ray region (Gurzadyan, 1985), the wavelength of resonance line of Li II is 199 Å (Faraggiana et al., 1986).

The infrared lithium line at the wavelength 8126 Å was used by Pavlenko et al. (1995) and Rebolo et al. (1994, 1995) in the analysis of Li-rich stars of late spectral classes.

Reeves (2009) shows that the abundances of the light chemical elements such as Li, Be, and B are dependent on the nuclear interactions of elementary particles.

Lithium can not survive under the high temperatures in internal layers of stars. According to Spite & Spite (2010) ${}^7\text{Li}$ is destroyed when the temperature reaches the value of $2.5 \cdot 10^6$ K and ${}^6\text{Li}$ is destroyed when the

temperature is higher than $2 \cdot 10^6$ K.

The Big Bang nucleosynthesis was responsible for the origin of the isotope ${}^7\text{Li}$ and negligible amount of ${}^6\text{Li}$ one as it was discussed by Reeves (2009), Spite & Spite (2010), and Knouth et al. (2002). But only 10 percents of currently observed abundance of ${}^7\text{Li}$ isotope is the result of primordial nucleosynthesis (Knouth et al., 2002).

In the series of papers since 1970's Reeves and collaborators have found that the Galactic cosmic rays are responsible for production of ${}^6\text{Li}$ isotope, which is a product of spallation reactions between the Galactic cosmic rays and the interstellar C, N, and O nuclei, therefore Li is a fragmentation of C, N, and O nuclei.

In this scenario the part of ${}^7\text{Li}$ isotope is only 10 to 25 percents of total lithium production as it was shown by Reeves et al. (1970), Reeves (2009), and Knouth et al. (2002). The nature of cosmic rays sources is continued to be debated (Ramaty et al., 2000).

Modern investigations show that the stellar nucleosynthesis is responsible for major part of ${}^7\text{Li}$ isotope. The increase of ${}^7\text{Li}$ abundance for stars with $[\text{Fe}/\text{H}] > -0.5$ indicates the existence of stellar source of ${}^7\text{Li}$ isotope and also proves that lithium can be a result of some physical processes in the stellar interiors, for example the Cameron-Fowler mechanism in AGB stars (Reeves, 2009; Spite & Spite 2010; Knauth et al., 2003; Lambert, 2004).

Numerous observations of lithium in hundreds of stars at various evolutionary stages (pre-MS, MS, post-MS) provide the evidence of some processes which modify the surface lithium abundance. The definition of the evolutionary phase of Li-rich stars is absolutely critical for understanding the processes that create the lithium in stellar atmospheres (Ruthti et al., 2011). According to investigation of Prantzos (2012) intensive theoretical and observational works about production and evolution Li in the stellar source remains elusive at present.

2. The lithium abundances in the atmospheres of MCP stars and the cooler stars.

Gopka et al. (2007, 2008, 2010) proposed that MCP stars are binary systems with NS companion. Let's overview shortly the most important results of investigations of lithium in stellar atmospheres with special attention to MCP stars. The main efforts will be devoted to the observational results which directly or indirectly support our hypothesis.

It is known, that the progenitors of MCP stars can be Herbig AeBe objects (Braithwaite et al., 2010; Hubrig et al., 2012). These stellar objects are at the pre-main sequence evolutionary stage. Their masses are between 2 and 10 M_{\odot} .

Recall that Herbig (1947, 1950a, 1950b, 1957, 1960)

identified the objects that are at the early stages of the star formation characterized by a significant amount of circumstellar matter around any of them and shaded by dense clouds of dust and gas.

The Herbig AeBe objects are located in star-forming areas, are essentially the protostars on the stage of compression, they exhibit the emission lines in the spectra (hydrogen, helium, S II, O II, and other elements) and the lines of lithium in absorption. The spectra of these objects are characterized by variations of line profiles including P Cyg type profiles which testify the movement of matter from the star with velocities up to hundreds kilometers per second. They are also characterized by variability of brightness and polarization, the energy distribution in the spectrum shows two peaks.

It seems interesting to discuss here T Tauri type stars which are not strongly distinct from Herbig AeBe objects. T Tau stars have masses less than two solar mass, its ages are accepted to be young objects which do not cross the MS zero-age line.

Both Herbig AeBe and T Tauri stars have the accretion disks, and the outflow of matter, which is inextricably linked to the magnetic field of the discs.

The origin of accretion and outflow along the magnetic lines, "frozen" in the disk, and the origin of the magnetic field configuration in the disk was pointed for example by Grinin & Tambovsheva (2012). It was found that the magnetospheres of Herbig AeBe stars occupies the area of about 2-3 radii of the star for the most rapidly rotating stars, whereas for T Tauri stars it extends up to 5-10 radii of the star.

The spectra of Herbig AeBe and T Tauri stars exhibit the lines of lithium in absorption. As it will be discussed here after we guess that MCP stars can be the next evolutionary phase of Herbig AeBe.

The enrichment of lithium occurs at an earlier stage of evolution, as it was shown by Grankin (2012).

The lithium abundance is known for a relatively small number of MCP stars, Kochukhov (2008) pointed a dozen stars. The number of MCP stars with identified lines of Li in their spectra could be higher, but the variations of Li line wavelength with rotational phase in some stars results in the decrease of the number of Li stars due to misidentification of shifted Li line as it was pointed by Polosukhina et al. (1973, 1999), Faraggiana et al. (1996), and Gerbaldi & Delmas (1996).

An important reason of the small number of MCP stars with known Li abundance is that the lithium is expected to be essentially ionized (Faraggiana et al., 1986). The calculation shows that for the temperature of T Tau stars (the object with lower temperatures than those of MCP stars) the dominate state of lithium is Li II, therefore, the main part of lithium atoms in the atmospheres of MCP stars are ionized atoms (Gurzadiyn, 1985) but the lines of ionized lithium are beyond the optical wavelength region, as it was men-

tioned here before.

The strong magnetic field is the reason of additional problem in the identification of the lithium line in the spectra of MCP stars. Kochukhov (2008) analysed the lithium line 6708 Å as a function of the strength of magnetic field for 17 magnetic Ap stars and obtained that the line profile changes noticeably in the strong magnetic field stronger than 5 kGs.

Faraggiana et al. (1986) calculated that the equivalent width of lithium line 6708 Å should be 1, 8, 35, and 69 mÅ for temperatures 9000, 8000, 7000, and 6500 K respectively if the abundance of lithium in the stellar atmosphere is equal to $\log N(\text{Li})=3$ (the upper limit of cosmic lithium abundance).

Very strong lithium lines at 6708 Å have been discovered in the spectra of only several stars of asymptotic red giants branch (AGB), namely in intermediate mass AGB stars WZ Cas and WX Cyg by McKellar (1941) and Feast (1954). Faraggiana et al. (1999) found that the variability of equivalent widths is strong, for example WZ Cas shows the equivalent widths in the range from 10.7 Å to 3.43 Å in direct relation with variations of T_{eff} , the heavy blending of Li 6708 Å line by molecular lines for these AGB stars was also noted.

It was supposed that Cameron-Fowler mechanism is responsible for high lithium content at the surface of the intermediate-mass AGB stars. As the result of the action of this mechanism, lithium could be transported to the surface of stars, since the convective envelope contacts with the H-burning shell where ^3He -enrichment takes place from proton-proton reaction chain (Ruchti et al., 2011).

Kipper & Wallerstein (1990) investigated the late type SC stars with temperatures as low as $T_{eff}=2320-3750$ K and found that these stars exhibit the equivalent widths of Li 6708 Å line near 500 mÅ. Kipper & Wallerstein (1990) obtained the abundances of Li in SC stars to be equal to $\log N(\text{Li})=-1.6$ (in the scale $\log N(\text{H})=12$).

Ruchti et al. (2011) found only eight Li-rich giants in the sample of over 700 metal-poor stars. The abundances of Li for these eight stars show the values $\log N(\text{Li})=2.30-3.63$. According to this work, only one per cent of all giants are Li-rich stars and the frequency of Li-stars occurrence is independent of the metallicity. The lithium lines in the spectra of lithium-rich giants are very strong, for example the equivalent width of Li line in the star J142546.2-154629 is 540 mÅ. The lithium line at 6103 Å is also enhanced in the spectra of lithium-rich giants. The Li-rich giants in the sample investigated by Ruchti et al. (2011) are consistent with old age and low-masses stars, with masses less than 1 M_{\odot} . Li-rich AGB and RGB stars, according to Ruchti et al. (2011), show the range of masses 0.8-5 M_{\odot} . The frequency of Li-rich objects among these type stars is very low.

The Li-rich stars pose the new questions. Koch et al. (2011) concluded that new results about high Li-content in dwarfs are not easily understood in the frame of simple evolutionary mechanisms. They found very high abundance of lithium, namely $\log N(\text{Li})=4.21$, in the atmosphere of super-Li turnoff dwarf in the metal-poor globular cluster with the age of 12 Gyr (Koch et al., 2012; Koch et al., 2011). Earlier a dwarf with $\log N(\text{Li})=4.29$ was discovered in the young open cluster NGC 6633 (the age is only 700 Myr) by Deliyannis et al. (2002).

The investigation of lithium abundances in magnetic stars began in the 60th of the former century and this problem is still not clear. It is possible to point papers by Wallerstein (1965), Wallerstein & Merchant (1965), Wallerstein & Conti (1968), Wallerstein (1968), Gerbaldi et al. (1995), Faraggiana et al. (1986), Polosukhina et al. (1999, 2000), Shavrina et al. (2000, 2001, 2003, 2004, 2005a, 2005b, 2009), Drake et al. (2005), Kochukhov et al. (2004), Kochukhov (2008), etc. The list can be continued.

For two MCP stars HR7575 and γ Equ Wallerstein (1965) and Wallerstein & Merchant (1965) found the ratio ${}^6\text{Li}/{}^7\text{Li}=0.5$ and the Li abundance $\log N(\text{Li})=3$ (in the scale $\log N(\text{H})=12$). These authors concluded that some MCP stars show a higher lithium content, than that of some F and G stars. It was pointed that the highest content of ${}^6\text{Li}$ isotope is observed when the ratio of ${}^6\text{Li}/({}^7\text{Li}+{}^6\text{Li})$ is in the range from 0.19 to 0.47. These high values of the ${}^6\text{Li}/{}^7\text{Li}$ ratio for MCP stars can shed light on the possible physical mechanisms of production and preservation of both isotopes, probably indicating the spallation production.

An important remark of Wallerstein (1965) is that the abundance of ${}^6\text{Li}$ is significantly higher in MCP stars and it surely indicates on the local lithium production, but the author can not prove that the spallation has occurred on the stellar surface.

It is important to note that Wallerstein & Conti (1968) were unable to find lithium lines in other six investigated Ap stars. These authors supposed that lithium isotopes are synthesized on the stellar surfaces, but the relation to other spectroscopic peculiarities of Ap stars, especially to the stars without lithium, was not understood.

Later a possibility of nucleosynthesis by spallation reactions for Przybylski's star (HD101065, the prototype of roAp stars) was theoretically shown by Goriely (2007). Goriely was the first who studied the interaction of the stellar photosphere material with the flux of high energy particles. The result was the production of heavy elements in stellar atmospheres. The observed abundance pattern of Przybylski's star (including the possible actinides with short decay times) was obtained as a result of numerical fit of a net of spallation reactions in the atmosphere. Lithium isotopes also can be synthesized in these reactions.

Warner (1966) was the first who noted the presence of lithium in the Przybylski's star and estimated the isotopic ratio ${}^6\text{Li}/{}^7\text{Li}=0.3$. Shavrina et al. (2003) made the detailed spectrum synthesis of this star at the wavelength of lithium doublet 6708 Å. It has been shown that lithium is present in a complex blend and the abundance of lithium is 3.1 dex (in the scale $\log N(\text{H})=12$). The isotopic ratio ${}^6\text{Li}/{}^7\text{Li}$ was found to be close to 0.3. Note that for freshly synthesized lithium in cosmic rays this ratio is higher and equal to 0.5-0.8 (Knauth et al., 2003).

Faraggiana et al. (1986) using high resolution spectrum of the Li 6708 Å region, concluded, that there is no correlation between the intensity of 6708 Å feature and the other properties of MCP stars. They resumed that the accurate theoretical model of lithium production is absent, so all situations are possible and the mechanisms of Li synthesis remain fully unidentified.

Shavrina et al. (2009) evaluated the lithium abundance in the atmosphere of HR465 as $\log N(\text{Li})=5.4$ in the phase of enhanced lanthanides (the spectrum was observed in 2004, Bs 1500 Gs), which is 2 orders of magnitude higher than the cosmic lithium abundance. In the phase of enhanced lines of chromium and even higher magnetic field value (Bs=4500 Gs) the lithium line is not detected. Remember that HR465 has period of spectral variability of 23 years, when the strong lines of chromium in the spectrum of this star are changed by strong lines of lanthanides.

The method of modelling of the Li line red asymmetry was proposed by Shavrina et al. (2005) for γ Equ ($T_{\text{eff}}=7750$ K, $\log g=4$). Later Shavrina et al. (2006) studied the lithium abundance and the isotopic ratio ${}^6\text{Li}/{}^7\text{Li}$ in several roAp stars with narrow lines.

For the star HD137949 the errors in Li abundance value due to uncertainty of model atmosphere parameters were studied. So, for the models with effective temperatures and surface gravities equal to $T_{\text{eff}}=7750$ & $\log g=4.5$, $T_{\text{eff}}=7500$ & $\log g=4.5$, and $T_{\text{eff}}=7500$ & $\log g=4.5$, the values of lithium abundance were found as $\log N(\text{Li})=4.1$, 3.6 and 3.9 respectively.

One of the interesting results of this study was the red asymmetry of the lithium line Li 6708 Å for γ Equ in the spectra obtained with short exposures. It appears to be possible to fit the observed profile for 6708 Å line in two ways, the first is to increase the isotopic ratio ${}^6\text{Li}/{}^7\text{Li}$, the second is to decide that the profile could be formed in the matter flow falling on the star, and to shift the profile in accordance with the observed radial velocity.

We constructed the synthetic profiles of Pr III 6706.7 Å and Li I 6708 Å lines for γ Equ in two ways. The first: the red asymmetry of lithium line profile was modelled by enhanced ${}^6\text{Li}$ abundance. The best fit to spectra observed at Nordic telescope with spectral resolution $R=170000$ was reached with $v \sin i=8$ km s⁻¹ and ${}^6\text{Li}/{}^7\text{Li}=0.5$.

The second way is to explain the red asymmetry by fall of lithium formation layers on the star after sudden kicking upward due to shock wave (Shibahashi et al. 2004). Authors of this paper showed that the line profile variations show the monotonic blue-to-red motion only for the lines formed in the high atmosphere near the magnetic polar regions. The results are illustrated by Fig. 1.

In terms of our model of MCP stars as a binary system with NS such approach would be consistent with reality: in certain positions of binary system, we can observe both the incident flux of high-energy plasma and the magnetic pole region, as the main place of the lithium production. Fig. 2 shows the model of MCP star as a binary system with NS.

The proposed hypothesis of MCP stars origin is consistent with the fact that available observations of Li-rich MCP stars clearly detect the falling flux of matter on the pole regions of the stars. Is this mechanism responsible for the observed red asymmetry in γ Equ and other roAp stars is a problem for future studies and discussions, but the red asymmetry is one more detail which supports the picture of our model of the MCP star phenomenon (Gopka & Ulyanov, 2008; Gopka et al., 2010). In this case the problem of ${}^6\text{Li}$ origin will disappear.

3. The origin of binaries with MCP star and neutron star companions.

The question of the origin of lithium in the atmospheres of MCP stars is a part of a larger problem of the MCP stars origin. Where is the switch that distributes the stars on the MS as 80 percents without anomalies in their atmospheres and 20 percents with an abnormal chemical composition?

In other words, where to find such a large number of supernovae to each MCP star? Our point of view is that the better understanding of the star formation is necessary. Let's consider the observations in the areas of star formation.

Brown (2001) analyzed the double (and multiple) systems in the young association Sco 2 and found that the systems with B0-B3 primaries are more frequent than the systems with B4-B9, A, and F primaries.

What does it mean? What is the possible way to interpret it and how it relates to the origin of MCP stars? The answer is: directly.

Our model answers the question about the appearance of a large number of protostars with masses close to the presupernova masses on stage of formation of double systems because this process may occur in dense star-forming regions. Naturally, it can happens in the next way.

The evolution of more massive protostars in a binary system should be faster, so the size of the primary star

should decrease, and the size of the secondary companion appeared to be larger than the primary one because of the slow contraction. The secondary companion should be closer to the filling of its Roche lobe.

As the birthplace of stars is characterized by increased the density of dust, the filling of the Roche lobe for the second component in the initial stage of star formation is almost guaranteed. Under the assumption of the Roche lobe filling for less massive protostar companion the exchange of mass through the Lagrange point from less massive star to more massive star should start.

As a result, the evolution of more massive primary protostar is accelerated even more, while the less massive star should lost loses its mass and the rate of compression. The primary star in such binaries works as a "vacuum cleaner".

The process of "vacuum cleaner" changes the evolution of the most massive binary systems and changes (increases) the population of binaries with more massive primaries as it is illustrated by Fig. 3.

That is why the relative number of binary systems with massive primary companions should increase in comparison with the fraction of binaries with less massive primaries.

The second consequence of the "vacuum cleaner" is that the double systems of intermediate mass at the stage before MS are formed as a result of mass exchange in the double systems with large mass differences.

Sirotkin (2004) published the results of numerical simulation of mass exchange in binary systems and found that in the case of less massive component is closer to fill its Roche lobe, the mass transfer can occur in a dynamic time scale. These calculations support our hypothesis and allow to point the duration of effective "vacuum cleaner" to be of the same order as a dynamic time scale. That is why the results of this process can be easily detected even for young binaries.

The third consequence of "vacuum" process is that the "greedy" stars in the binary systems with the masses of primaries of 8-10 M_{\odot} in the progenitor state (it corresponds to spectral type near B2), quickly evolves through the type II supernova explosions to neutron star remnants.

A fourth consequence of the "vacuum cleaner" process is that the number of binary pairs with NS and low-massive stars (MCP stars) on the MS will be more numerous on the MS than the number of pairs with massive primaries. This is confirmed by observational data obtained by Kochukhov & Bagnulo (2006). These low-mass stars previously lost their masses to more massive companions. At the moment of explosion of more massive companion it lost almost 6 M_{\odot} , and enriched the atmosphere of low-massive star and the interstellar medium by r-process elements.

One of the results of supernova explosion is also the redistribution of angular momentum of the system.

The rotation of future MCP star should be braked, as it follows from the observations of rotational velocities of modern MCP stars.

Artemenko (2012) points the observational evidence of effective mechanism of braking the rotation of stars with observed lithium at the early evolutionary stages in the Taurus-Auriga region of star formation. T Tauri type stars in the mass range $0.3-3.0 M_{\odot}$ show approximately constant angular velocity during the first 10 million years of evolution. It outlines the existence of effective braking mechanisms which prevents the increase of rotational velocity with the compression of the star.

4. Conclusion: the consequence of our supposition of lithium origin in binary stars.

The problem of lithium origin in stellar atmospheres of stars today is one of the unsolved problems of astrophysics. We propose to have a look at this problem from the point of view of the most promising physical mechanism of lithium production, namely the synthesis of this element in the binary systems of intermediate mass stars at the early evolutionary stages.

Ambartsumian (1958) was the first who showed that the stellar associations are non-stable systems, consist of many young O, B0, B1, B2 spectral type hot giants, named B associations. It was discussed by later investigations, as an example Tetzlaff et al. (2011) published a catalog of runaway stars which were lost by these associations.

The explanation of mechanism of stellar formation in OB associations, as well as in the case of T-associations needs improvements. Binns et al. (2007) made the review of main properties of OB associations and tried to explain the origin of galactic cosmic rays by supernova explosions in these stellar complexes.

The distribution of binaries similar to that found by Brown (2001) is one the main characteristics of B associations. Based on the observed distribution of binaries obtained by Brown (2001) we did ascent on the evidence of overpopulation of binaries with primordial stars in pre-supernova state.

We suggest the evolutionary scenario of binary system with initial massive OB component and less massive component. The massive component attracts the matter from less massive component and after increasing of its mass accelerates the evolution and goes to Supernova II type explosion and to the neutron star. The atmosphere of less massive component should be irradiated by the high-energy particles from neutron-star component. The spallation reactions in this relativistic flux can product lithium.

The similar systems were observed by Martin (1994), Martin et al. (1994) and Rebolo et al. (1994, 1995). These authors detected binary systems with compact

objects such as neutron stars and Li-rich objects. For system Cen X-4 containing a neutron star and K-type star with $T_{eff}=4250$ K, the equivalent width of lithium line is $480 \text{ m}\text{\AA}$ corresponds to lithium abundance $\log N(\text{Li})=3.3$ dex (Rebolo et al. 1994, 1995).

This system belongs to the subclass of low mass X-ray binaries. The characteristic feature of such subclass is that during the period of several years or some weeks one can observe strong outbursts reaching the peak of X-ray luminosities of about $5 \cdot 10^{38} \text{ erg s}^{-1}$. At this time we can observe both lithium absorption and H_{α} emission in the photosphere of secondary component.

Fujimoto et al. (2008) theoretically examined the production of Li and the high isotopic ratio ${}^6\text{Li}/{}^7\text{Li}$ on the surface of low-mass secondary through the spallation of C,N,O nuclei by hot neutrons ($>10\text{MeV}$) in the transient soft X-ray radiation of a neutron star.

The supposed scenario have very important consequences from the point of view of stellar evolution theory. Let us point few of them.

1. The formation of lithium in MCP star can be explained by spallation reactions in the matter flow moving toward the star (namely to the magnetic poles). It is naturally interpreted in the framework of MCP stars phenomenon model proposed by Gopka & Ulyanov (2008) and Gopka et al. (2010).

The main counter-argument is improbable large number of supernovae, which then should evolve to NS. In our explanation of the phenomenon of MCP stars, we interpret the observational data of binary systems in stellar formation regions, which could explain the increased frequency of systems with companions at the stage of presupernova formation. The birthplaces of these systems are the OB associations (Ambartsumian, 1958) with overpopulation of B-type stars.

2. An important result of our consideration is the understanding of the nature and the evolutionary status of Herbig-AeBe stars as binary systems and progenitors of MCP stars. This is clear from the upper scenario. Fig. 1 by Gopka et al. (2010) and Fig. 1 by Grinin & Tambovtseva (2011) are similar.

According to Martin (1994) in order to detect the binary companions the lithium 6708 \AA resonance doublet could be used. Its equivalent width is the function of effective temperature of of the star (when it is assumed the mass of $1.5 M_{\odot}$ for invisible star). The equivalent width increases from 4 to 147 and 192 $\text{m}\text{\AA}$ if the temperature decreases from 18000, 12000, and 9000 K (spectral classes B2, B8, and A2) respectively. The spectral lines with above pointed strengths can be easily detected for stars with spectral types B8 and later.

3. The binary systems with NSs in which the mass of optical stars are less than $5 M_{\odot}$ are most likely formed as the result of the decay of triple or more multiple systems. As it was shown by Dewey & Cordes (1987) and Hinkle et al. (2005) the binary

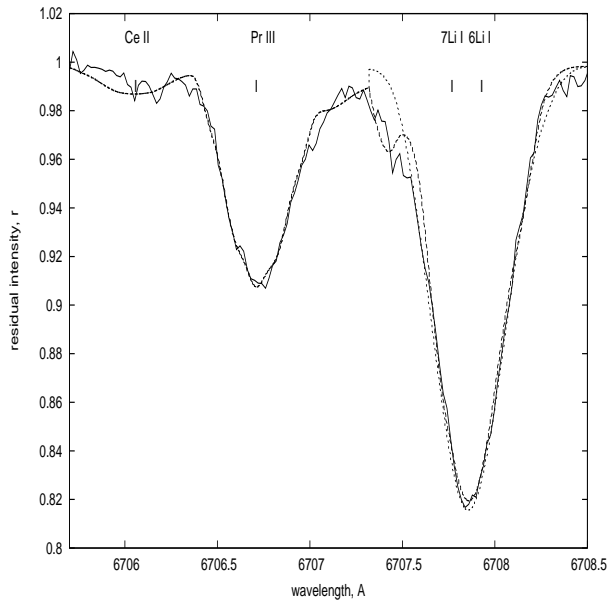


Figure 1: The spectrum of γ Equ in the vicinity of Li I 6708 Å line. Solid line - observations, NORDIT telescope. Dashed line - synthetic spectrum calculated with $\log N(\text{Li}) = -8.40$, ${}^6\text{Li}/{}^7\text{Li} = 0.5$, $v\text{ sini} = 8 \text{ km s}^{-1}$. Dotted line - synthetic spectrum calculated with ${}^6\text{Li}/{}^7\text{Li} = 0.08$ (solar value), $v\text{ sini} = 3 \text{ km s}^{-1}$. and red shifted by $\Delta\lambda = 0.065 \text{ \AA}$ (2.9 km s^{-1}).

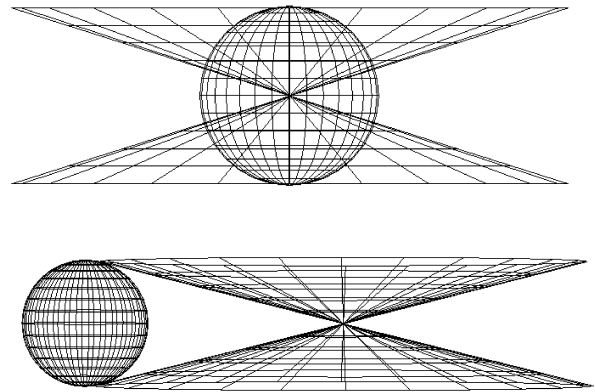


Figure 2: The supposed model of MCP stars as a stable magneto-dynamic configuration: star-neutron star at early stages of stellar formation (Gopka et al., 2007, 2008, 2010). This model confirms the observed kinematics of the circumstellar outflow for both progenitors of MCP stars on the stage before MS (Herbig AeBe objects), and for stars of T Tau type. The position of NS is the point of intersection of two cones. Two panels show the double system at different phases.

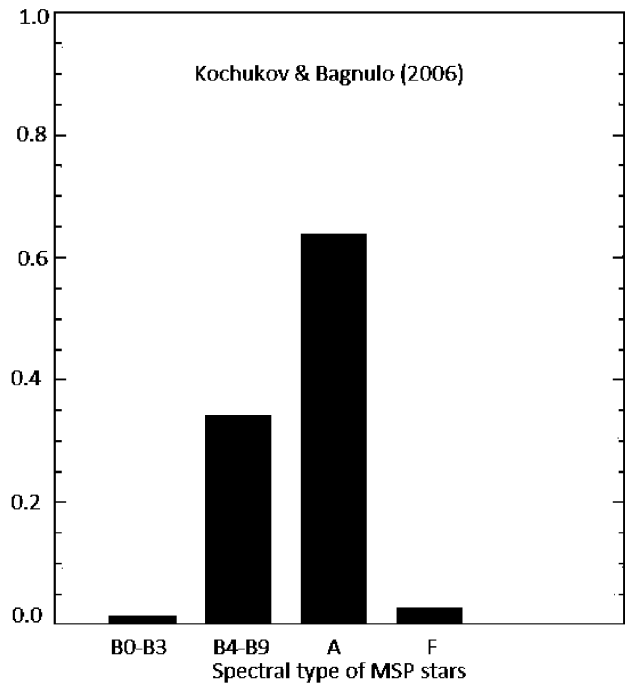
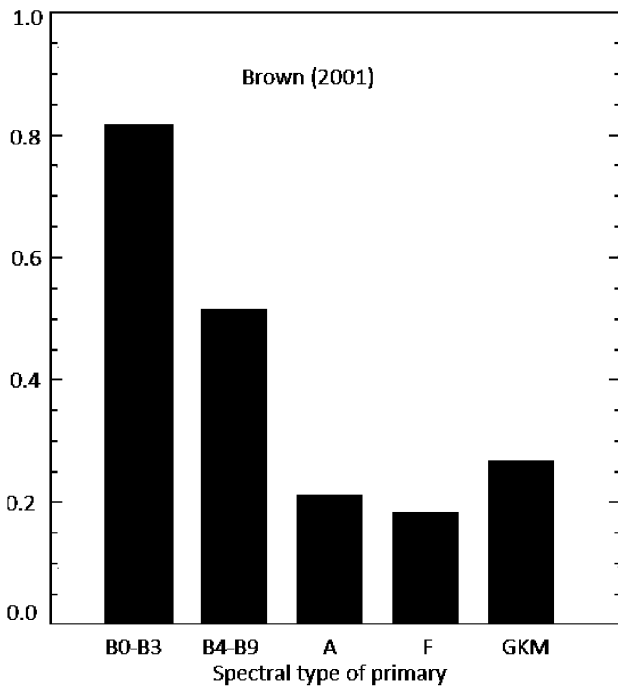


Figure 3: Upper panel: the distribution of observed fraction of stellar systems as ratio of the number of multiple systems to the total number of systems as a function of spectral type of the primary (Brown, 2001). Bottom panel: the distribution of MCP stars as a function of spectral type. The data are taken from Kochukhov & Bagnulo (2006).

system remains binary after the supernova explosion only if its mass is more than one half of the total mass of the binary system before the explosion. For example, the system T Tauri is a gravitationally bound multiple star with the total mass of about $6 M_{\odot}$ (Kohler, 2008).

Li-rich RGB giants and AGB supergiants can be considered as probably dissipated triple or multiple systems with NS.

4. The lowest limit of the optical star mass in this scenario is not confined which has been confirmed by observational data.

The proposed mechanism of lithium formation needs additional observational confirmation.

Acknowledgements. This work was supported in part by Mid-career and General Researcher Programs, and Science and Technology grants 2011-0028001 and 2011-00106996 respectively, through the National Research Foundation (NRF) funded by the Ministry of Education of Korea. One of the authors was granted by the Swiss National Science Foundation (SCOPE project No. IZ73Z0 -128180/1).

References

- Ambartsumian V.A.: 1958, *Review of Modern Physics*, **30**, 944.
- Anthony-Twarog B.J., Delyannis C.P., Twarog B.A. et al., 2009, *ApJ*, **138**, 1171.
- Artemenko S.: 2012, report, *Conf. "Stellar Atmospheres"*, KrAO, Ukraine.
- Asplund M., et al.: 1999, *A&A*, **346**, L17.
- Asplund M.: 2000, *ASP IUA Symp.*, **198**, 448.
- Binns W.R., Wiendenbeck M.E., Arnould M. et al.: 2007, *Space Sci. Rev.* **130**, 439.
- Braithwaite J., Akgun T., Aleciance F., et al.: 2010, *Highlights of Astronomy*, **15**, 161.
- Brown A.: 2001, *AN*, **322**, 43.
- Deliyannis C.P., Steinhauer A., Jeffries R.D.: 2002, *ApJ*, **577**, L39.
- Dewey R.J. & Cordes J.M.: 1987, *ApJ*, **321**, 780.
- Drake N.A., Nesvacil N., Hubrig S., et al.: 2005, *IAU Symp. Proc. IAU*, **228**, 89.
- Faraggiana R., Gerbaldi M., Castelli F., & Floquet M.: 1986, *A&A*, **158**, 200.
- Faraggiana R., Gerbaldi M., & Delmas F.: 1996, *ApSS*, **238**, 169.
- Faraggiana R., Gerbaldi M., Molaro P., et al.: 1999, *MmSAI*, **62**, 189.
- Feast M.W.: 1954, *Les Processus Nucleaires dans les Astres, Communications presentees au cinquieme Colloque International d'Astrophysique tenu a Liege les 10-12 Septembre, 1953*, p. 413.
- Ford A., Jeffries R.D., Smalley B., et al.: 2002, *A&A*, **393**, 617.
- Fujimoto S.-I., Matsuba R., & Arai K.: 2008, *ApJ*, **673**, L51.
- Gerbaldi M., & Delmas F.: 1996, *ApSS*, **238**, 169.
- Gerbaldi M., Faraggiana R., & Castelli F.: 1995, *A&A Suppl.*, **111**, 1.
- Gopka V.F., Ulyanov O.M., & Andrievsky S.M.: 2007, *OAP*, **20**, 62.
- Gopka V.F., Ulyanov O.M., & Andrievsky S.M.: 2008, *KPNT*, **24**, 36.
- Gopka V.F., Ulyanov O.M., Yushchenko A.V., et al.: 2010, *AIP Conf. Proc.*, **1269**, 454.
- Goriely S.: 2007, *A&A*, **466**, 619.
- Grankin K.N.: 2012, report, *Conf. "Stellar Atmospheres"*, KrAO, Ukraine.
- Grinin V.P. & Tambovtseva L.V.: 2012, *Astronomy Reports*, **55**, 704.
- Gurzadyan G.A.: 1985, *Stellar flares*.
- Herbig G.H.: 1946, *PASP*, **58**, 163.
- Herbig G.H.: 1950a, *ApJ*, **111**, 11.
- Herbig G.H.: 1950b, *ApJ*, **111**, 15.
- Herbig G.H.: 1957, *IAUS*, **3**, 3.
- Herbig G.H.: 1960, *ApJS*, **4**, 337.
- Hinkle K.H., Fekel F.C., Joyce R.R. et al.: 2005, *ASPC*, **336**, 173.
- Hubrig S., Cowley C., Faraggiana R. et al.: 2012, *The Messenger*, **148**, 21.
- Kipper T., & Wallerstein G.: 1990, *PASP*, **102**, 574.
- Knauth D.C., Federman S.R., & Lambert D.L.: 2003, *ApJ*, **586**, 268.
- Koch A., Lind K. & Rich R.M.: 2011, *ApJ*, **738**, 29.
- Koch A., Lind K., & Thompson J.B., & Rich R.M.: 2012, **673**, L51.
- Kochukhov O., Drake N.A., Piskunov N., & de la Reza R.: 2004, *A&A*, **424**, 935.
- Kochukhov O. & Bagnulo S.: 2006, *A&A*, **450**, 763.
- Kochukhov O.: 2008, *A&A*, **483**, 557.
- Kohler R.: 2008, *JPhCS*, **131a**, 2028.
- Lambert D.: 2004, *AIPC*, **743**, 206.
- Martin E.L.: 1994, *ASPC*, **62**, 315.
- Martin E.L., Rebobolo R., Casares J., & Charle P.A.: 1994, *ApJ*, **435**, 791.
- McKellar A.: 1941, *The Observatory*, **64**, 4.
- Meissner K.W., Mundie L.G., & Stelson P.H.: 1948, *Phys. Rev.*, **74**, 932.
- Pavlenko Ya.V., Rebolo R., Martin E.L., & Garcia Lopez R.J.: 1995, *A&A*, **303**, 807.
- Polosukhina N. et al.: 1973, *Izv. KrAO*, **47**, 118.
- Polosukhina N, Kurt D., Hack M., et al.: 1999, *A&A*, **351**, 28.
- Polosukhina N., Kurtz D., Hack M., et al.: 2000, *A&A*, **357**, 920.
- Prantzos N.: 2012, *A&A*, **542**, 67.
- Ramaty R., Scully S.T., Lingenfelter R.E., et al.: 2000, *ApJ*, **534**, 747.
- Rebolo R., Magazzu A., & Martin E.L.: 1994, *arXiv:astro-ph/9410089v1 28 Oct. 1994*.
- Rebolo R., Martin E.L., Casares J., et al.: 1995, *MmSAI*, **66**, 437.
- Reewes H.: 2009, *Light Elements in the Universe. Proceeding IAU Symposium*, **258**, 469.

- Reeves H., Fowler W.A., & Hoyle F.: 1970, *Nature*, **226**, 727.
- Ruchti G.R., Fulbright J.P., Rosemary F.G., et al.: 2011, *ApJ*, **743**, 107.
- Shavrina, A.V., Polosukhina N.S., Tsymbal V., & Khalak V.: 2000, *Astronomy Reports*, **44**, 235.
- Shavrina, A.V., Polosukhina N.S., Zverko J., et al.: 2001, *A&A*, **372**, 571.
- Shavrina, A.V., Polosukhina N.S., Pavlenko Y.V., et al.: 2003, *A&A*, **409**, 707.
- Shavrina A., Polosukhina N., Khan S., et al.: 2004, *IAU Symposium*, **224**, 711.
- Shavrina A.V., Polosukhina N.S., Pavlenko Ya.V. et al.: 2004, *Astronomy Reports*, **47**, 573.
- Shavrina A.V., Polosukhina N.S., Khan S. et al.: 2005a, *KPNT Suppl.*, **5**, 500.
- Shavrina A.V., Polosukhina N.S., Khan S. et al.: 2005b, *Astronomy Reports*, **50**, 295.
- Shavrina A.V., Polosukhina N.S., Khan S. et al.: 2006, *Astronomy Reports*, **83**, 560.
- Shavrina A.V., Polosukhina N.S., Kudryavtsev D.O. et al.: 2009, *KFNT Suppl.*, **6**, 222.
- Shibahashi H., Kurtz D.W., Kambe E., Gough D.O.: 2004, IAU Symposium, No. 224. Cambridge, UK: Cambridge University Press, p. 829. Edited by Zverko J., Ziznovsky J., Adelman S.J., Weiss W.W.
- Sirotkin F.V.: 2004, *OAP*, **17**, 84.
- Spite M. & Spite F.: 2010, *IAU Simp. AIP Conf. Proc.*, **268**, 1.
- Tetzlaff N., Neuhauser R., & Hohle M.M.: 2011, *MNRAS*, **410**, 190.
- Wallerstein G.: 1965, *ApJ*. **141**, 311.
- Wallerstien G., Herbig G.H., & Conti P.S.: 1965, *ApJ*. **141**, 610
- Wallerstein G., Merchant A.E.: 1965, *PASP*, **77**, 140.
- Wallerstein G., & Conti P.S.: 1968, *ARAA*, **7**, 99.
- Warner B.: 1966, *Nature*, **211**, Issue 5044, 55.

THE MATHEMATICAL MODEL OF THE PHOTOMETRIC VARIABILITY AND CLASSIFICATION OF SEMIREGULAR PULSATING ASYMPTOTIC GIANTS BRANCH STARS

L. S. Kudashkina

Odessa National Maritime University
Odessa, Ukraine
kuda2003@ukr.net

ABSTRACT. The modern review of the stars which are located at the position of asymptotic giant branch at the HR-diagram is presented. The most interesting problems connected to these objects are noted, as well as attention is paid to classification and to the evolutionary status. We provided mathematical modeling of the mean light curve of the semiregular supergiant S Per. It is shown, that by means of the periodogram analysis, it is possible to determine the period of the main variability and to provide further detailed classification of semiregular pulsating stars, approximating their mean light curves with a trigonometric polynomial. It is offered to use the photometric period for estimates of physical parameters of pulsating stars.

Key words: variable stars, pulsations, data analysis

After in the center of the star will burn out helium, having formed a carbon-oxygen core, reactions will move to a layer around of a core where helium was still kept, and in higher layers burning hydrogen proceeds. At this stage, a star again turns to red giants, forming asymptotic giant branch (AGB) at the HR-diagram.

We carried out research of semiregular AGB stars using methods of mathematical modeling and their making subsequent classification. The algorithms and programs developed by I.L.Andronov were used for the analysis of photometric signals. They were described by Andronov (1994, 1997, 2003).

All AGB stars are pulsating.

Pulsating instability arises at certain stages of stellar evolution, therefore classification of pulsating variable stars on duration of the period, the shape of the light curve, to the spectral type and other observational parameters reflects their evolutionary status, that is characteristic to group of stars with certain ranges of mass, age and chemical composition.

The basic problems solved now, concerning AGB stars, is in computation of dynamic models of atmospheres, definition of a pulsation mode, studying of the mechanism of the mass loss and the further evolution of stars.

One of the main questions of the theory of stellar pulsations is the mode, in which AGB stars pulsate.

For the solution of the problem about the mode of stellar pulsation, it is necessary to classify all observations and types of stellar activity.

Any ways of classification of stars on variability types lean on a general view of a light curve and a spectral class. However, such approach is not always successful, if it is a question of semiregular variables (SR). For them often it is impossible to consider the general light curve as it contains parts, characteristic for stars of various types. This is probably because SR-stars, in the majority, first, multiperiodic and all components of this multiperiodicity prove very actively, thus having similar amplitude with the main variability. And, secondly, the period of the basic variation also changes (Kudashkina, 2003).

Subclasses of SR-stars are strongly mixed. Especially it concerns stars of subtypes SRb. Kerschbaum and Hron (1992) introduced their division into 'red' and 'blue', based on statistical researches of the periods, amplitudes, temperatures, mass loss rates, presence the dust shell and features of spectra. Properties of stars in visual and infra-red areas of a spectrum have been used in their work. The same authors specify, that SRa-stars are intermediate objects between long period Mira-type stars and SRb-stars.

For example, the star AF Cyg may be quite a prototype of a separate class of stars (as, for example, RV Tau). This object shows consecutive pulsations periods 'switching' between two main values (Andronov, Chernysheva, 1989).

It is necessary to notice, that the SRc-class, in fact, marks only stars which are supergiants, sometimes with variability of type SRa, but more often the type of variability is not certain in any way. As a representative of the SRc-class, we shall consider the star S Per.

S Per is the supergiant, belongs to stars with harmonious variability. For the periodogram analysis, the database of the French Association of Variable Stars Observers (AFOEV) and the methods of the analysis of multiperiodic fluctuations, described by Andronov (1994, 1997), were used.

The period value is $P=809.^d91$ (Kudashkina & Andronov, 2000). Actually, at the periodograms, there is not a single high peak, but there are two. The first corresponds to a period of $P=16173^d \pm 158^d$. with which average brightness changes (we shall notice, that the interval of observations exceeds 20000 days), and the second peak is dual $P_1=809.^d6 \pm 0.^d22$ and $P_2=768.^d8 \pm 0.^d31$.

Extended researches of the period show the following. Having divided all existing light curve about for hundred years into six intervals, for each interval we applied the periodogram analysis. The results are presented in Table 1. Each following value of the period for a given interval is computed for the residuals of observations from a best sine fit (the 'prewhitening'), $S(f)$ – height of peak at the periodogram, which is a square of the correlation coefficient between the observations and the sine fit.

In last time interval, the light curve of S Per has a regular form with the stable period of 816.8 days (Fig. 1). We consider, that the star pulsates in a fundamental mode.

Using the dependence 'the period - absolute bolometric magnitude', published by Feast (1989) for supergiants, we shall estimate M_{bol} for S Per.

$$M_{bol} = -7.20 \cdot \lg(P) + 12.8$$

We obtain $M_{bol} \approx -8.17$.

Abramyan (1984) has determined the following parameters for S Per, using infrared-observation and dependences between luminosity, mass, effective temperature and the period: $M_V = -6.1$, $M_{bol} = -8.7$, $M/M_\odot = 26.3$, $T_{ef} = 2950$ K. Spectral class M4Ia-M4.5Iab.

Let's take advantage of these values of mass and effective temperature for estimates of radius of a star.

We use classical relations,

$$\lg(L/L_\odot) = -0.4(M_{bol} - 4.7)$$

where L_\odot – luminosity of the Sun.

We have from here $L \approx 140605 L_\odot$.

For absolutely black body

$$L = 4\pi R^2 \sigma T_{ef}^4,$$

we receive $R = 1.0 \cdot 10^{14}$ cm or, about, $1400 R_\odot$.

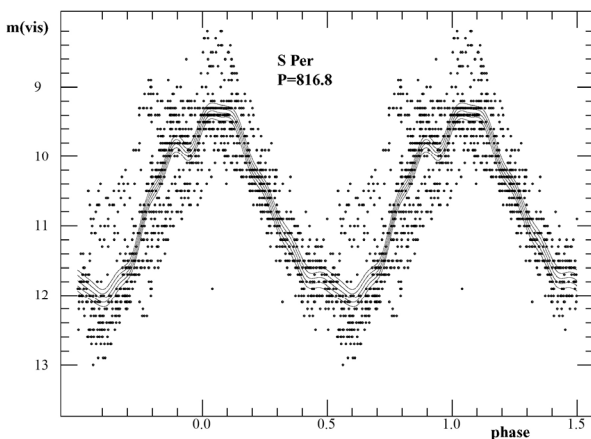


Figure 1: Phase light curve of the star S Per on the observational data-base AFOEV and its approximation by a trigonometric polynomial of statistically optimal degree $s=8$ (Andronov, 1994; Andronov & Baklanov, 2004).

Table 1: The results of the periodogram analysis for S Per.

Interval (JD+24...)	Period values	S(f)
23500-25000 (1500 ^d)	991. ^d 46 ± 18. ^d 64 431.43 ± 9.84 643.99 ± 45.50	0.94 0.48 0.40
25000-29000 (4000 ^d)	834.15 ± 3.26 489.88 ± 2.08 1631.76 ± 25.04	0.44 0.36 0.33
29000-32000 (3000 ^d)	768.91 ± 7.16 544.26 ± 4.04 998.83 ± 15.20	0.75 0.53 0.39
39400-43200 (3800 ^d)	909.40 ± 6.52 787.89 ± 8.45 1090.17 ± 15.31	0.83 0.55 0.45
43200-47000 (3800 ^d)	759.33 ± 5.48 599.31 ± 6.07 298.55 ± 1.65	0.42 0.35 0.33
47000-51000 (4000 ^d)	816.82 ± 1.55 2463.06 ± 40.01 1106.98 ± 8.90	0.77 0.44 0.38

As to $T_{ef} = 2900$ K estimated by Alvarez and Mennessier (1997), this corresponds to a spectral class of about M8. However, at them it is a question of stars-giants of the Mira-type. Nevertheless, the radius of S Per seems to be overestimated. In this connection, it is interesting to substitute the obtained value in the known formula from the theory of stellar pulsations (Cox, 1980)

$$P_0 = Q \sqrt{\frac{(R/R_\odot)^3}{(M/M_\odot)^2}},$$

where R_0 , M_0 – are solar radius and mass, respectively.

For our value of period of $P_0 = 816.^d8$, $Q \approx 0.077$, that, generally speaking, should agree with theoretical values (Q from 0.06 till 0.08) for semiregular variables.

Conclusions. Thus, the extensive and non-uniform class of semiregular variables requires the close approach and audit which quite with advantage can be lead, using modern mathematical methods and already existing observation material.

In the present work it is shown, that stable light curve and a period of pulsations can be used to estimate of physical parameters of a star.

All variations of the photometric parameters inherent to considered stars, for example, the form of a light curve in visual area, undoubtedly, are connected to physical properties of a star. Therefore it is possible to make classification of semiregular variable stars on these parameters. Similar work has been done by Chinarova and Andronov (2001). Average values of parameters of light curves for 173 SR-stars of various subtypes were received as a result. This result can serve as the basis for mathematical modeling of the complicated processes taking place in a star and its envelope, influencing on the shape of the light curve.

Acknowledgment. The author thanks Professor I.L.Andronov for statement of a problem and useful discussions.

References

- Abramyan G.: 1984, *Astrophysics* **20**, 2, 239.
- Andronov I.L.: 1994, *Odessa Astron. Publ.* **7**, pt. 1-2, 49.
- Andronov I.L.: 1997, *Astron. Astrophys. Suppl. Ser.* **125**, 207.
- Andronov I.L.: 2003, *Astron. Soc. Pacif. Conf. Ser.* **292**, 391.
- Alvarez R., Mennessier M.-O.: 1997, *Astron. And Astrophys.* **317**, 761.
- Andronov I.L., Chernysheva I.V.: 1989, *Astron. Circ.*, 1538, 18.
- Andronov I.L., Baklanov A.V.: 2004, *Astronomy School's Report* **5**, 264.
- Chinarova L.L., Andronov I.L.: 2001, *Odessa Astron. Publ.* **13**, 116
- Feast M., Glass I., Whitelock P., Catchpole R.: 1989, *Mon. Not. Roy. Astron. Soc.* **241**, 375.
- Kerschbaum F., Hron J.: 1992, *Astron. Astrophys.* 263, 97.
- Cox, J. P.: 1980, *Theory of Stellar Pulsation*, Princeton U. Press.
- Kudashkina L.S., Andronov I.L.: 2000, *The Impact of Large-Scale Surv. on Puls. Star Res. ASP Confer. Ser.* **203**, L. Szabados & D.W. Kurtz, eds., P.119.
- Kudashkina L.: 2003, *Kinematics and physics of celestial bodies* **19**, 3, 193.

COMMENTS ON ENVIRONMENTAL EFFECTS IN THE ORIGIN OF ANGULAR MOMENTA IN GALAXIES

Elena Panko¹, Paulina Pajowska², Włodzimierz Godłowski³, Piotr Flin⁴

¹ Nikolaev National University, Kalinenkov Astronomical Observatory, Nikolskaya, 24, Nikolaev, 54030, Ukraine *panko.elena@gmail.com*

² Opolski University, Institute of Physics, ul. Oleska 48, 45-052 Opole, Poland *paoletta@interia.pl*

³ Opolski University, Institute of Physics, ul. Oleska 48, 45-052 Opole, Poland *godlowski@uni.opole.pl*

⁴ Jan Kochanowski University, Institute of Physics, 25-406 Kielce, ul. Swietokrzyska 15, Poland *sfflin@cyf-kr.edu.pl*

ABSTRACT. We examine the orientations of galaxies in 43 rich Abell galaxy clusters belonging to superclusters and containing at least 100 members in the considered area as a function of supercluster multiplicity. It is found that the orientation of galaxies in the analyzed clusters is not random and the alignment decreases with supercluster richness, although the effect is statistically significant only for azimuthal angles. The dependence of galaxy alignment on cluster location inside or outside a supercluster and on supercluster multiplicity clearly shows the importance of environmental effects on the origin of galaxy angular momenta. The comparison with alignment of galaxies in a sample of rich Abell clusters not belonging to superclusters is made too.

Key words: galaxies, angular momenta.

1. Introduction

One of the most important but unsolved until now problems in modern extragalactic astronomy and cosmology is the origin of large scale structures. At present the Λ CDM model is commonly accepted as the basis by which cosmic structures were born. In the model the Universe is considered to be spatially flat, homogeneous and isotropic at an appropriate scale. However, the dimension of that scale is changing with the growth in our knowledge of the Universe. In addition, it is also commonly accepted that currently observed structures originated from nearly isotropic distributions in the early Universe. The departure from isotropy, as estimated by the CMBR is on the order of $\delta\rho/\rho \simeq 10^{-5}$. About half a century ago the main

problems were connected with the types of perturbations, their amplitude, and scale (mass or length). In the Λ CDM model the structures were formed in the primordial, adiabatic, nearly scale invariant, Gaussian, random fluctuations.

Numerous different theories of galaxy origins predict various means by which galaxies gained angular momentum (Peebles 1969, Zeldovich 1970, Sunyaev & Zeldovich 1972, Doroshkevich 1973, Shandarin 1974, Wesson 1982, Silk & Efstathiou 1983, Bower et al. 2005). Since different scenarios forecast different distributions for the angular momenta of galaxies in structures (Peebles 1969, Doroshkevich 1973, Shandarin 1974, Silk & Efstathiou 1983, Catelan & Theuns 1996, Li 1998, Lee & Pen 2002, Navarro et al. 2004, Trujillo et al. 2006), testing galaxy orientations can be used to check the scenarios of galaxy origins. Normally studies of the orientation of galaxy planes were performed.

Godłowski & Flin (2010) studied the orientation of galaxy groups in the Local Supercluster, and found a strong alignment of the major axis of the groups with directions towards the supercluster center (Virgo cluster) as well as with the line joining the two brightest galaxies in the group. The interpretation of these observational features is as follows. The brightest galaxies (believed to be the most massive ones) of the group originated first. As a result of gravitational forces, other galaxies were attracted to them and a filament was formed at the end.

Similar results were obtained by Paz et al. (2011), where the authors found a strong alignment between the projected major axis of group shapes and the surrounding distribution of galaxies to scales of $30h^{-1}Mpc$. Smargon et al. (2011) searched for two types of cluster alignments using pairs of clusters:

the alignment between the projected major axes of the clusters displayed a weak effect up to $20h^{-1}Mpc$, whereas the alignment between the major axis of one cluster with the line connecting the other cluster in the pair displayed a strong alignment on scales up to $100h^{-1}Mpc$. Also, a statistically significant anisotropy for the galaxy groups and cluster orientations for a sample of the Jagellonian field was noted by Flin & Vavilova (1996) and Vavilova (1999).

The other possibility for interpreting the (Godłowski & Flin, 2010) result is that the galaxies form at a pre-existing filament. Consistent with that argument are the results of Jones et al. (2010), who found that the spins of spiral galaxies located within cosmic web filaments tend to be aligned along the larger axis of the filament. Jones et al. (2010) interpreted it as “fossil” evidence, indicating that the action of large scale tidal torques effected the alignment of galaxies located in cosmic filaments. The relationship between alignment and the surrounding neighborhood was observed in a study of orientations in the vicinity of voids by Varela et al. (2011), a continuation of an earlier study of galaxy orientations in regions surrounding bubble-like voids (Trujillo et al., 2006). Varela et al. (2011) found that the observed tendency in the alignment of galaxies is similar to that observed in numerical simulations of the distribution of dark matter, i.e. in distributions of the minor axis of dark matter halos around cosmic voids, which suggests a possible link to the evolution of both components.

The large scale distribution is usually known as the “Cosmic Web.” In practice the “Cosmic Web” has four components which are: long filaments, walls, voids, and rich, dense regions – so called galaxy clusters. Thus, we should investigate the alignment of galaxies and clusters in such structures as well.

In Godłowski et al. (2010), Paper I hereinafter, a sample of 247 rich Abell clusters was analyzed. It was found that the alignment of members in rich structures containing more than 100 galaxies is a function of the group mass, in the sense that the alignment increases with the richness of the group. In view of such features, it is interesting to see if clusters belonging to the larger structures exhibit the same type of alignment as the entire sample of clusters. For that reason, we Godłowski et al. (2011, Paper II hereinafter) analyzed the alignment of galaxy cluster members for clusters belonging to superclusters. The problem was not investigated previously, although the alignment of galaxies in superclusters has been investigated many times.

In Paper II the alignment of galaxies in the sample of 43 rich Abell galaxy clusters belonging to a supercluster and having at least 100 members was investigated. It was found that the orientation of galaxies in the analyzed clusters is not random. However, significant differences were found with the

results obtained in Paper I, in which an increase of alignment was found for rich Abell clusters as a function of cluster richness. On the contrary, other clusters belonging to superclusters do not show such an effect. In Paper I galaxies in the sample studied were split into three bins according to supercluster multiplicity. They were: a subsample of superclusters containing only 4 structures, a subsample of superclusters containing 5–7 structures, and finally a subsample of superclusters containing 8–10 clusters. However, because the analysis was based on only 3 bins, it was difficult to determine the statistical significance of the results. In the present paper we decided to analyse the orientation of galaxies in clusters belonging to supercluster in more detail, without binning on clusters properties such as richness or BM type. In essence, we used the likelihood of membership in a supercluster as the parameter which characterizes each analyzed cluster.

2. Observational data

Input data for the present study made use of the PF Catalogue of galaxy structures (Panko & Flin, 2006). That Catalogue was constructed by finding structures in the Muenster Red Sky Survey (MRSS) (Ungruhe et al., 2003) in conjunction with the Voronoi tessellation technique applied to find structures. The MRSS is a large-sky galaxy catalogue covering an area of about 5000 square degrees in the southern hemisphere. It is the result of scanning 217 ESO plates, yielding positions, red magnitudes, radii, ellipticities, and position angles for about 5.5 million galaxies, and is complete to $r_F = 18.3^m$. As a result, there are 6188 galaxy structures called clusters. Structure ellipticities and position angles were determined by means of the standard covariance ellipse method. We have selected a sample of 247 very rich clusters containing at least 100 members each that are identified with an ACO cluster (Abell et al., 1989) – see Paper I for more details. Unfortunately there are not obvious correlation between “rich” PF clusters and Abell’ richness classes. The PF catalogue was also used as the basis for supercluster search (see, for example, Panko, 2011) and 54 superclusters containing at least 4 clusters each were detected. We found that 43 of a total of 247 rich PF clusters belong to superclusters, and they were chosen for detailed analysis. However, it should be noted that three clusters, 0347-5571, 2217-5177, and 2234-5249, have two possible identifications with superclusters of different multiplicity, so must be counted in two bins, which formally enlarged our sample to 46 clusters.

3. Results and Discussion

Studies of galaxy alignments are usually done by analyzing distributions of the angles connected with the orientation of the galaxy plane; namely the position angle of the great axis of the galaxy image P and the angles describing the orientation of the normal to the galaxy plane: δ_D and η . The polar angle δ_D is the angle between the normal to the galaxy plane and the main plane of the coordinate system; the azimuthal one η is angle between the projection of this normal onto the main plane and the direction toward the zero initial meridian and positional angle (see for example Flin & Godłowski 1986, Paper I). In the present paper, as well as in Paper II, we analyzed the sample of 43 very rich clusters (having 100 and even more members) belonging to superclusters.

The existence of an alignment for each particular cluster belonging to our sample was analyzed in Paper I (Table 4). On that basis it was possible to analyze the frequency of alignments in our sample of galaxy clusters attributed to superclusters (Table 1). To first order, the data indicate that anisotropy decreases with supercluster multiplicity.

Table 1: The frequency of anisotropy of very rich clusters located in superclusters.

Multiplicity	The angle P	The angle δ_D	The angle η
N=4	0.84	0.74	0.84
N=5-7	0.31	0.90	0.79
N=8-10	0.43	0.57	0.43

It is also possible to analyze the alignment of clusters belonging to superclusters in more detail. The standard method of approach for galactic alignments is an analysis of the distribution of the angles, which provides information connected with the orientation of galaxies. That approach was proposed by Hawley & Peebles (1975), who analyzed the distribution of position angles using χ^2 testing, Fourier testing, and first autocorrelation testing. One should note that there were several modifications and improvements to the original Hawley & Peebles (1975) method (Flin & Godłowski 1986, Kindl 1987, Godłowski 1993, 1994, Aryal & Saurer 2000, Godłowski et al., 2010). Godłowski (2012) made a significant improvement to the original Hawley & Peebles (1975) method and showed its usefulness in the analysis of galaxy orientations in clusters. In Godłowski (2012) the mean values of the analyzed statistics were computed. The null hypothesis H_0 assumed that the mean value of the analyzed statistics was that expected for the case of a random distribution of analyzed angles. The results

were compared with theoretical predictions as well as with the results obtained from numerical simulations.

Following the Godłowski (2012) method, we analyzed our sample of 43 clusters belonging to superclusters. In Paper II we analyzed only the χ^2 statistic and statistics obtained on the basis of Fourier testing.

χ^2 statistics was studied as

$$\chi^2 = \sum_{k=1}^n \frac{(N_k - N_{0,k})^2}{N_{0,k}} \quad (1)$$

where N_k is the number of galaxies within k -th angular bin and as $N_{0,k}$ is the expected number of galaxies per bin, n is the number of bins.

If the theoretical probability function PF is uniform, then $N_{0,k}$ are equal.

In all applied statistical tests, the entire range of the investigated θ angle (as θ we accept $\delta_D + \pi/2$, η or P).

If deviation from isotropy is a slowly varying function of the angle, one can use the Fourier test (Hawley & Peebles, 1975):

$$N_k = N_{0,k}(1 + \Delta_{11} \cos 2\theta_k + \Delta_{21} \sin 2\theta_k) + \dots \quad (2)$$

If the theoretical probability function PF is symmetric with respect to the value $\theta = \pi/2$, we obtain the following expressions for the Fourier coefficients:

$$\Delta_{11} = \frac{\sum_{k=1}^n (N_k - N_{0,k}) \cos 2\theta_k}{\sum_{k=1}^n N_{0,k} \cos^2 2\theta_k} \quad (3)$$

$$\Delta_{21} = \frac{\sum_{k=1}^n (N_k - N_{0,k}) \sin 2\theta_k}{\sum_{k=1}^n N_{0,k} \sin^2 2\theta_k} \quad (4)$$

The probability function has amplitude

$$\Delta_1 = (\Delta_{11}^2 + \Delta_{21}^2)^{1/2} \quad (5)$$

with the standard deviation of the amplitude

$$\sigma(\Delta_1) \approx \left(\frac{2}{nN_0}\right)^{1/2}. \quad (6)$$

The amplitude Δ was calculated using higher Fourier coefficients till 4θ , according Godłowski (1994).

Here we extend our analysis in comparison with Paper II using autocorrelation and Kolmogorov - Smirnov (K-S) testing. Autocorrelation test we applied in form:

$$C = \sum_{k=1}^n \frac{(N_k - N_{0,k}) \cdot (N_{k+1} - N_{0,k+1})}{\sqrt{N_{0,k}N_{0,k+1}}} \quad (7)$$

Because of the small number of galaxies in some clusters, we made 1000 simulations of the distribution of position angles in 43 fictitious clusters, each cluster with the number of galaxy members identical to the

real cluster. On this basis we obtained the probability density function (PDF) and the cumulative distribution function (CDF) seen in Fig. 1 and Fig. 2. The expected value for the analyzed statistics and its variance were computed as well. In Table 2 we present the average values of the analyzed statistics, the corresponding standard deviations, the standard deviations in the sample, and the standard deviations for the distribution of P angles. Details of the applied statistics were presented in previous papers (Paper I and Godłowski, 2012).

It is now possible to compare the results obtained for the actual sample of 43 clusters with that obtained from numerical simulations (right hand side of Table 2). If we assume that the true distribution of position angles is uniform, then an exact value for the probability that the analyzed statistic included a specific chosen value can be obtained from CDF (Figs. 1 and 2).

However, one should note that our procedure computes the mean values of the analyzed statistics. When the errors are normally distributed (Gaussian), which is the case at least for some statistics analyzed in Godłowski (2012), the parameters are estimated by the maximum-likelihood method. The distribution should have an asymptotic normal (Gaussian) appearance, which was checked by Godłowski (2012) with the use of the Kolmogorov - Lilliefors test (Lilliefors, 1967). There it was shown that a Gaussian approximation works well, which made the interpretation of the results much easier. For the sample of all 43 clusters located in superclusters the distribution of position angles of galaxy members in the cluster is anisotropic and the departure from isotropy is usually greater than 3σ (see Table 2), with the exception of the first autocorrelation test where the effect is less than 2σ . For the angles which gave the spatial orientation of galaxy planes (δ_D and η angles) the anisotropy is even greater than in the case of position angles P . In our opinion that can be attributed to incorrectly assumed shapes for the galaxies. That problem was analyzed in detail by Godłowski & Ostrowski (1999) and Godłowski (2011). Those studies were based on Tully's NGC Catalogue (1988). In that catalogue, while calculating galaxy inclination angles, Tully assumed that the "true" ratio of axes for galaxies is 0.2, which, as we have shown in the above papers, is a rather poor approximation, especially for non-spiral galaxies (Godłowski, 2011). For that reason, the previous study concentrated on the analysis of position angles. In our present analysis, presented below, the effect is not especially important because, for the case of analyzing the spatial orientation of galaxy planes, our interest is only to show how the alignment changes with membership of the clusters in a supercluster as well as with supercluster multiplicity.

The main goal of this study is connected with finding trends appearing in the data. In Paper I, while analyzing

entire samples of 247 rich Abell clusters, we found that the alignment increases with cluster richness. In the analyzed sample of 43 clusters of galaxies belonging to superclusters we do not observe that effect (Table 3). This conclusion is significantly different from the result obtained in Paper I for the whole sample of 247 rich Abell clusters. We suppose that such a difference can be traced to environmental effects during the formation of superclusters. Note that the distributions of analyzed angles are anisotropic in both cases: for the entire collection of 247 rich Abell clusters and for the subsample of 43 clusters belonging to superclusters.

In Paper II we presented an analysis of 43 clusters (Table 4.), binned according to supercluster multiplicity. One can observe that the anisotropies seem to decrease with supercluster richness. For that reason, in the present paper we decided to perform an unbinned analysis of the linear regression between values of the analyzed statistics and supercluster multiplicity. The results are presented in the Table 5. We analyzed statistics $T = \frac{a}{\sigma(a)}$, the Students' T distribution with $n - 2$ degrees of freedom. For $n = 46$ at the significance level $\alpha = 0.05$, the critical value $T_{\text{crit}} = 1.68$. We tested the H_0 hypothesis that the value of the analyzed statistic does not depend on supercluster richness against the H_1 hypothesis that it decreases with supercluster richness. From Table 5 we can conclude that only in the case of the η angle, the anisotropy decreases with the supercluster richness and is statistically significant on a significance level of 0.05.

4. Conclusions

In the present paper we investigated a sample of 43 rich Abell galaxy cluster belonging to a supercluster and containing at least 100 members in the considered area. We found that the orientation of galaxies in the analyzed cluster was not random. However, in contrast with the results of Godłowski et al. (2010), we detect that for our sample the alignment of galaxies does not depend on cluster richness. The differences between samples analyzed in these studies are as follows. In Godłowski et al. (2010), we analyzed a sample of 243 rich Abell galaxy clusters, while in the present paper we analyzed only subsamples of galaxies belonging to supercluster. Nevertheless, for both samples we observed that the distributions of analyzed angles P , δ_D and η , which specify the orientation of galaxies in space, are not random. We also found that the alignment decreases with supercluster richness, although the effect is statistically significant only for azimuthal angles (η angles). The results obtained, which include the dependence of galaxy alignment on cluster location inside or outside a supercluster as well as supercluster multiplicity, clearly support

Table 2: The theoretical (random) and observational values of statistics.

Test	Simulations				Observations	
	\bar{x}	$\sigma(x)$	$\sigma(\bar{x})$	$\sigma(\sigma(x))$	PA	
χ^2	34.9592	1.2843	0.0406	0.0287	38.772	1.574
$\Delta_1/\sigma(\Delta_1)$	1.2567	0.0983	0.0031	0.0022	1.797	0.148
$\Delta/\sigma(\Delta)$	1.8846	0.1027	0.0032	0.0023	2.339	0.148
C	-0.9750	0.8593	0.0274	0.0192	0.611	1.120
λ	0.7729	0.0392	0.0012	0.0009	0.932	0.057

Table 3: The results of the linear regression analysis: value of the analyzed statistics as a function of the cluster richness for clusters belonging to superclusters.

angle	χ^2	$\Delta_1/\sigma(\Delta_1)$	$\Delta/\sigma(\Delta)$	C	λ
	$a \pm \sigma(a)$	$a \pm \sigma(a)$	$a \pm \sigma(a)$	$a \pm \sigma(a)$	$a \pm \sigma(a)$
P	0.028 ± 0.039	-0.0004 ± 0.0037	-0.0029 ± 0.0037	0.027 ± 0.028	0.0004 ± 0.0014
δ	0.026 ± 0.037	-0.0008 ± 0.0023	0.0020 ± 0.0024	0.031 ± 0.032	0.0004 ± 0.0011
η	0.125 ± 0.040	0.0060 ± 0.0030	0.0082 ± 0.0028	0.112 ± 0.041	0.0018 ± 0.0009

Table 4: The statistical analysis: value of the analyzed statistics for different supercluster multiplicities.

angle	Test	$N = 4$	$N = 5 - 7$	$N = 8 - 10$
P	χ^2	43.30 ± 2.42	34.99 ± 2.11	36.65 ± 1.55
	$\Delta_1/\sigma(\Delta_1)$	1.99 ± 0.25	1.50 ± 0.16	1.89 ± 0.32
	$\Delta/\sigma(\Delta)$	2.57 ± 0.23	2.08 ± 0.18	2.42 ± 0.36
	C	2.53 ± 1.60	-0.99 ± 1.27	-0.37 ± 4.05
	λ	1.01 ± 0.08	0.81 ± 0.06	1.01 ± 0.21
δ_D	χ^2_c	54.52 ± 10.69	48.68 ± 4.57	89.07 ± 18.56
	$ \Delta_{11}/\sigma(\Delta_{11}) $	3.13 ± 0.63	2.76 ± 0.57	6.41 ± 0.84
	$\Delta_c/\sigma(\Delta_c)$	4.76 ± 0.72	4.40 ± 0.34	6.97 ± 1.09
	C_c	29.73 ± 9.48	22.53 ± 4.46	51.59 ± 16.36
	λ_c	2.22 ± 0.33	2.01 ± 0.13	3.39 ± 0.55
η	χ^2	83.60 ± 12.09	95.57 ± 9.74	43.01 ± 5.44
	$\Delta_1/\sigma(\Delta_1)$	5.43 ± 0.86	5.83 ± 0.71	2.02 ± 0.29
	$\Delta/\sigma(\Delta)$	6.30 ± 0.88	7.31 ± 0.66	3.19 ± 0.38
	C	49.31 ± 12.34	54.25 ± 10.50	5.26 ± 2.93
	λ	2.24 ± 0.28	2.37 ± 0.19	1.07 ± 0.13

Table 5: The results of linear regression analysis: value of the analyzed statistics as a function of supercluster multiplicity.

angle	χ^2	$\Delta_1/\sigma(\Delta_1)$	$\Delta/\sigma(\Delta)$	C	λ
	$a \pm \sigma(a)$	$a \pm \sigma(a)$	$a \pm \sigma(a)$	$a \pm \sigma(a)$	$a \pm \sigma(a)$
P	-1.093 ± 0.772	0.018 ± 0.074	0.001 ± 0.074	-0.249 ± 0.563	0.014 ± 0.029
δ	6.839 ± 2.937	0.527 ± 0.181	0.435 ± 0.195	4.282 ± 2.651	0.206 ± 0.126
η	-7.863 ± 3.553	-0.574 ± 0.255	-0.558 ± 0.256	-7.772 ± 3.668	-0.178 ± 0.078

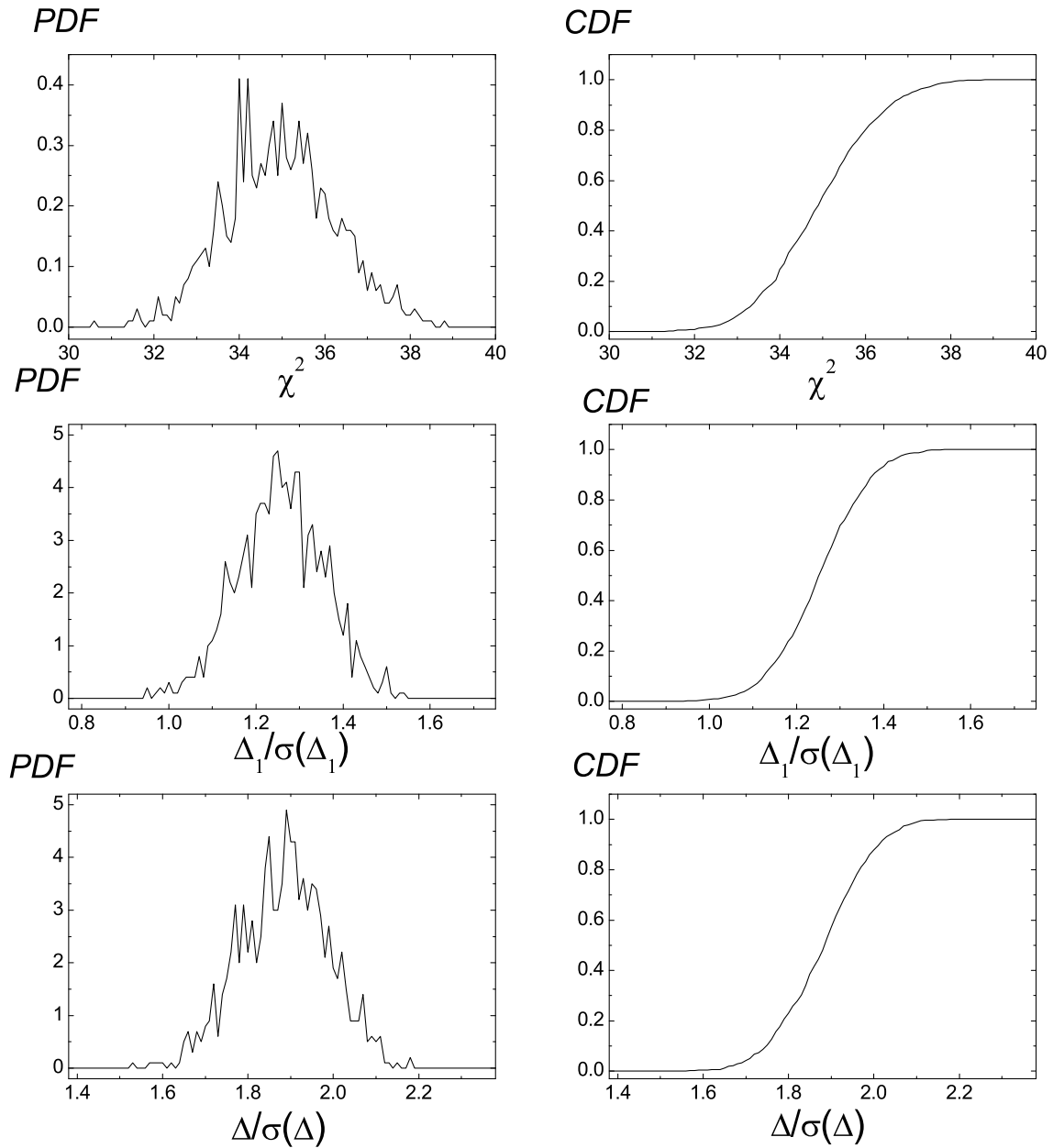


Figure 1: Probability density function (PDF, left panel) and cumulative distribution function (CDF, right panel) for statistics χ^2 , $\Delta_1/\sigma(\Delta_1)$ and $\Delta/\sigma(\Delta)$.

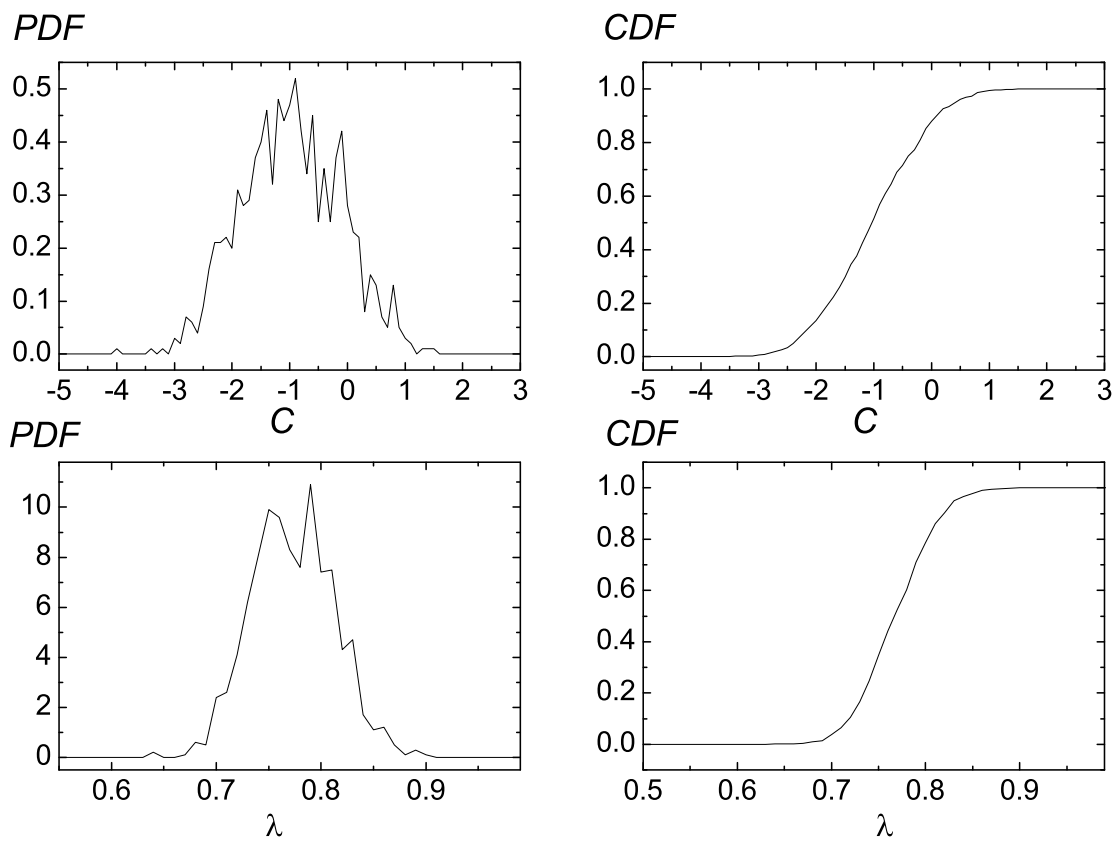


Figure 2: Probability density function (PDF, left panel) and cumulative distribution function (CDF, right panel) for statistics C and λ .

the influence of environmental effects on the origin of galaxy angular momenta. The problem of obtaining the angular momenta of galaxies in a structure is rather complicated since several mechanisms play roles. According to the major scenarios for galaxy formation, in some cases the angular momentum of galaxies results from local anisotropic collapse of protostructures, in others due from a tidal torque mechanism. Moreover, clusters can merge, introducing additional factors which influence the observed distribution of galaxy angular momenta. This suggests that environment played a crucial role in the origin of galaxy angular momentum. In a very simple and naive picture, if the alignment of galaxies is primordial, the strongest effect should be observed in small structures. In the present paper we analyzed only the sample very rich clusters. For final confirmation or rejection of this hypothesis, it is necessary to enlarge the analysis taking into account a sample of poorer clusters. Fortunately, our basic PF Catalogue (Panko & Flin, 2006) will allow us to perform such an analysis in the future.

Acknowledgements. This research has made use of the NASA Astrophysics Data System, and was partially supported by grant BS052 of Jan Kochanowski University (Kielce, Poland).

References

- Abell G.O., Corwin H.G., Jr., Olowin R.P.: 1989, *ApJS*, **70**, 1.
- Aryal B., Saurer W.: 2000, *A&A*, **364**, L97.
- Bower R.G., Benson A.J., Malbon R., Helly J., Frenk C.S., Baugh C.M., Cole S., Lacey C.G.: 2006, *MNRAS*, **370**, 645.
- Catelan P., Theuns T.: 1996 *MNRAS*, **282**, 436.
- Doroshkevich A.G.: 1973, *ApL*, **14**, 11.
- Flin P., Godłowski W.: 1986, *MNRAS*, **222**, 525.
- Flin P., Vavilova I.B.: 1996, *Proceedings of the 27th Meeting of the Polish Astronomical Society, held in Poznan, September 12, 1995*, edited by Marek J. Sarna and Peter B. Marks, p.63.
- Godłowski W.: 1993, *MNRAS*, **265**, 874.
- Godłowski W.: 1994, *MNRAS*, **271**, 19.
- Godłowski W.: 2011, *Acta Physica Polonica B*, **42**, 2323.
- Godłowski W.: 2012, *ApJ*, **747**, 7.
- Godłowski W., Flin P.: 2010, *ApJ*, **708**, 902.
- Godłowski W., Ostrowski M.: 1999, *MNRAS*, **303**, 50.
- Godłowski W., Panko E., Flin P.: 2011, *Acta Physica Polonica B*, **42**, 2313, Paper II.
- Godłowski W., Piwowarska P., Panko E., Flin P.: 2010, *ApJ*, **723**, 985, Paper I.
- Hawley D.I., Peebles P.J.E.: 1975, *AJ*, **80**, 477.
- Jones B., van der Waygaert R., Aragon-Calvo M.: 2010 *MNRAS*, **408**, 897.
- Kindl A.: 1987, *AJ*, **93**, 1024.
- Lee J., Pen U.: 2002, *ApJ*, **567**, L111.
- Li, Li-Xin.: 1998, *Gen. Rel. Grav.*, **30**, 497.
- Lilliefors H.W.: 1967, *J. Am. Stat. Assoc.*, **62**, 399.
- Navarro J.F., Abadi M.G., Steinmetz M.: 2004, *ApJ*, **613**, L41.
- Panko E.: 2011, *Baltic Astr.*, **20**, 131.
- Panko E., Flin P.: 2006, *Journ. Astro. Data* **12**, 1.
- Paz D.J., Stasyszyn F., Padilla N.D.: 2008, *MNRAS* **389**, 1127.
- Peebles P.J.E.: 1969, *ApJ*, **155**, 393.
- Shandarin S.F.: 1974, *Sov. Astr.* **18**, 392.
- Silk J., Efstathiou G.A.: 1983, *The Formation of Galaxies, Fundamentals of Cosm. Phys.* **9**, 1.
- Smargon A., Mandelbaum R., Bahcall N., Niederste-Ostholt M.: 2011, arXiv:1109.6020.
- Sunyaev A.R., Zeldovich Ya.B.: 1972 *A&A*, **20**, 189.
- Trujillo I., Carretro C., Patiri S.G.: 2006, *ApJ* **640**, L111.
- Ungruhe R., Seitter W., Durbeck H.: 2003, *Journ. Astr. Data*, **9**, 1.
- Varela J. Rios J.B., Trujillo I.: 2011, astro-ph 1109.2056.
- Vavilova I.B.: 1999, *Kinematics Phys. Celest. Bodies*, **15**, 69.
- Wesson P.S.: 1982, *Vistas Astron.*, **26**, 225.
- Zeldovich B.Ya.: 1970, *A&A*, **5**, 84.

A CURRENT APPLICATION OF THE METHODS OF SECULAR AND STATISTICAL PARALLAX

D.G. Turner

Department of Astronomy and Physics, Saint Mary's University
Halifax, Nova Scotia B3H 3C3, Canada, *turner@ap.smu.ca*

ABSTRACT. The methods of secular and statistical parallax for homogeneous groups of Galactic stars are applied in a practical (classroom) exercise to establish the luminosity of bright B3 V stars. The solar motion of 20 km s^{-1} relative to group stars exceeds their random velocities of $\pm 10 \text{ km s}^{-1}$, a condition adopted for preference of secular parallax to statistical parallax. The group parallax of $\langle \pi_{\text{ups}} \rangle = 5.81 \pm 0.83 \text{ mas}$ and derived luminosity $\langle M_V \rangle = -0.98 \pm 0.33$ for B3 V stars from upsilon components of proper motion should be close to the true value. The weighted mean *Hipparcos* parallax of $\langle \pi_{\text{Hip}} \rangle = 5.75 \pm 0.27 \text{ mas}$ for the same sample, and implied luminosity of $\langle M_V \rangle = -1.00 \pm 0.15$, confirm the secular parallax solution. Both solutions are close to $M_V = -0.83$ for ZAMS stars of the same type, implying that Malmquist bias in the selection of stars mainly accounts for the presence of unresolved binaries, slightly evolved objects, and rapidly rotating stars in the sample.

Key words: methods: statistical — parallaxes — stars: fundamental parameters.

1. Introduction

The method of statistical parallax was important to Galactic astronomers of the last century, but seems of minor interest today, most current Galactic research involving instead the astrophysics of galaxies like the Milky Way. Yet there are still occasions where the technique can be involved in current problems in Galactic astronomy, so the author continues to instruct students in the methodology for courses in Galactic astronomy taught at his home institution. The problem outlined here is used as a learning exercise for application of the technique, but proves to be of more than just pedagogical interest since it addresses current questions regarding luminosity calibrations.

2. Statistical and Secular Parallaxes

The technique involves the use of proper motions

and radial velocities to establish the space motion of a group of stars relative to the Sun, and is explained very well by Mihalas & Routly (1968), Mihalas & Binney (1981), and Scheffler & Elsässer (1988). The basic premise is that the Sun's motion relative to nearby stars in the Galaxy creates a baseline of observation, similar in nature to that created by the Earth's annual orbital motion around the Sun, from which one can triangulate the distances to stars from their temporal angular displacements, namely their proper motions across the sky. The angular motions of nearby stars resulting from their different distances from the Sun are often masked by individual space motions and observational uncertainties, but it is possible to evaluate an average for an entire homogeneous group once the Sun's motion relative to the group is measured (in km s^{-1}). The individual space motions of group stars are not known *a priori*, which is why the technique devolves to a statistical approach that yields a mean parallax for the group from their proper motions and radial velocities.

The first step in any study involving statistical parallax is to isolate a group of stars with a common set of parameters and then establish the Sun's motion relative to the group. Radial velocities can be used for the latter purpose, as outlined by Mihalas & Routly (1968) and Mihalas & Binney (1981), provided the stars in the group are randomly distributed on the sky. Failing that, they may be sufficiently randomly distributed in Galactic longitude to establish a space motion for the group reliably, at least for motion in the Galactic plane.

There are two components of any star's proper motion: one reflecting the Sun's motion relative to the star, denoted as the upsilon υ component, and the other perpendicular to it reflecting solely the star's space motion, denoted as the tau τ component. The former is dominated by the Sun's motion relative to the group of stars, while the latter is presumably random for a large enough sample. The two components can be calculated from the direction of the solar motion relative to the group, the solar apex, denoted by right ascension A and declination D , and the observed proper motion components, μ_α in right ascension, and μ_δ in declination. Three equations are needed to solve

for the position angle ψ and angular distance λ of each star from the direction to the solar apex since there are ambiguities in the sine function for angles of 0° – 180° . The upsilon and tau components of proper motion for each star then follow from the equations of spherical and Cartesian geometry:

$$v = \mu_\alpha \cos \delta \sin \psi - \mu_\delta \cos \psi$$

$$\tau = \mu_\alpha \cos \delta \cos \psi + \mu_\delta \sin \psi.$$

The secular parallax is then calculated from a knowledge of the Sun's motion v_\odot relative to the group:

$$\langle \pi \rangle = \frac{4.74 \langle v \sin \lambda \rangle}{v_\odot \langle \sin^2 \lambda \rangle}$$

where the triangular brackets on both sides of the equation represent straight averages. The statistical parallax is calculated differently using:

$$\langle \pi \rangle = \frac{4.74 \langle |\tau| \rangle}{\langle |v_R + v_\odot \sin \lambda| \rangle}$$

involving the use of absolute values for tau and radial velocity difference. Secular parallaxes are predicted to work best when the solar motion dominates the group random velocities, and statistical parallaxes otherwise.

Weights assigned to individual stars in the method of secular parallax vary according to the sine of a star's angular distance from the solar apex for the group, in order to maximize the influence of those stars displaying the largest degree of angular displacement produced by the Sun's motion. An alternate version using the maximum likelihood technique was developed by Clube & Dawe (1980a,b). For classroom exercises the standard methodology provides the most direct approach to solving practical problems, and is the technique followed here.

3. A Practical Example: B3 V Stars

Class exercises are normally chosen to be completed within a time span not exceeding a week or two, which limits the quantity and type of data that can be analyzed. For the present purpose an exercise was developed to find the mean absolute magnitude of B3 V stars using the methods of secular and statistical parallax in conjunction with information available from *The Bright Star Catalogue* (Hoffleit & Jaschek 1982). There are 88 bright stars classified as B3 V that have coordinates, proper motions, and radial velocities summarized by Hoffleit & Jaschek (1982). For the exercise the author also calculated unreddened visual magnitudes V_0 by removing small amounts of reddening and extinction for affected stars. The exercise was first developed in an era prior to the general availability of high-speed computers, so ease of calculation was originally a concern. The availability of *The Hipparcos and*

Tycho Catalogues (ESA 1997) in recent years has also provided an improved set of proper motions, as well as absolute parallaxes that allow one to test the results.

An essential step in deriving secular and statistical parallaxes is to establish the solar motion relative to the group, since the resulting values of A and D are necessary for calculating the angles λ and ψ for each star in the group, while v_\odot is required for solving the parallaxes. Omission of that step greatly reduces the accuracy of the solutions, since one must rely on parameters derived for quite different stars to obtain comparable values. For the sample of B3 V stars considered here, solutions for the solar motion relative to the group are given in Table 1 for the epochs 1900.0 and 2000.0. Proper motion data for the former were taken from Hoffleit & Jaschek (1982), and for the latter from ESA (1997). The radial velocities are those cited by Hoffleit & Jaschek (1982). Differences between solutions in v_\odot for the two epochs are the result of rounding errors in the calculations.

Table 1: Parallax Solutions for B3 V Stars.

Parameter	Epoch (1900)	Epoch (2000)
A (solar motion)	$265^\circ.384$	$266^\circ.145$
D (solar motion)	$43^\circ.112$	$43^\circ.071$
v_\odot (km s $^{-1}$)	20.0465	20.0466
$\langle V_0 \rangle$	5.20 ± 0.12	5.20 ± 0.12
$\langle \pi_{\text{ups}} \rangle$ (mas)	6.07 ± 0.91	5.81 ± 0.83
$\langle \pi_{\text{tau}} \rangle$ (mas)	5.34 ± 0.58	4.42 ± 0.51
$\langle \pi_{\text{Hip}} \rangle$ (mas)	...	5.20 ± 0.38
$\langle \pi_{\text{Hip}} \rangle_{\text{wgt}}$ (mas)	...	5.75 ± 0.27
$\langle M_V \rangle_{\text{ups}}$ (B3 V)	-0.88 ± 0.34	-0.98 ± 0.33
$\langle M_V \rangle_{\text{tau}}$ (B3 V)	-1.16 ± 0.26	-1.57 ± 0.27
$\langle M_V \rangle_{\text{Hip}}$ (B3 V)	...	-1.22 ± 0.19
$\langle M_V \rangle_{\text{Hipwgt}}$ (B3 V)	...	-1.00 ± 0.15

The calculation of mean secular and statistical parallaxes follows from the equations given previously, with solutions given in Table 1 for upsilon ($\langle \pi_{\text{ups}} \rangle$) and tau ($\langle \pi_{\text{tau}} \rangle$) components, as well as for revised *Hipparcos* parallaxes (van Leeuwen 2007). The desired mean absolute magnitude follows from the standard formula: $\langle M_V \rangle = \langle V_0 \rangle + 5 \log \langle \pi \rangle + 5$. In the case of revised *Hipparcos* parallaxes, mean and weighted mean parallaxes were calculated for the sample, with weights assigned according to the cited absolute uncertainty in the parallax (not the relative uncertainty), and the resulting absolute magnitude was calculated as both a straight average and a weighted average, with the uncertainty in the mean dereddened magnitude for the stars included. The observed scatter in the absolute magnitudes inferred from individual *Hipparcos* parallaxes is $\pm 0^m.77$, with values of M_V ranging from $+0.10$ to -4.05 .

Information about the luminosities of B3 V stars has also been established from older parallaxes and membership in open clusters, as well as from zero-

age main sequence (ZAMS) calibrations. For example, the ZAMS of Turner (1976) implies $M_V = -0.83$ for stars with the intrinsic colour of B3 V stars, $(B-V)_0 = -0.20$, and spectral type calibrations for B3 V stars imply $M_V = -1.5$ (Turner 1980) or $M_V = -1.7$ (Blaauw 1963; Keenan 1963).

The Sun's 20 km s^{-1} motion relative to the sample of B3 V stars exceeds the random motions of the stars relative to one another of $\pm 10 \text{ km s}^{-1}$, so the secular parallax $\langle \pi \rangle_{\text{ups}}$ should be closer to the true parallax than the statistical parallax $\langle \pi \rangle_{\text{tau}}$. Malmquist bias is expected to be important for the sample, given that *The Bright Star Catalogue* is magnitude limited, thereby sampling preferentially the most luminous stars of spectral type B3 V. In that case the derived luminosity from secular parallax should be greater than the true mean value for the class. Interestingly enough, the secular parallax produces a luminosity that is only $0^{\text{m}}.15$ more luminous than the value expected for ZAMS stars, but $\sim 0^{\text{m}}.6$ less luminous than standard literature values for class V dwarfs. If there are unresolved binaries, slightly evolved objects, or rapidly rotating stars in the sample, then the luminosity derived from the secular parallax is in excellent agreement with the ZAMS, but not class V, value. It appears that Malmquist bias in this instance actually accounts for the presence of unresolved binaries, slightly evolved objects, and rapidly rotating stars in the sample.

Spectral type- M_V calibrations make use of spectral classifications of mixed quality in the literature. Stars identified spectroscopically as B3 V may therefore include subgiants and slightly evolved objects. That is not the case for spectral classifications in *The Bright Star Catalogue*, which are generally of high quality. The small discrepancy between the value of M_V derived for B3 V stars using secular parallax and those in published calibrations is therefore not unusual.

The weighted mean *Hipparcos* parallax for the sample, $\langle \pi_{\text{Hip}} \rangle_{\text{wgt}} = 5.75 \pm 0.27 \text{ mas}$, confirms the secular parallax, $\langle \pi_{\text{ups}} \rangle = 5.81 \pm 0.83 \text{ mas}$. The mean luminosity for sample B3 V stars, $\langle M_V \rangle = -1.00 \pm 0.15$, therefore coincides closely with the secular parallax value, $\langle M_V \rangle = -0.98 \pm 0.33$. An unweighted average for *Hipparcos* parallaxes gives a value $\sim 0^{\text{m}}.2$ more luminous, implying that the smallest parallaxes are associated with the largest cited uncertainties. That is not entirely self-evident, since some stars with the largest parallaxes in the sample actually have relatively large cited uncertainties.

An identical conclusion was found for Cepheid variables studied by *Hipparcos* (Turner 2010), namely Cepheids of small parallax are typically associated with large cited uncertainties. That is why researchers prefer stars with small relative parallax uncertainties for calibration purposes. For *Hipparcos* parallaxes, however, it appears that many stars with small parallax uncertainties also deviate significantly, i.e. by

several σ , from the true parallax, in other words the cited precision may be overstated (Turner 2010). The methods of secular and statistical parallax may therefore continue to serve as useful tools for calibration purposes.

4. Discussion

Presented here is an application of secular and statistical parallax to the study of a homogeneous group of Galactic stars, in a manner useful for classroom demonstrations or research assignments. The sample considered here consists of 88 stars in *The Bright Star Catalogue* classified as B3 V. The solution generates a luminosity for the stars close to the value expected for a selection of ZAMS stars of that spectral type contaminated by unresolved binaries, slightly evolved objects, and rapidly rotating stars. The expected Malmquist bias applying to the sample selection appears to account implicitly for the latter effect. The result is confirmed by *Hipparcos* parallaxes for stars in the same sample, a rare instance where alternate solutions can be used to check the consistency of results from secular and statistical parallax.

The numerical simplicity of the method stands in contrast to more complicated versions, for example the maximum likelihood technique developed by Clube & Dawe (1980a,b). It may therefore be possible to extend the type of class exercise posed here to problems of greater astronomical interest, for example the luminosities of important distance calibrators such as the Cepheids discussed by Clube & Dawe (1980b).

References

- Blaauw, A.: 1963, *Basic Astronomical Data*, ed. K.Aa. Strand, (Univ.Chicago Press: Chicago), p. 383.
 Clube, S.V.M., Dawe, J.A.: 1980a, *MNRAS*, **190**, 575.
 Clube, S.V.M., Dawe, J.A.: 1980b, *MNRAS*, **190**, 591.
 ESA: 1997, *The Hipparcos and Tycho Catalogues*, ESA SP-1200 (ESA: Noordwijk).
 Hoffleit, D., Jaschek, C.: 1982, *The Bright Star Catalogue*, (Yale Univ. Obs.: New Haven).
 Keenan, P.C.: 1963, *Basic Astronomical Data*, ed. K.Aa. Strand, (Univ.Chicago Press: Chicago), p. 78.
 Mihalas, D., Routly, P.M.: 1968, *Galactic Astronomy*, (W.H. Freeman & Co.: San Francisco).
 Mihalas, D., Binney, J.: 1981, *Galactic Astronomy: Structure and Kinematics*, (W.H. Freeman & Co.: New York).
 Scheffler, H, Elsässer: 1988, *Physics of the Galaxy and Interstellar Matter*, (Springer-Verlag: Berlin).
 Turner, D.G.: 1976, *AJ*, **81**, 97.
 Turner, D.G.: 1980, *ApJ*, **240**, 137.
 Turner, D.G.: 2010, *Ap&SS*, **326**, 219.
 van Leeuwen, F.: 2007, *A&A*, **474**, 653.

INVESTIGATION OF THE PHOTOMETRIC SYSTEM OF CCD-PHOTOMETER AND THE AZT-3 TELESCOPE

S.N. Udovichenko

Astronomical observatory, Odessa National University, T.G. Shevchenko Park, Odessa
Ukraine, *astro@paco.odessa.ua*

ABSTRACT. The investigation of the photometric system consisting from photometer with CCD detector Sony ICX429ALL, VRI filters and the AZT-3 telescope was carried out. The transformation coefficients from the instrumental values of magnitudes and color indices to the Johnson-Cousins system in the VRI passbands are presented. The instrumental system of telescope and standard system have satisfactory agreement.

Key words: Photometry, transformations coefficients

1. Introduction

The 48 cm reflecting telescope of Astronomical observatory Odessa National University AZT-3 started to operate in astronomical station near Odessa in 1967. The telescope has four changeable operational modes: direct focus, the Cassegrain, Newton and the the Coude focuses. The photometer was mounted in the Newtonian focus (aperture ratio 1: 4.5, field of view 15') in hermetic chamber with thermoelectric (Peltier) cooler, which provide a temperature difference between the CCD detector and the environment of about $-30^{\circ}\text{C} - -40^{\circ}\text{C}$. The filters turret contains three windows with filters corresponding to the VRI passbands of the Johnson-Cousins system (Bessell, 1990). The filters were made from special sort of domestic glass and the transmission curves of the filters are close to the passbands of the standard system. The photometer had been successfully used for observations of variable stars and other celestial objects. After the addition new filters it was necessary to examine the instrumental photometric system of the telescope. The transmission of standard photometric UBVRI Johnson-Cousins system and CCD detector ICX429ALL (from Sony CCD Instruction Manual) is shown on Fig. 1.

2. Reduction of images

CCD images contain the both information about sky objects and noise. The noise consists from a

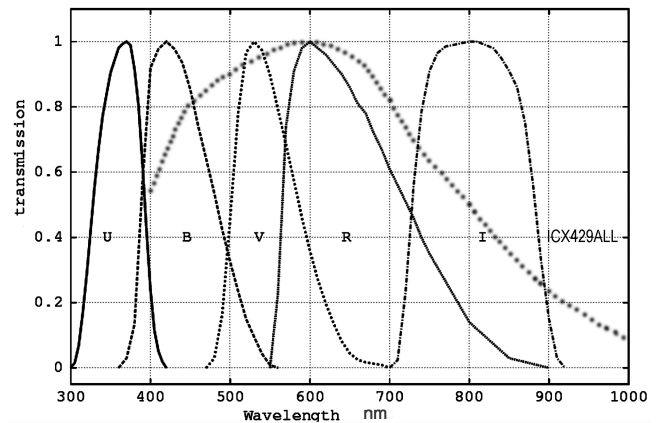


Figure 1: The transmission of standard photometric UBVRI Johnson-Cousins system and CCD detector ICX429ALL.

sky background, readout noise and thermal noise. Besides, there is a photometric error of a field which appear as a result of not uniform sensitivity of pixels and the various optical effects dispersion of light in a telescope, optical filters and the chamber. The standard procedure was used to correct each image by division on a "flat field", which obtained by measurement of the twilight sky during evening or morning time. The average image "master-flat" has been calculated from 10-15 individual images. Also the average "master-dark" was used for subtraction for the same temperature and time, as images of standard stars. The exposure time was choosing to get the relation a signal/noise 100-300 and accuracy of photometry not worse 0.01 - 0.02^m.

3. Determination of transformation coefficients

The reduction of the CCD frames were carried out using the MUNIPACK software (Motl, 2003-2012). The method of aperture photometry was used. It de-

Table 2: List of standard stars.

Number of Landolt's catalog	RA (J2000)	Dec (J2000)	V	B-V	U-B	V-R	R-I
104 456	12:42:54	-00:32:06	12.362	0.622	0.135	0.357	0.337
104 457	12:42:54	-00:28:49	16.048	0.753	0.522	0.484	0.490
104 460	12:43:03	-00:28:21	12.886	1.287	1.243	0.813	0.693
104 461	12:43:07	-00:32:21	9.705	0.476	-0.030	0.289	0.290
104 350	12:43:15	-00:33:21	13.634	0.673	0.165	0.383	0.353
104 484	12:44:20	-00:30:57	14.406	1.024	0.732	0.514	0.486
104 485	12:44:24	-00:30:16	15.017	0.838	0.493	0.478	0.488
104 490	12:44:33	-00:25:53	12.572	0.535	0.048	0.318	0.312
107 599	15:39:09	-00:14:28	14.675	0.698	0.243	0.433	0.438
107 601	15:39:14	-00:13:26	14.646	1.412	1.265	0.923	0.835
107 602	15:39:19	-00:15:29	12.116	0.991	0.585	0.545	0.531
107 626	15:40:06	-00:17:28	13.468	1.000	0.728	0.600	0.527
107 627	15:40:08	-00:17:22	13.349	0.779	0.226	0.465	0.454
107 484	15:40:17	-00:21:13	11.311	1.237	1.291	0.664	0.577
107 636	15:40:41	-00:14:54	14.873	0.751	0.121	0.432	0.465
107 639	15:40:45	-00:17:11	14.197	0.640	-0.026	0.399	0.404
107 640	15:40:50	-00:16:48	15.050	0.755	0.092	0.511	0.506
HD 89904	10:17:21	+34:24:47	5.878	0.15	-	0.075	-
HD 90040	10:18:24	+34:13:28	5.500	1.18	-	0.602	-

termines a brightness of a stellar object by integrating a signal in a small area on a frame. The point spread function that represents the spatial distribution of the signal from stellar object is rotationally symmetric. The background has been estimated from neighboring pixels as another "aperture" that has an annular shape. The readout from stars with subtracted background convert to instrumental magnitude m_0 using the Pogson's law:

$$m_0 = -2.5 \lg(I/I_0), \quad (1)$$

where I_0 is a signal from an object of reference flux F_0 . The ratio between flux and signal is not known, it is lawful to choose any reference signal I_0 , providing a fact that only a difference of magnitude between two objects make sense - the difference is independent of choice of a reference I_0 . In the C-Munipack software, the reference flux was set to 10^{10} . As a point of view of the photometer coverage small quantity of the stars, they are practically on equal air mass, and calculation of extinction for difference air mass inside the image not made, but only for a whole of image.

The relation between magnitudes and colors in instrumental and standard systems (Hardie, 1967) is possible to write, as:

$$M = m_0 + \zeta_m + \epsilon C, \quad C = \zeta_c + \mu c_0, \quad (2)$$

where M , C – magnitudes and color indices in standard system, m_0 , c_0 – magnitudes and color indices in instrumental system, ϵ , μ – transformation coefficients, ζ_m , ζ_c – constants of zero-point.

Stars were measured during several nights and found an average value. For research of photometric system 19 standard stars from catalog was used, which list is presented in Table 2 (Landolt, 1992). The transformation coefficients are calculated by linear least squares method and presented in Table 1.

Table 1: Transformation coefficients.

Passband	ζ_m	ϵ
V_c	-1.293 ± 0.010	0.014 ± 0.039
R_c	-1.951 ± 0.009	0.021 ± 0.055
I_c	-4.628 ± 0.003	0.029 ± 0.019
Color indices	ζ_c	μ
V-R	0.501 ± 0.014	0.956 ± 0.076
R-I	0.472 ± 0.007	0.984 ± 0.048

The dependence of the magnitudes in standard and instrumental systems in filter V and its approximation of the linear function is shown on Fig. 2a. The inclination coefficient equal 1.0085 ± 0.0084 , that indicate a good agreement between instrumental and standard systems in the passband V. The same dependencies were obtained in passbands R and I and their values are not presented in this paper.

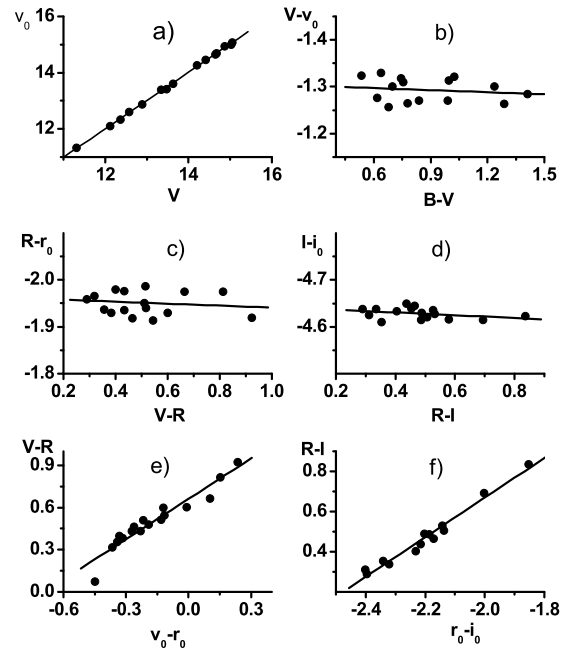


Figure 2: a) Dependence of the magnitudes in standard and instrumental systems in filter V_c ; b,c,d) Dependence of the magnitude differences V_c , R_c , I_c on the color indices B-V, V-R, R-I; e,f) Dependence of the color indices V-R, R-I in standard and instrumental systems $v-r$, $r-i$

The dependencies of the magnitude differences V, R, I on the color indices B-V, V-R, R-I and their approximations of the linear function are presented in Fig. 2(b,c,d). All dependencies have a small positive slope, and differences do not exceed 0.05^m . The dependencies of the color indices V-R, R-I in standard and instrumental systems $v-r$, $r-i$ have a positive gradient, and linear coefficients are close to 1. In general, the instrumental system of telescope and standard system have satisfactory agreement. The transformation coefficients for magnitudes and color indices from the instrumental to the standard system of the VRI passbands are determined by measurements of photometric standards.

References

- Bessell M.S.: 1979, *PASP*, **91**, 589.
 Bessell M.S.: 1990, *PASP*, **102**, 1181
 Hardie R.H.: 1967, In book: "Astronomical techniques", Edited by Hiltner, Publish."Mir".
 Landolt A.U.: 1992, *Astron. J.*, **104.**, 340.
 Motl D.: 2003-12, <http://c-munipack.souceforge.net>

SOME EVOLUTIONARY ASPECTS OF THE BINARY STELLAR SYSTEMS CONTAINING NEUTRON STAR

Oleg O. Ulyanov ¹, Sergei M. Andrievsky ², Vera F. Gopka ²,
Angelina V. Shavrina ³

¹ Institute of Radio Astronomy of NASU, Krasnoznamennaya str. 4, Kharkov 61002, Ukraine

² Department of Astronomy and Astronomical Observatory, Odessa National University, Shevchenko Park, Odessa, 65014, Ukraine

³ Main Astronomical Observatory of NASU, Zabolotnogo str. 27, Kyiv 03680, Ukraine

ABSTRACT. The obvious lack of the binary stellar systems that contain neutron stars (NS) is observed at present. Partly it is caused by the fact that it is very difficult to detect neutron star in a binary system if this relativistic component does not manifest itself as a radio pulsar. Among 1879 pulsars that are listed in the ATNF pulsar catalogue, only 141 pulsars are known to be the companions in binary systems. Only 81 objects having median mass estimation of more than $0.2 M_{\odot}$ constitute the binary systems with pulsars. Nevertheless, such systems should be much more numerous and their investigation is of the great interest because thier structure and evolution can certainly help in our understanding of many unique properties that are seen in some stars.

Introduction

Some difficulties of a detection of the NS as sources of the radio emission (<http://www.atnf.csiro.au/research/pulsar/psrcat/>) are discussed in Refs. (McLaughlin et al., 2006; Kondratiev et al., 2008; Kondrattiev et al., 2009; Malofeev et al., 2007; Zakharenko et al., 2010). Analysis of the different stages of the close binary system evolution with a NS, as one of the companion stars, shows that at the early stage of this evolution the ultra-relativistic electron-positron plasma produced and ejected by NS can hit the atmosphere gas of its companion normal star. At the same time, an usual stellar wind of the normal star will eventually screen NS magnetic field. During some period both winds from NS and normal star will create sources of X-ray emission located at the surfaces of both companions.

The detection of the annihilation line at 511 keV from such systems could be considered as observed manifestation of the above mentioned interaction between NS and normal star in the binary system, in

addition to the detection of X-ray radiation. An appearance of the chemical composition anomalies in the companion star atmosphere can also be possible in this case.

There are papers (Tutukov et al., 1985; Iben et al., 1997; Fedorova & Tutukov, 1994; Fedorova & Tutukov, 1992; Fedorova, 1997) in which two most probable evolutionary scenarios are proposed. The first scenario is connected with an expansion of the donor under the action of the X-ray and gamma-ray radiation generated by the NS (acceptor) (Fedorova, 1997). In this scenario, the generation of X-ray and gamma-ray radiation by the NS is a result of accretion of the wind of a companion star. The expansion of the upper layers of the donor in this model is caused by the energy absorption of the NS X-ray and gamma-radiation in the relatively deep layers of the donor. This model implies that donor fills its entire Roche lobe and its material is lost through the first Lagrangian point.

According to this scenario, under the influence of the hard radiation emitted by NS, the donor (companion normal star) passes through the cyclic stages of the orbital period change. At the same time, as a whole, the orbital period decreases, similarly to that as this occurs in cataclysmic binary stars (Fedorova & Tutukov, 1994; Fedorova & Tutukov, 1992; Fedorova, 1997).

Moreover, this scenario predicts the secular increase of the semi-major axis due to an increase of the Roche lobe radius of the donor, and corresponding increase of the mass exchange rate. The most contrasting manifestation of this effect should be observed in the range of the hard radiation fluxes from 10^{10} to 10^{12} $erg/(cm^2 sec)$, and for the range of the donor masses from 0.1 to $2.0M_{\odot}$. This process must occurs in the so-called Jeans mode (Gopka et al., 2007), when for a long time the conditions $a_m \cdot (M_1 + M_{NS}) = const$ are satisfied, where a_m is the size of the semi-major axis, M_1 is the mass of the donor, M_{NS} is the mass of the NS (acceptor).

The second scenario describes evolutionary evaporation of the donor due to the presence of the so-called induced stellar wind. In this case, it is assumed that the hard radiation of acceptor heats the relatively thin upper layers of the donor, which have the low density. Cooling in this scenario is achieved due to an induced stellar wind that leads to the gradual evaporation of the donor. In contrast to the first scenario, in this case the size of the semi-major axis of the binary system will decrease with a time. At the early stages of evolution, this decrease is caused by the loss of the binary system moment of inertia due to the stellar wind. However, in the case of an extremely close binary system the gravitational radiation losses must play a more significant role. The qualitative analysis of the interaction in the close binary system with a young NS, as one of the components (Gopka et al., 2007; Gopka et al., 2010; Gopka et al., OAP-20, 2007; Gopka et al., 2008), shows that at the early stage of this evolution heating of the upper atmosphere of the companion can be achieved not only due to the NS hard radiation, but also due to its ultra-relativistic electron-positron plasma ejection. In this case, plasma ejected by NS can hit the atmosphere layers of the companion star. The depth of the heating is supposed to be not uniform. Such an ununiformity can be connected with a concrete geometry of the magnetic field in the donor atmosphere (Ulyanov, 2010). For example, as far as the synchrotron energy losses are proportional to the component of the magnetic field perpendicular to the charge flow, zones near the magnetic poles will be heated at larger depths compared to other zones of the donor atmosphere. Let us note that ionization will be the basic source of energy loss for the ultra-relativistic electrons and positron, which have relatively low kinetic energies (Ginzburg, 1979). These losses will occur in the upper and relatively thin layers of a companion star (Ulyanov, 2010).

Detailed analysis of different types of the losses of the ultra-relativistic electron-positron plasma in the companion atmosphere was performed in (Ulyanov, 2010). The losses caused by the inverse Compton effect, that takes place near the companion (because of an interaction of the electron-positron ultra-relativistic plasma with optical photons), are not essential in comparison with other basic types of the energy losses (Ulyanov, 2010; Ginzburg, 1979). During this period of binary system evolution both winds create the sources of X-ray radiation on the surfaces of companion stars. As it was already mentioned, observational manifestation of such an interaction (besides the X-ray radiation) might be detection of the annihilation line at 511 keV (Ulyanov, 2010; Kontorovich et al., 2010). An appearance of the chemical anomalies in the atmosphere of the companion is also possible (for instance, some lines of the unstable radioactive isotopes were registered in spectra of some stars) (Gopka et al., 2005; Gopka et al., 2008).

An interaction of two objects in the system containing NS can lead to the gradual screening of the NS magnetic field, and corresponding weakening of the ultra-relativistic plasma flow. This may cause the "switch off" of the X-ray and gamma-ray sources of radiation in the atmosphere of the normal companion star. At the same time, X-ray emission from the NS surface can become stronger. Further evolution strongly depends on the diffusion of the NS magnetic field through the acquired accretion crust.

Observation Data

Let us examine the observational facts available at present that characterize evolution of the binary systems which contain NS.

There is ATNF catalogue (<http://www.atnf.csiro.au/research/pulsar/psrcat/>), where important properties are gathered for all pulsars. In this catalogue, the listed pulsars are the members of binary systems with primary companions of different types. In fact these are close binary systems. After examining of the whole amount of available data in ATNF catalogue, one can make the following conclusions:

- 1) in the binary systems the secular decrease of the magnetic field strength on the pulsar surface is observed (Fig. 1.);
- 2) the well known effect of the evolutionary decrease of the pulsar rotation period is observed;
- 3) the general stabilization of the pulsar kinematic parameters connected with the decreasing of the magnitude of \dot{P} and with an increase of the so-called characteristic age $Age = P/(2\dot{P})$, (where Age is characteristic age of pulsar, P is the period of the rotation of NS around its own axis, \dot{P} is the first-order derivative of the P) is observed (Fig. 2.);
- 4) on average, for the lower masses of the normal companions, the decrease of the semi-major axis is observed (excluding the companion mass range from $0.1M_{\odot}$ to $2M_{\odot}$) (Fig. 3.);
- 5) the mass decrease of the normal companion as a function of an increase of the pulsar characteristic age is observed (Fig. 4.).

Possible Interpretation of the Observation Data

It is easy to interpret the first three dependences mentioned above (items 1-3 and Fig. 1-2. The secu-

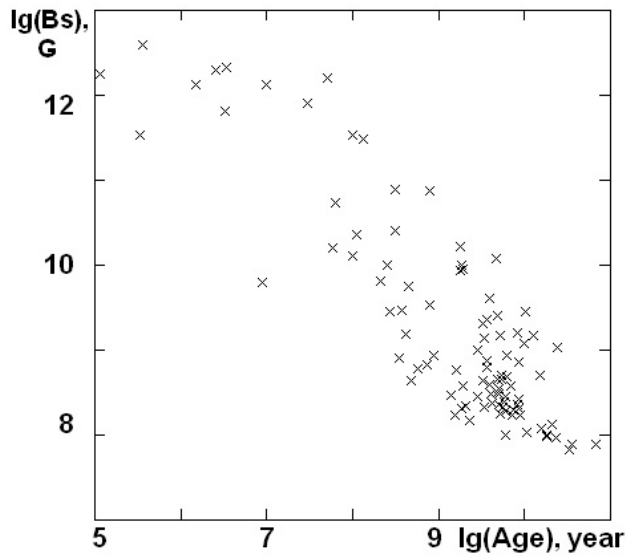


Figure 1: Distribution of the magnitude of the surface strength of magnetic field (B_s) of pulsars in binary systems as a function of their characteristic ages ($Age = \tau$).

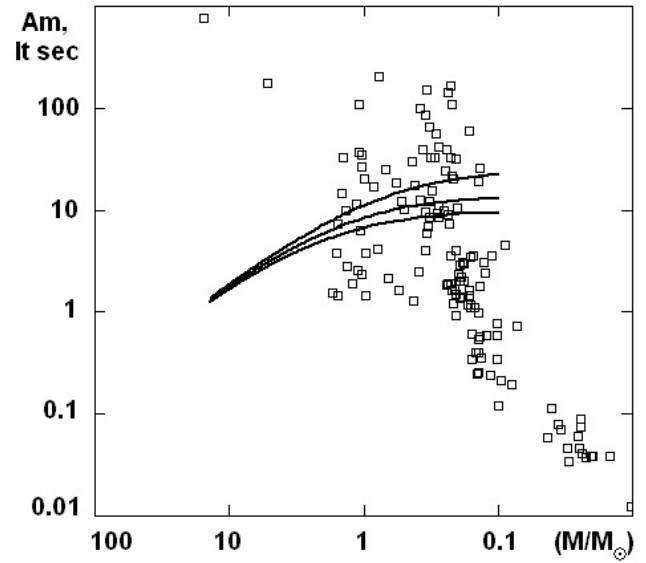


Figure 3: Distribution of the magnitude of the semi-major axis of the binary systems (a_m) depending on the median mass of the normal companions. Solid lines illustrate qualitative behaviour under the Jeans mode conditions corresponding to $0.8M_\odot$, $1.4M_\odot$, $2.0M_\odot$ pulsar masses (respectively from the top to bottom).

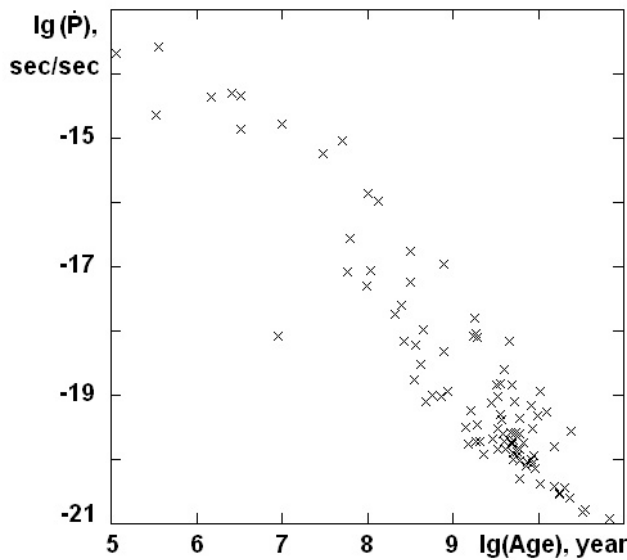


Figure 2: Distribution of the first derivatives for the pulsar rotation periods (\dot{P}) as a function of pulsar characteristic ages.

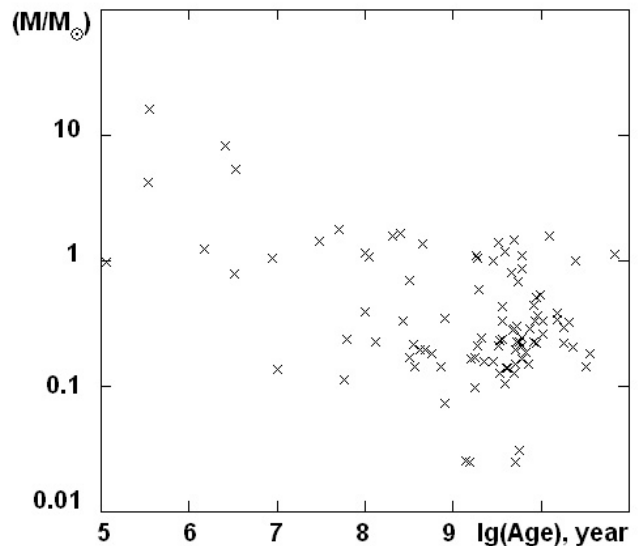


Figure 4: Distribution of the median mass of the normal companions (M/M_\odot) as a function of the pulsar characteristics.

lar decrease of the magnetic field strength on the pulsar surface (Fig. 1.) most probably is connected to its screening with the material falling on the pulsar surface from its normal companion. This possibility was indicated in a number of papers (for example, see Bisnovaty-Kogan, 2006 and references therein). Here we will only note that the rate of accretion must correlate with the intensity of the hard radio emission, produced with the same particles via the warming-up of pulsar surface up to extremely high temperatures. The second aspect is the fact that the magnetic field will be preserved inside the core of pulsar/NS for a long time, but when the accretion stops the magnetic field must float to its surface as a result of diffuse processes. The threshold value of magnetic induction on the NS surface, above which we observe the NS as a radio pulsar, according to the ATNF catalog data corresponds to $B_s > 6.7 \cdot 10^7$ Gauss.

Similar explanation involves the evolutionary decrease of the pulsar rotation periods. In this case (Fig. 2.), the so-called effect of the slight twist occurs, when the donor twists the pulsar, increasing its torque. The effect is connected with an increase of the conservatism of such kind of the binary system (Fig. 2.). This is confirmed by the decrease in the first-order derivative of the pulsar rotation period. When the magnetic field strength on the pulsar surface decreases, the corresponding decrease in the kinematic losses of pulsar (caused either by magneto-dipole emission or by current losses) takes place. It is quite probable that the accretion on pulsar surface is stabilized or completely discontinued as pulsar characteristic age increases.

Items 4, 5 (Fig. 3-4) can be grouped together due to the fact that total mass of both companions, sizes of semi-major axes and orbital periods are coupled via the third Kepler law. Although the general trend (Fig. 4) probably indicates to a decrease of the mass of the NS companion in the binary systems, the behavior of these systems in the range of the masses $M_1 \in [0.1M_\odot; 2M_\odot]$ should be considered in more detail. For example, in the range of masses $M_1 \in [0.1M_\odot; 2M_\odot]$ the companion normal star can lose very rapidly part of its mass as a result of the tidal destruction, directed explosions, or a series of the directed micro explosions/bursts.

Conclusions

The analysis of the presented data shows that in the close binary systems containing NS, the secular decrease of the magnetic field strength on the NS surface is observed. This decrease of the magnetic field strength most probably is connected with the accretion from the companion star on the NS surface. A threshold below which the NS/pulsar cannot be observed as a radio source is about $6.7 \cdot 10^7$ Gauss.

The observed secular decrease of the first derivative of the rotation period of the pulsars most likely corresponds to the fact that between the pulsar and its companion star a deep negative feedback is established, which effectively suppresses any fluctuations in the rate of the accretion on the NS surface and/or fluctuation in the luminosities of the hard radiation.

The evolutionary decrease of the semi-major axis of the binary systems and the simultaneous decrease of the mass of the normal star companions over the large time intervals testifies in a favour of the hypothesis about evolutionary evaporation (or destruction with the subsequent evaporation) of the companion star.

This hypothesis is also supported by the presence of numerous single millisecond pulsars with a large characteristic age, whose companion stars are not seen.

In the range of companion masses from $0.1M_\odot$ to $2M_\odot$, the most complex manifestation of the evolutionary phenomena in the binary systems are observed. It is quite probable that in this mass range the Jeans accretion mode operates.

References

- <http://www.atnf.csiro.au/research/pulsar/psrcat/>
M.A.McLaughlin, A.G.Lyne, D.R.Lorimer, M.Kramer, A.J.Faulkner, R.N.Manchester, J.M.Cordes, F.Camilo, A.Possenti, I.H.Stairs, G.Hobbs, N.D'Amico, M.Burgay, J.T.O'Brien: *Nature*, 2006, **439**, 817.
V.I.Kondrattiev, M.Burgay, A.Possenti, M.A.McLaughlin, D.R.Lorimer, R.Turolla, S.Popov, S.A.Zane: *40 Years of Pulsars, Magnetars and More*, 2008, American Institute of Physics, Montreal.
V.I.Kondrattiev, M.A.McLaughlin, D.R.Lorimer, M.Burgay, A.Possenti, R.Turolla, S.B.Popov, S.A.Zane: *Astrophys. J.*, 2009, **702**, 692.
V.M.Malofeev, O.I.Malov, and D.A.Teplykh: *Astrophys. Space Sci.*, 2007, **308**, No.1, 211.
V.V.Zakharenko, A.V.Markova, Y.Y.Vasylyeva: *Radio Physics and Radio Astronomy*, 2010, **15**, No.3, 263.
A.V.Tutukov, A.V.Fedorova, E.V.Ergma, L.R.Yungel'son: *Pis'ma Astron. Zh.*, 1985, **11**, 123.
I.J.Iben, A.V.Tutukov, A.V.Fedorova: *Astrophys. J.*, 1997, **486**, 955.
A.V.Fedorova, A.V.Tutukov: *Astronomy Reports*, 1994, **38**, 377.
A.V.Tutukov, A.V.Fedorova: *Astronomicheskii Zhurnal*, 1992, **69**, 271.
A.V.Fedorova: *Dual Stars*, 1997, Spaceinfo Pub., Moscow.
V.F.Gopka, O.M.Ulyanov, S.M.Andrievsky: *Origin of Matter and Evolution of Galaxies*, 2007, American Institute of Physics, Sapporo.
V.F.Gopka, O.M.Ulyanov, S.M.Andrievsky: *Origin*

- of Matter and Evolution of Galaxies*, 2010, American Institute of Physics, Osaka.
- V.F.Gopka, O.M.Ulyanov, S.M.Andrievsky: *Odessa Astron. Publ.*, 2007, **20**, 62.
- V.F.Gopka, O.M.Ulyanov, S.M.Andrievsky: *Kinematics and Physics of Celestial Bodies*, 2008, **24**, 36.
- O.M.Ulyanov: *Origin of Matter and Evolution of Galaxies*, 2010, American Institute of Physics, Osaka.
- V.L.Ginzburg: *Theoretical Physics and Astrophysic*, 1979, Pergamon Press, Oxford.
- V.M.Kontorovich, O.M.Ulyanov, A.B.Flanchik: *Origin of Matter and Evolution of Galaxies*, 2010, American Institute of Physics, Osaka.
- V.F.Gopka, A.V.Yushchenko, S.Goriely, A.Shavrina, Y.K.Woon: *Origin of Matter and Evolution of Galaxies*, 2005, American Institute of Physics, Tokyo.
- V.F.Gopka, A.V.Yushchenko, V.A.Yushchenko, I.V.Panov, Ch.Kim: *Kinematics and Physics of Celestial Bodies*, 208, **24**, 89.
- G.S. Bisnovatyi-Kogan: *Physics Uspekhi*, 2006, **49**, 53.

FUNDAMENTAL PARAMETERS AND CHEMICAL COMPOSITION OF CEPHEID X SGR.

I.A. Usenko¹, A.Yu. Knyazev², L.N. Berdnikov³, V.V. Kravtsov^{3,4}

¹ Department of Astronomy of I.I. Mechnikov Odessa National University
T.G.Shevchenko Park, Odessa 65014 Ukraine, *igus99@ukr.net*

² South African Large Telescope, P.O. Box 9, Observatory, Cape Town, 7935
South Africa, *aknyazev@sao.ac.za*

³ Sternberg Astronomical Institute, Moscow University, Moscow, 119899 Russia
lberdnikov@yandex.ru

⁴ Universidad Católica del Norte, Avenida Angamos 0610, Antofagasta, Chile
vkravtsov@ucn.cl

ABSTRACT. Five high-resolution spectra of unusual Cepheid X Sgr have been obtained during its pulsational period. For the first time we obtain accurate fundamental parameters and abundances of chemical elements, in particular of sodium, magnesium and aluminium. We estimate the mean $T_{\text{eff}} = 6143 \pm 30$ K; $\log g = 2.00$; $V_t = 4.35 \text{ km s}^{-1}$. The estimated effective temperature and surface gravity are relatively high compared to the typical values characteristic of Cepheids with pulsational period around 7 days. A deficit of carbon ($[\text{C}/\text{H}] = -0.26 \pm 0.04$ dex), overabundances of sodium ($[\text{Na}/\text{H}] = +0.31 \pm 0.04$ dex) and aluminium ($[\text{Al}/\text{H}] = +0.21 \pm 0.08$ dex) are typical for Cepheids passing through the first dredge-up phase. However, an obvious overabundance of magnesium ($[\text{Mg}/\text{H}] = +0.19 \pm 0.04$ dex) is unusual. The abundance of iron ($[\text{Fe}/\text{H}] = -0.02 \pm 0.01$ dex) is very close to the solar one. Abundances of α -elements, (those of Fe-group, as well as "light" and "heavy", s- and r-process elements) are comparable to the solar values, except for several elements showing slight over- or underabundances.

1. Introduction

X Sgr is one of the most famous objects among Cepheid variables. Being 7-days pulsational period's variable, the longest for so called "bump" Cepheids, it demonstrates an unusual character of its absorptional lines: they have splitting character, showing additional blue- or red- shifted absorption features in the line profiles (Sasselov & Lester, 1990). Moreover, these ones show remarkable changes during the pulsational period (see, for example, Figure 1 from Mathias et al., 2006). At that this fact concern only strong

low-excitational lines, but the absence of phase lag between weak metal lines forming low in the atmosphere and $\text{H}\alpha$ (which is formed higher) is obvious (Mathias et al., 2006). Kovtyukh et al. (2003) and Mathias et al. (2006) attempted to explain the strange behaviour of X Sgr line profiles. The former group of authors interprets this fact as the combined effect of strong line broadening (rotation and macro-turbulence) and non-radial oscillation, excited through resonances. Mathias et al. (2006) in turn suggest either the shock waves propagation per pulsation period as a result of κ -mechanism acting in the star or a binary nature of the star as a possible cause of unusual behaviour of spectral lines. Nevertheless, the evolutionary status of X Sgr still remain uncertain. Despite the fact that the star is quite bright ($\langle V \rangle = 4.^m6$), its fundamental parameters and chemical composition are poorly studied. Indeed, two CCD spectra in red region 5380 - 8710 Å and two photographic plate spectra in blue region 4300 - 4600 Å were obtained and analyzed by Luck & Lambert (1981) and Giridhar (1983), respectively. Luck & Lambert (1981) obtained their spectra near the minimum ($\phi = 0.47$) and maximum ($\phi = 0.06$) of light, whereas the spectra gathered by Giridhar (1983) correspond to the descending branch ($\phi = 0.258$ and 0.394 , respectively). In addition, the number of elements with determined abundances did not exceed thirteen items. The ultimate goal of this study is to determine precise fundamental parameters and chemical composition using of X Sgr using five newly-obtained, high-resolution spectra, gathered at different phases of its pulsational cycle.

2. Observations and data reduction

The observations have been carried out in August 2011 with GIRAFFE (Grating Instrument for Radiation Analysis with a Fibre Fed Echelle) spectrograph mounted at the Coudé focus of the 1.9m telescope at the South African Astronomical Observatory (SAAO), South Africa. Five spectra of this Cepheid have been obtained during weekly observational set. Information about X Sgr spectroscopic observations and heliocentric radial velocity measurements is given in Table 1. Phases were calculated according to the ephemeris published by Berdnikov & Caldwell (2001):

$$HJD_{max} = 2451653.5600 + 7.01281E \quad (1)$$

Table 1: Observations of X Sgr and radial velocities measurements.

Spectrum	HJD 2450000+	Phase	Exp. (min.)	RV (km s ⁻¹)	σ (km s ⁻¹)
1080044	5784.4374	0.047	40	-26.12	0.22
1080107	5785.3798	0.182	40	-19.42	0.20
1080198	5788.4230	0.616	20	-3.45	0.18
1080243	5789.4562	0.763	19	+1.26	0.21
1080284	5790.4428	0.904	44	-21.60	0.29

GIRAFFE allows to obtain high-resolution CCD echelle spectra ($R = 39\,000$) due to two dispersional prisms optimized for the blue (3770-5560 Å) and red (5200-10400 Å) spectral ranges. For our observations we used the red prism and a fiber with a projection diameter of 2". The detector was a 1024 × 1024 pixel TEK6 CCD camera. The total recorded spectral range (4300-6750 Å) contains 48 spectral orders.

At the beginning of each night and before each exposure, we observed the spectra of a hollow-cathode (Th+Ar) lamp, which allowed us to take into account all temperature trends by cross-correlating the 2D images of comparison spectra during the reduction. On each night, we also observed CAMERA FLATS to correct the pixel sensitivity and FIBER FLATS to find the position of spectral orders and to apply a correction for the spectral sensitivity effect along each order (blaze correction).

The data have been reduced using the standard XSPEC2 software (Balona, 1999). The procedure included: (1) background subtraction; (2) search for and extraction of the 1D fragments corresponding to individual orders from the 2D images; (3) blaze correction; (4) construction of the dispersion curves from hollow-cathode lamp spectra; (5) wavelength calibration; (6) applying the heliocentric correction; (7) determination of the radial velocity by means of the cross-correlation technique.

Phase-folded radial velocity (RV) curve approximated by the cubic spline is represented in Figure 1.

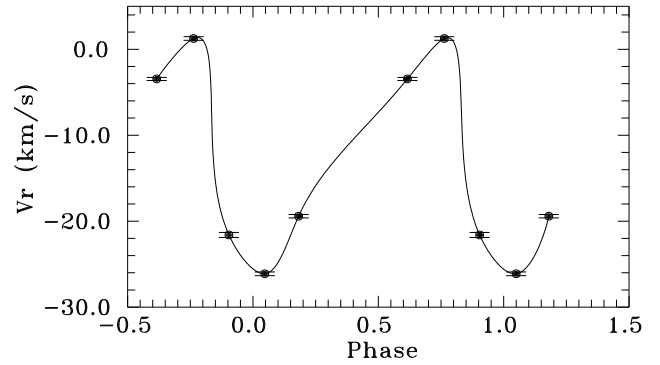


Figure 1: Radial velocity curve of X Sgr folded with the dominant pulsational period of 7.01281 days, approximated by the cubic spline.

We used the DECH 20 software package (Galazutdinov, 1992) to normalise the individual spectra to the local continuum, to identify the lines of different chemical elements and to measure the equivalent widths (EWs) of the individual spectral lines.

2. Fundamental parameters and chemical composition

For each spectrum we have obtained a set of fundamental parameters and individual elemental abundances. Effective temperatures has been evaluated using spectroscopic criteria based on the depth ratios for selected pair of spectral lines most sensitive to the temperature changes (Kovtyukh & Gorlova, 2000). This method provides an internal accuracy in determining T_{eff} of ~ 10 -30 K. Surface gravity has been derived using the ionization equilibrium condition for Fe I and Fe II atoms with an accuracy of ~ 0.15 dex. Microturbulent velocity V_t , has been deduced (with an accuracy of 0.25 km s^{-1}) following the standard procedure assuming that the abundance of ionized iron Fe II determined from a set of lines should be independent of their equivalent widths (Kovtyukh & Andrievsky, 1999).

The results are summarised in Table 2.

Table 2: Atmosphere parameters of X Sgr

Spectrum	Phase	T_{eff} (K)	log g	V_t (km s ⁻¹)
1080044	0.047	6367±10	2.10	4.30
1080107	0.182	6223±28	2.00	4.50
1080198	0.616	5791±25	1.90	4.30
1080243	0.763	5900±50	2.00	4.40
1080284	0.904	6435±38	2.10	4.30
Mean		6143±30	2.00	4.35

Figure 2 shows the variations of the effective temperature in dependence of the pulsational phase.

Table 3: Elemental abundance for X Sgr spectra

Element	1080044			1080107			1080198			1080243			1080284		
	[E/H]	σ	NL	[E/H]	σ	NL	[E/H]	σ	NL	[E/H]	σ	NL	[E/H]	σ	NL
C I	-0.29	0.21	6	-0.10	0.13	8	-0.41	0.23	8	-0.29	0.33	6	-0.29	0.21	9
O I	+0.35	0.00	1	+0.04	0.36	3	+0.11	0.17	2	+0.16	0.04	2	+0.23	0.06	2
Na I	+0.22	0.22	2	+0.34	0.19	6	+0.22	0.12	5	+0.42	0.32	6	+0.38	0.13	5
Mg I	+0.24	0.04	3	+0.07	0.19	5	+0.09	0.35	3	+0.25	0.20	4	+0.18	0.14	3
Al I	-0.16	0.04	2	+0.29	0.19	2	+0.20	0.14	2	+0.45	0.15	2	+0.27	0.07	2
Si I	+0.06	0.19	15	+0.21	0.14	11	+0.04	0.11	11	+0.02	0.14	12	-0.05	0.17	8
Si II	-	-	-	+0.43	0.00	1	+0.20	0.00	1	-0.43	0.00	1	-0.34	0.00	1
S I	-0.09	0.11	2	+0.28	0.32	3	+0.17	0.25	3	+0.03	0.22	4	+0.10	0.34	4
Ca I	-0.18	0.20	11	-0.15	0.09	10	+0.02	0.22	19	-0.01	0.08	7	-0.01	0.21	15
Sc II	-0.07	0.26	5	-0.18	0.12	5	-0.17	0.26	4	-0.06	0.26	3	-0.05	0.17	10
Ti I	+0.01	0.22	32	+0.03	0.27	28	+0.13	0.24	31	+0.05	0.26	23	+0.18	0.25	16
Ti II	-0.15	0.13	9	+0.16	0.19	7	-0.01	0.13	5	+0.01	0.07	4	-0.10	0.14	7
V I	+0.33	0.26	10	+0.30	0.24	9	+0.09	0.22	8	+0.26	0.14	6	+0.25	0.22	8
V II	-0.20	0.28	4	-0.11	0.00	1	+0.05	0.42	3	+0.01	0.23	3	-0.04	0.17	4
Cr I	-0.11	0.30	25	+0.20	0.23	33	+0.03	0.25	25	+0.06	0.24	25	+0.16	0.20	16
Cr II	+0.07	0.22	8	-0.10	0.19	8	-0.13	0.19	7	-0.07	0.22	7	-0.07	0.23	6
Mn I	-0.13	0.17	9	+0.04	0.21	9	-0.12	0.21	11	+0.00	0.31	7	-0.08	0.21	7
Fe I	-0.03	0.17	111	-0.03	0.18	94	-0.02	0.16	94	-0.01	0.17	82	+0.00	0.16	70
Fe II	-0.03	0.15	26	-0.03	0.19	26	-0.02	0.18	28	-0.02	0.13	29	+0.00	0.14	21
Co I	-0.00	0.23	16	+0.10	0.19	15	-0.15	0.23	12	+0.13	0.57	12	+0.23	0.23	7
Ni I	-0.23	0.20	53	-0.03	0.21	46	-0.10	0.21	38	+0.00	0.20	36	+0.03	0.21	29
Cu I	+0.16	0.23	2	+0.11	0.40	3	+0.03	0.00	1	+0.43	0.00	2	+0.32	0.23	3
Zn I	-0.24	0.43	3	-0.39	0.19	2	-0.40	0.12	2	-0.06	0.50	2	-0.36	0.08	3
Sr I	-	-	-	-	-	-	-0.08	0.00	1	-	-	-	-	-	-
Y II	+0.04	0.23	6	+0.07	0.27	7	-0.08	0.14	4	+0.09	0.40	6	-0.04	0.32	5
Zr II	+0.15	0.54	3	-0.03	0.31	6	-0.03	0.36	4	-0.17	0.26	4	+0.23	0.23	6
Ru I	+0.04	0.00	1	+0.11	0.00	1	-	-	-	-	-	-	-	-	-
La II	+0.15	0.21	3	+0.17	0.34	3	+0.22	0.23	3	+0.15	0.19	5	+0.30	0.27	7
Ce II	+0.00	0.23	9	-0.05	0.16	5	-	-	-	-0.11	0.26	7	-0.01	0.09	6
Pr II	-0.35	0.03	3	-0.05	0.24	2	+0.01	0.04	2	+0.06	0.44	2	+0.24	0.09	2
Nd II	-0.16	0.18	10	-0.26	0.31	7	-0.08	0.26	10	+0.05	0.25	8	-0.00	0.30	8
Sm II	-0.05	0.23	2	-0.03	0.00	1	+0.09	0.12	3	-0.10	0.39	2	-0.06	0.28	3
Eu II	+0.10	0.33	2	+0.11	0.17	2	+0.26	0.07	2	-0.05	0.00	1	+0.11	0.05	2
Gd II	-0.53	0.00	1	+0.24	0.00	1	+0.05	0.00	1	-0.34	0.00	1	-0.23	0.00	1

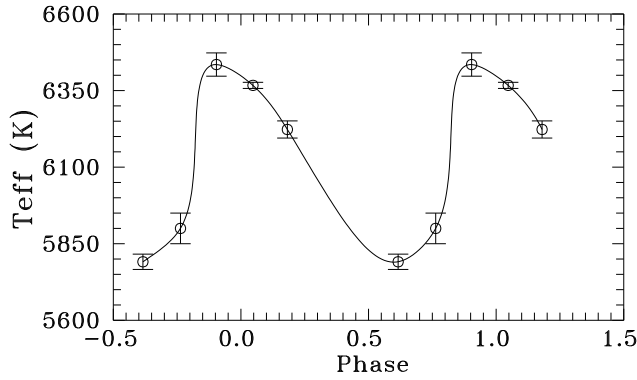


Figure 2: The effective temperature variations of X Sgr during its pulsational period, approximated by the cubic spline.

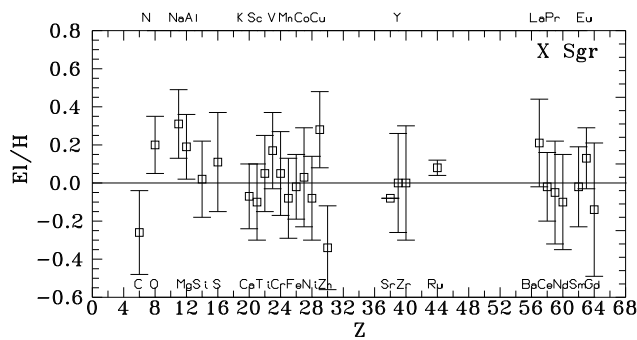


Figure 3: Average elemental abundances obtained for X Sgr using our observations.

Because of the pronounced splitting and variation of the absorption lines of X Sgr, we cannot use the Gaussian approximation to measure the equivalent widths of the lines assigned for the analysis. Therefore we used the equivalent widths obtained by forth integration only, except for the individual lines of "key elements" of yellow supergiant evolution (C, O, Na, Mg, Al), - in this case the relation between the line depths and equivalent widths have been applied.

All the atmosphere models and chemical composition for each spectrum were calculated using the version of the WIDTH9 code on the basis of the interpolation of Kurucz (1992) models grid with the "solar" log gf values, adopted from Kovtyukh & Andrievsky (1999). The data on the elemental abundances derived from individual spectra of X Sgr are given in Table 3 whereas Table 4 lists the average ones in comparison with the Luck & Lambert (1981) and Giridhar (1983) data. The least reliable estimates of the elemental abundances resulting from the analysis of a single spectral line are given in the parentheses in Table 3. Figure 3 gives a graphical representation of the data listed in Table 4.

Table 4: Average elemental abundances for X Sgr

Element	This work			Other authors	
	[El/H]	σ	NL	L&L ¹	SG ²
C I	-0.26	0.22	37	-0.15	-
O I	+0.20	0.15	10	+0.07	-
Na I	+0.31	0.18	24	-	-
Mg I	+0.19	0.17	18	-	-
Al I	+0.21	0.23	10	-	-
Si I	+0.06	0.16	57	+0.07	-
Si II	-0.04	0.42	4	-	-
S I	+0.11	0.26	16	-	-
Ca I	-0.07	0.17	62	+0.24	-0.20
Sc II	-0.10	0.20	27	-0.13	-
Ti I	+0.08	0.24	130	-0.03	+0.13
Ti II	-0.05	0.15	32	-	+0.13
V I	+0.26	0.22	41	+0.37	-
V II	-0.06	0.26	15	-	-
Cr I	+0.09	0.25	124	+0.33	+0.20
Cr II	-0.07	0.19	36	-	+0.20
Mn I	-0.08	0.21	36	-	-
Fe I	-0.02	0.17	451	+0.02	+0.07
Fe II	-0.02	0.16	130	+0.01	+0.07
Co I	+0.03	0.26	61	+0.09	-
Ni I	-0.08	0.22	202	+0.09	-
Cu I	+0.28	0.20	11	-	-
Zn I	-0.34	0.22	12	-	-
Sr I	-0.08	-	1	-	-
Y II	+0.00	0.26	28	-	-
Zr II	+0.00	0.30	23	-	-
Ru I	+0.08	0.04	2	-	-
La II	+0.21	0.23	21	+0.32	-
Ce II	-0.02	0.18	27	-	-0.20
Pr II	-0.05	0.27	11	-	-
Nd II	-0.10	0.25	43	-	-
Sm II	-0.02	0.21	11	-	-0.20
Eu II	+0.13	0.16	9	-	-
Gd II	-0.14	0.35	4	-	-

NL - number of lines

¹ - Luck & Lambert (1981)

² - Giridhar (1983)

4. Conclusions

As seen from Table 2, the mean value of the effective temperature 6143 ± 30 K, is in good agreement with 6125 K and close to 6100 K deduced by Luck & Lambert (1981) and Giridhar (1983), respectively. Our surface gravity value of 2.00 formally coincides with Giridhar's estimates (2.00) and is in agreement within the error bars with the value (1.90) reported by Luck & Lambert (1981). ones, but the Microturbulent velocity of 4.35 km s^{-1} agrees within the error of measurement with the value of 4.25 km s^{-1} given by Giridhar (1983) and is considerably higher than the value of 3.00 km s^{-1} obtained by Luck & Lambert (1981). Kovtyukh et al. (2003) have noted the fact that X Sgr

like another three Cepheids, suspected to have non-radial pulsations (V1334 Cyg, EV Sct and BG Cru), has rather high T_{eff} , - above 6000 K. In turn we would note the relatively high value of surface gravity for a classical Cepheid with pulsational period near 7 days.

With respect to the elemental abundances obtained in the present study, we would like to summarize the following points:

1. The iron abundance is very close to solar one, and is in good agreement with the results published by Luck & Lambert (1981). Giridhar (1983) has obtained higher value of +0.07 dex.
2. Carbon is found to be underabundant in agreement with the findings by Luck & Lambert (1981). The obtained oxygen abundance is unfortunately unreliable due to the line blending.
3. We estimated for the first time the abundances of the "key elements" of yellow supergiants evolution. All three elements Na, Mg and Al are found to be enhanced in the atmosphere of the star. The overabundance of magnesium is very unusual, taking into account that the most Cepheids and nonvariable supergiants demonstrate its deficit as a result of MgAl process after first dredge-up.
4. α - elements abundances are close to the solar ones.
5. The same can be noted for the elements of Fe-group, as well as for "light" and "heavy" - s-process and r-process elements: their abundances demonstrate either slight enrichment or deficit with respect to the solar values. The abundances of the majority of these elements were obtained for the first time for this star.

The obtained in this study results suggest that X Sgr is probably a Cepheid after first dredge-up phase. Indeed it shows deficit of carbon, overabundance of nitrogen ($[N/H] = +0.6$ dex according Luck & Lambert (1981)), sodium and aluminium. At the same time the unusual overabundance of magnesium is in disagreement, however.

References

- Balona L.A.: 1999, *Internal SAAO Report SAAO, CapeTown*, **1**.
- Berdnikov L.N., & Caldwell, J.A.R., 2001, *J. Astron. Data*, **7**.
- Galazutdinov G.A.: 1992, *Preprint SAO RAS*, **92**.
- Giridhar S.: 1983, *J. Astroph.*, **4**, 107.
- Kovtyukh V.V., Andrievsky, S.M.: 1999, *A&A*, **351**, 597.
- Kovtyukh V.V., Gorlova N.I.: 2000, *A&A* **358**, 587.
- Kovtyukh V.V., Andrievsky S.M., Luck R.E., Gorlova N.I.: 2003, *A&A*, **401**, 661.
- Kurucz R.: 1992, *In: The Stellar Populations of Galaxies, (eds) B.Barbuy and A.Renzini, IAU Symp.*, **149**, 225.
- Luck R.E., Lambert D.L.: 1981, *ApJ*, **245**, 1018.
- Mathias P., Gillet D., Fokin A.B., Nardetto N., Kervella P., Mourad D.: 2006, *A&A*, **457**, 575.
- Sasselov D.D., Lester J.B.: 1990, *ApJ*, **362**, 333.

MODELLING OF THE SEMI-DETACHED BINARY STAR WZ CORVI

N.A. Virnina¹, S. Zola^{2,3}, T. Krajci⁴

¹ Odessa National Maritime University, Odessa, Ukraine, *virnina@gmail.com*

² Astronomical Observatory, Jagiellonian University, ul. Orla 171, 30-244 Krakow, Poland

³ Mt. Suhora Observatory, Pedagogical University, ul. Podchorazych 2, 30-084 Krakow, Poland

⁴ Astrokolhoz Observatory, PO Box 1351, Cloudcroft, 88317, New Mexico, USA

ABSTRACT. We present results from modeling of multicolor light curves of the semi-detached, Algol-type binary system WZ Corvi. We analyzed VR data gathered in 2010 and new BVR_cI_c observations collected in 2012. Two models for WZ Crv are considered: the first was derived under the assumption that the temperature of the primary component, having the dominant contribution to total system light, corresponds to spectral type F7, and the second model, in which the temperature of the secondary was estimated from the colors observed at the flat bottom of the primary minimum. The new set of observations shows almost no difference in maxima heights, obvious in the earlier, 2010 data. However, primary minimum in V and R is deeper than in the 2010 light curve. We explain the variable shape of the system light curve as spot(s) present on primary or secondary component(s) due to their magnetic activity. Based on the derived solutions, we calculate relative physical (assuming the primary component to be a Main Sequence star) parameters of WZ Crv for both models.

Key words: Stars: binary; stars: individual: WZ Crv.

1. Introduction

Eclipsing binary WZ Corvi ($\alpha_{J2000.0} = 12^h44^m15.2^s$, $\delta_{J2000.0} = -21^\circ25'35''$) is a poorly studied Algol-type system, discovered by Luyten (1937). During the Edinburg-Cape Blue Object Survey (Kilkenny et al., 1997), from five spectra, the spectral classes of components have been determined to be F7 and late G.

Since its discovery, multicolor observations of WZ Crv have been obtained only in 2010 (Virnina et al. 2011). They collected and subsequently analyzed VR_c observations and discovered that the phase curve is asymmetric: the second maximum is brighter than the first one.

Virnina et al. (2011) also noticed the flat bottom of the primary minimum, and from $V - R$ color index they estimated the temperature of 5650 ± 66 K for

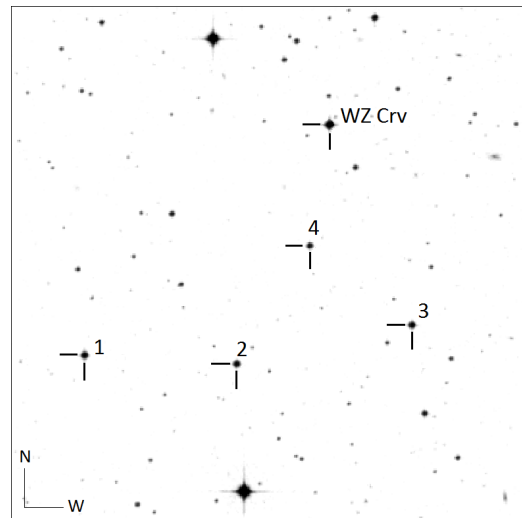


Figure 1: The position of WZ Crv and comparison stars. Field of view is $10' \times 10'$

the secondary (cooler) star. In the present paper we analyse new observations obtained in 2012, and illustrate variable magnetic activity of WZ Crv.

2. New Observations and Data Reduction

New observations of WZ Crv were obtained using the Schmidt-Cassegrain AAVSONet telescope Wright 28 (W28), $D = 280\text{mm}$, $F = 1717\text{mm}$, equipped with the 765×510 pixels CCD camera SBIG ST-7XME. With the scale of $1.074''/\text{pixel}$, that gives a field of view of $13.7' \times 9.1'$. In the period between February 18th and May 5th, 2012, twenty three runs were gathered in BVR_cI_c filters and the exposure times were: $B = 150$ s, $V = 70$ s, $R_c = 50$ s and $I_c = 70$ s. Altogether, in 2012 we have collected 396, 409, 414 and 381 single points in B , V , R_c and I_c filters, respectively. Scientific images have been calibrated for bias, flatfield and dark frames in a standard way.

Since the field of view of the W28 telescope is significantly smaller than that of TOA-150, used to

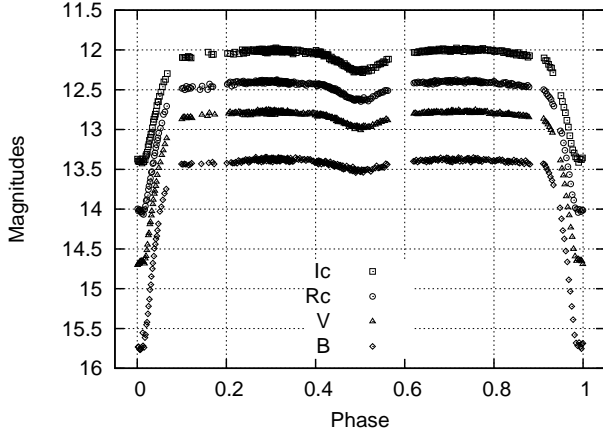


Figure 2: Phase curves, obtained from W28 robotic telescope of AAVSONet observatory in 2012.

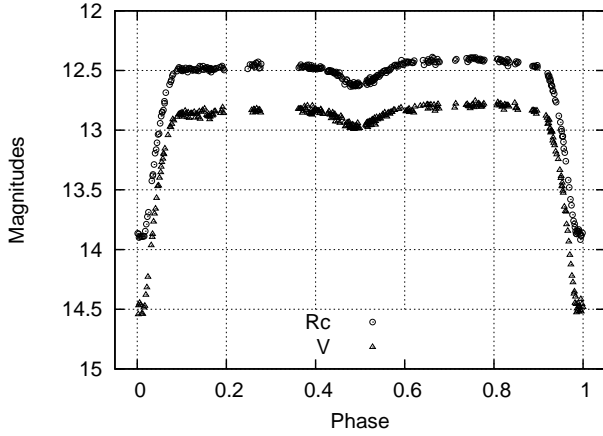


Figure 3: Phase curves, obtained on TOA-150 telescope of Tzec Maun observatory in 2010.

perform observations of WZ Crv in 2010, we had to choose other comparison stars to process photometry. We used the AAVSO software *SeqPlot* (<http://www.aavso.org/seqplot>), written by S. Beck, which is based on an original program by A. Henden, to extract from the AAVSO database the standard magnitudes of constant stars in the field of WZ Crv. Four comparison stars were chosen for "ensemble photometry" with the *MaxIm DL* software package. The coordinates and BVR_cI_c magnitudes of these stars are given in Table 1; their positions, together with the position of WZ Crv itself, are marked in Figure 1.

For direct comparison of the two sets of data, we recalibrated the VR_c observations collected in 2010, by using the same comparison stars as these for 2012 observations.

Making use of both datasets and *Peranso* (Vanmunster 2010) software, we have improved the ephemeris of WZ Crv:

$$\text{Min.I} = \text{HJD } 2455978.91668(45) + 1^d.78878(87) \cdot E$$

The period was calculated using the Lafler & Kinman method (1965); the initial epoch was measured from an individual minimum, observed in 2012, by approximating it with the algebraic polynomial of optimal degree $s = 6$ (MCV software, Andronov & Baklanov, 2004). The light curves phased with the above ephemeris are shown in Figures 2 and 3.

Table 1: Magnitudes of comparison stars.

#	USNO-B1.0	B	V	R_c	I_c
1	0684-0300004	14.356	13.688	13.299	12.934
2	0684-0299934	14.605	14.028	13.648	13.360
3	0685-0281718	14.486	13.826	13.458	13.112
4	0685-0281767	15.185	14.561	14.176	13.815

We measured instrumental magnitudes of 45 constant stars in the fields of WZ Crv, W Crv and V881 Per. The results have been compared with the standard magnitudes from the AAVSO database. We found the following transformation formulae for obtaining the standard magnitudes:

$$B - v = 1.081(\pm 0.018) \cdot (b - v) - 0.060(\pm 0.015)$$

$$V - r = 0.951(\pm 0.016) \cdot (v - r) + 0.018(\pm 0.008)$$

$$R_c - i = 0.968(\pm 0.055) \cdot (r - i) + 0.026(\pm 0.024)$$

$$r - I_c = 1.022(\pm 0.061) \cdot (r - i) - 0.034(\pm 0.027)$$

where B , V , R_c and I_c denote standard magnitudes, while b , v , r and i are instrumental. The effective wavelengths for each filter have been calculated to be: $\lambda_b = 447\text{nm}$, $\lambda_v = 546\text{nm}$, $\lambda_r = 649\text{nm}$ and $\lambda_i = 777\text{nm}$.

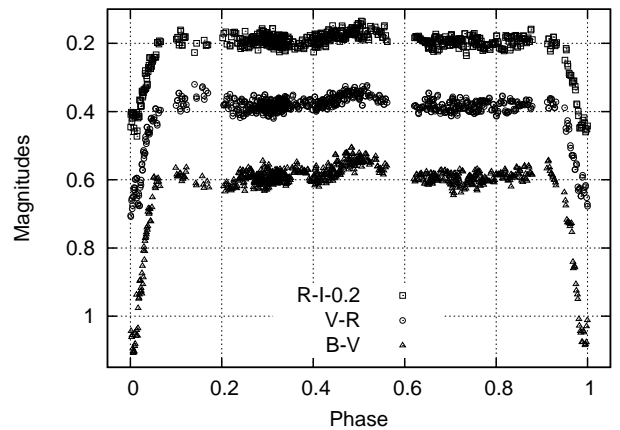


Figure 4: Phase curves of $b-v$, $v-r$ and $r-i$ color indices of WZ Crv, 2012.

In order to transform the instrumental measurements of the TOA-150 telescope to the standard system, we chose 58 constant stars in the field of WZ Crv. The resulting transformation formulae are:

$$V - r = 1.017(\pm 0.022) \cdot (v - r) - 0.026(\pm 0.010)$$

$$v - R_c = 0.950(\pm 0.041) \cdot (v - r) + 0.007(\pm 0.019)$$

where the meaning of V , R_c , v and r is the same as above. The effective wavelengths of the TOA-150 telescope are: $\lambda_v = 552\text{nm}$ and $\lambda_r = 636\text{nm}$. We applied transformation formulae to smoothed magnitudes in minima and maxima and the results are shown in Table 2.

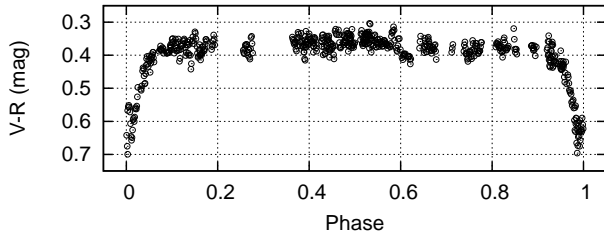


Figure 5: Variability of $v - r$ color index, 2010.

The asymmetry of the phase curves in maxima $\Delta max_V = max_{II} - max_I = -0.^m.033(\pm 0.^m.009)$ and $\Delta max_R = max_{II} - max_I = -0.^m.050(\pm 0.^m.004)$, which was clearly visible in 2010, in 2012 almost disappeared. However, the depth of the primary minimum in the new light curve is deeper both in V and R_c filters. Moreover, the $V - R_c$ color index in the primary minimum has changed - while in 2010 it was $(V - R_c)_{2010} = 0.^m.548(14)$, we measured it to be $(V - R_c)_{2012} = 0.^m.634(11)$ two years later.

We plotted the instrumental $b - v$, $v - r$ and $r - i$ colors observed in 2012 in Figure 4, while the $v - r$ instrumental color index derived from the 2010 data is shown in Figure 5. For phasing these data we used the same ephemeris as that for light curves. As it can be seen, there is rather high reddening in the primary minimum and WZ Crv becomes somewhat bluer at the secondary one.

Table 2: Standard magnitudes in minima and maxima with corresponding errors estimates.

	B	V	R_c	I_c
2012				
min_I	15.750(9)	14.649(9)	14.015(6)	13.407(6)
max_I	13.363(1)	12.782(2)	12.411(1)	12.030(2)
min_{II}	13.502(4)	12.974(3)	12.643(3)	12.291(3)
max_{II}	13.366(2)	12.779(1)	12.406(2)	12.021(2)
2010				
min_I		14.482(12)	13.934(7)	
max_I		12.803(8)	12.481(3)	
min_{II}		12.955(4)	12.647(3)	
max_{II}		12.770(4)	12.431(3)	

Additional evidence for the changing

shape of WZ Crv light curve can be found in the SuperWASP project database (<http://www.wasp.le.ac.uk/public/>). There have been more than 11000 points gathered by this project, after deleting bad points, 10462 points were left, which were divided into three subsets for observational seasons 2006, 2007 and 2008. The light curves (flux versus phase) are shown in Figures 4-6. We marked the original data by grey circles, while black points represent a smoothed light curve.

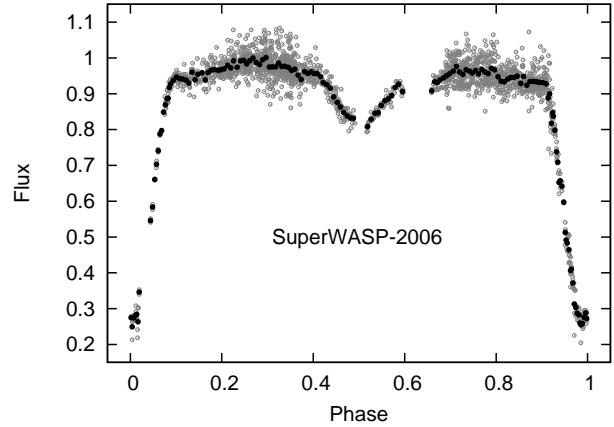


Figure 6: SuperWASP data, 2006.

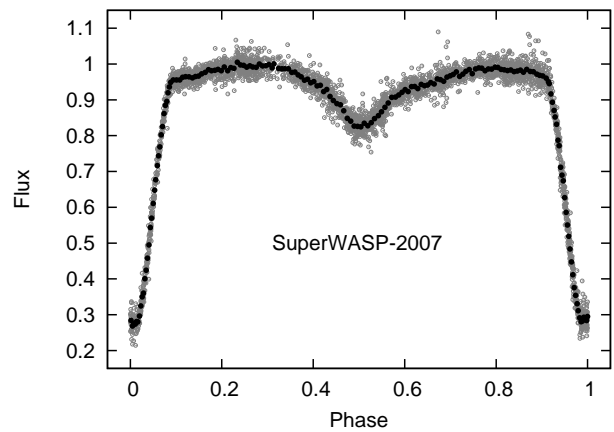


Figure 7: SuperWASP data, 2007.

3. Modeling the light curve

We used Wilson-Devinney code (Wilson & Devinney 1971; Wilson 1979; Wilson 1993) appended with Monte Carlo search algorithm (Zola 1997; Zola et al. 2010 and references therein) to obtain physical parameters of WZ Crv.

The light curves of this system are apparently unstable. The instability of the curve in close binary systems is usually explained by the presence of spots, caused by

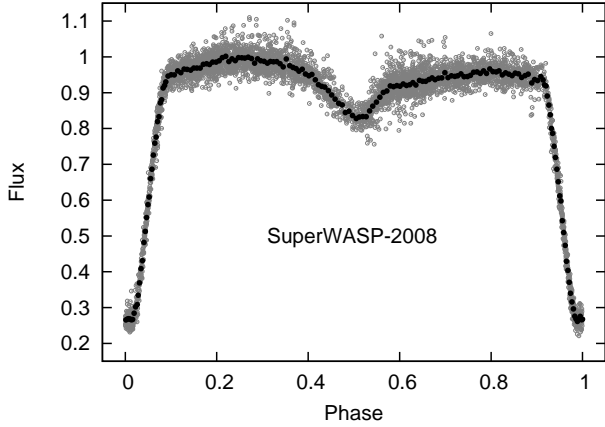


Figure 8: SuperWASP data, 2008.

magnetic activity of one or both components of the system. The main goal of this study was to determine the physical parameters of WZ Crv and to find a common solution for both 2010 and 2012 seasons. According to the spectral classification, obtained by Kilkenney et al. (1997), one may suggest, that the temperature of the hotter (primary) component should be 6200 K.

However, the flat bottom primary minimum indicates that at phase $\varphi = 0.0$ we see a total eclipse of the primary star, and only the rear face of the secondary (cooler) star is visible at that time. Therefore, the temperature of the secondary component could be independently evaluated from the color indices. In 2012 we collected four-color observations, thus the temperature determined from the color indices should be more reliable. However, in 2012, as it had been already shown, the primary minimum is deeper than that in 2010, and the color index $V - R_c$ is redder, indicating a lower temperature. To explain this, we assumed that in 2012 the depth and color at primary minimum could have been affected by a cool spot. Therefore, we eventually decided to determine the temperature of the secondary star from $V - R_c$ color index observed in 2010. According to Cox (2000), $V - R_c = 0^m.548(14)$ corresponds to temperature of $T_2 = 5510(\pm 87)$ K.

For each year we performed simultaneous computations in all available filters. The difference between color indices in minima indicates that the temperature difference between components should be significantly higher than 700 K. While searching for the common solution for both years, we applied two different approaches to light curve modeling. The first model (*Solution 1*) had been computed with a fixed temperature of the primary component to be $T_1 = 6200$ K as follows from the F7 spectral type and temperature of the secondary was adjusted. The second model assumed that the temperature of the secondary component is $T_2 = 5510$ K (*Solution 2*). In both cases we searched for a dark region in the

photosphere of each component to account for visible asymmetries and changes of the shape of light curves.

3.1. Solution 1

With the primary star temperature fixed at $T_1 = 6200$ K, the ranges for the other parameters were set up for four-color observations as follows: temperature of the secondary component between 3000K and 6000K, inclination between 70° and 90° , the mass ratio $q = M_2/M_1$ in the range of 0.1 - 0.9, and the luminosity of the primary component L_1 between 7 and 12.6. Following Lucy (1967) and Rucinski (1973), the gravity darkening exponents of both components and the bolometric albedo coefficients were set to the values of $g_{1,2} = 0.32$ and $A_{1,2} = 0.5$, respectively, which are appropriate for stars with convective envelopes. The limb-darkening coefficients were interpolated from the tables published by Claret et al. (1995) and Díaz-Cordovés et al. (1995).

Initially, we assumed that the third light could be present, but since its contribution in every band turned out to be negligible we proceeded with no third light solutions.

Parameters of the WZ Crv, including the position of the spot and its radius, are listed in Table 3. The resulting theoretical curves for 2012 are shown on Figure 9 with a solid line. The configuration of the system and the position of the dark spot were visualised at phase $\varphi = 0.11$ with the *Binary Maker* software (Figure 10). The theoretical and observed light curves for 2010 are plotted in Figure 11 while the configuration of the system (at phase $\varphi = 0.24$) is shown in Figure 12. The parameters of the system are listed in Table 3 for both 2010 and 2012.

Modeling yielded the temperature of the secondary star to be $T_2 = 4220$ K. The potential of the secondary star was $\Omega_2 = 3.56$ and this corresponds to filling the Roche lobe by the secondary component. The primary star was within its Roche lobe. The best fit was found for a dark spot to be on the secondary star.

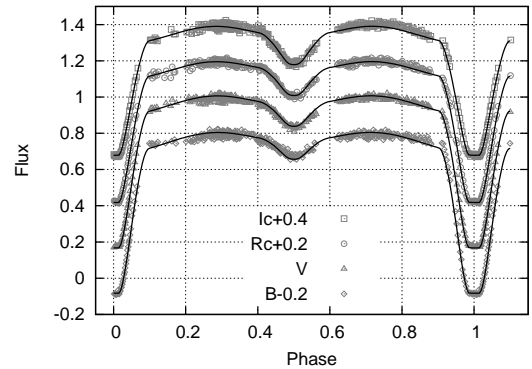


Figure 9: *Solution 1*: Synthetic curves (2012) are presented in solid lines, the grey symbols represent the original data.

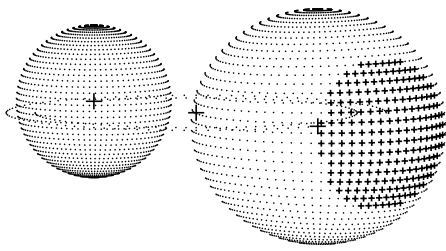


Figure 10: *Solution 1*: Configuration of the system (2012) at the phase $\varphi = 0.11$.

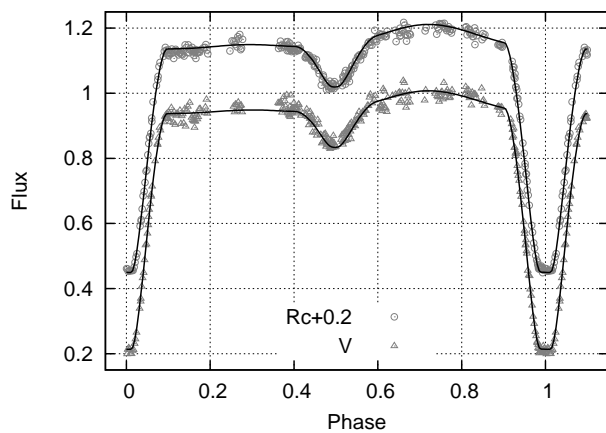


Figure 11: *Solution 1*: Synthetic curves (2010) are presented in solid lines, while the grey symbols represent the original data.

3.2. Solution 2

In the second solution, the temperature of the secondary star was fixed as $T_2 = 5510\text{K}$. The search range for the temperature of the primary star was between 7200 K and 13000 K. According to Lucy (1967) and Rucinski (1973) the gravity darkening exponents were set at $g_1 = 1.0$ and $g_2 = 0.32$, the bolometric albedo coefficients were set to be $A_1 = 1.0$ and $A_2 = 0.5$, for the primary and secondary, respectively. The same ranges as those for Solution 1 we set for inclination, potentials and the mass ratio. A dark spot was placed on the surface of the secondary component.

From the preliminary solution we found that the mass ratio was close to 0.75, and the secondary star filled its Roche lobe. Since this star is very distorted and the color corresponded to its back side, for the final solution the temperature of the secondary has been corrected to account for such a shape and resulted in a new T_2 value of 5630 K. From new computations we derived a model with the same parameters describing stars in 2010 and 2012. They are listed in Table 4. Figure 13 presents the synthetic light curves for 2012,

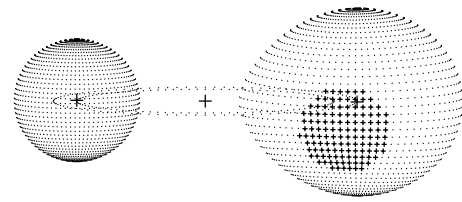


Figure 12: *Solution 1*: Configuration of the system (2010) at the phase $\varphi = 0.24$.

while the configuration of the system ($\varphi = 0.10$) is shown in Figure 14. The resulting light curve and data for 2010 and the configuration of the system ($\varphi = 0.24$) in that year could be seen in Figures 15 and 16, respectively.

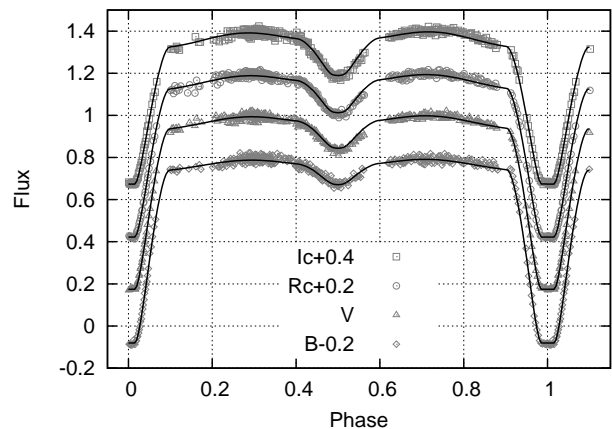


Figure 13: *Solution 2*: Synthetic curves (2012) are presented as solid lines, while grey symbols represent the observed data.

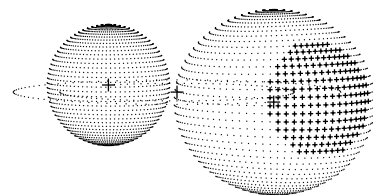


Figure 14: *Solution 2*: Configuration of the system (2012) at the phase $\varphi = 0.10$.

Table 3: Parameters of WZ Crv derived from modeling, *Solution 1*. Given uncertainties are those derived from the fit at the 90% confidence level. Stars radii are given in orbital separation units.

Parameter	2012	2010
i (deg)	84.7 ± 0.1	84.7 ± 0.1
T_1 (K)	*6200	*6200
T_2 (K)	4220 ± 5	4220 ± 5
Ω_1	5.413 ± 0.015	5.413 ± 0.015
Ω_2	3.561 ± 0.011	3.561 ± 0.011
$q(M_2/M_1)$	0.847 ± 0.005	0.847 ± 0.005
$L_1/(L_1 + L_2)$ (b)	0.7929 ± 0.0017	
$L_1/(L_1 + L_2)$ (v)	0.7475 ± 0.0015	0.7448 ± 0.0017
$L_1/(L_1 + L_2)$ (r)	0.6990 ± 0.0017	0.7052 ± 0.0018
$L_1/(L_1 + L_2)$ (i)	0.6363 ± 0.0035	
$L_2/(L_1 + L_2)$ (b)	0.2071 ± 0.0004	
$L_2/(L_1 + L_2)$ (v)	0.2525 ± 0.0005	0.2552 ± 0.0006
$L_2/(L_1 + L_2)$ (r)	0.3010 ± 0.0007	0.2948 ± 0.0008
$L_2/(L_1 + L_2)$ (i)	0.3637 ± 0.0014	
r_p (pole)	0.2181	0.2181
r_p (point)	0.2240	0.2240
r_p (side)	0.2203	0.2203
r_p (back)	0.2230	0.2230
r_s (pole)	0.3341	0.3341
r_s (point)	0.4199	0.4199
r_s (side)	0.3490	0.3490
r_s (back)	0.3765	0.3765
Spot parameters		
Star	2	2
longitude ($^\circ$)	90 ± 6	103 ± 10
latitude ($^\circ$)	178 ± 2	85 ± 1
radius ($^\circ$)	37.2 ± 0.5	27.9 ± 1.7
temperature	$0.925 \pm 0.002 T_2$	$0.751 \pm 0.022 T_2$

*-not adjusted

Table 4: Parameters of WZ Crv derived from modeling, *Solution 2*. Given uncertainties are those derived from the fit at the 90% confidence level. Stars radii are given in orbital separation units.

Parameter	2012	2010
i (deg)	85.7 ± 0.1	85.7 ± 0.1
T_1 (K)	10390 ± 26	10390 ± 26
T_2 (K)	*5630	*5630
Ω_1	5.321 ± 0.014	5.321 ± 0.014
Ω_2	3.270 ± 0.007	3.270 ± 0.007
$q(M_2/M_1)$	0.715 ± 0.004	0.715 ± 0.004
$L_1/(L_1 + L_2)$ (b)	0.8160 ± 0.0015	
$L_1/(L_1 + L_2)$ (v)	0.7516 ± 0.0015	0.7480 ± 0.0020
$L_1/(L_1 + L_2)$ (r)	0.6941 ± 0.0018	0.7009 ± 0.0023
$L_1/(L_1 + L_2)$ (i)	0.6338 ± 0.0022	
$L_2/(L_1 + L_2)$ (b)	0.1840 ± 0.0003	
$L_2/(L_1 + L_2)$ (v)	0.2484 ± 0.0005	0.2520 ± 0.0007
$L_2/(L_1 + L_2)$ (r)	0.3059 ± 0.0008	0.2991 ± 0.0010
$L_2/(L_1 + L_2)$ (i)	0.3662 ± 0.0013	
r_p (pole)	0.2164	0.2164
r_p (point)	0.2213	0.2213
r_p (side)	0.2183	0.2183
r_p (back)	0.2205	0.2205
r_s (pole)	0.3284	0.3284
r_s (point)	0.4626	0.4626
r_s (side)	0.3437	0.3437
r_s (back)	0.3756	0.3756
Spot parameters		
Star	2	2
longitude ($^\circ$)	84 ± 3	102 ± 11
latitude ($^\circ$)	175 ± 2	81 ± 2
radius ($^\circ$)	35.0 ± 0.2	29 ± 2
temperature	$0.897 \pm 0.016 T_2$	$0.751 \pm 0.025 T_2$

*-not adjusted

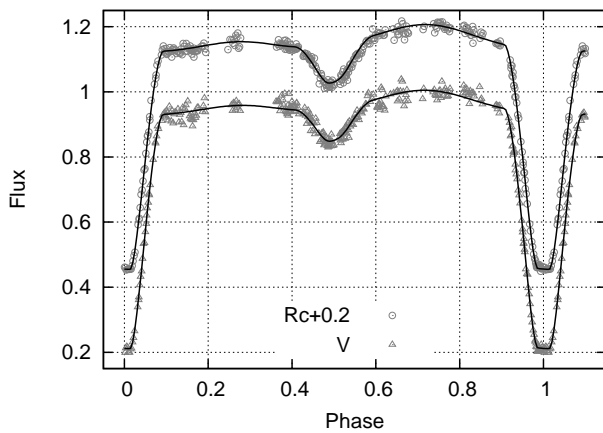


Figure 15: *Solution 2*: Synthetic curves (2010) are presented as solid lines, while grey symbols represent the original data.

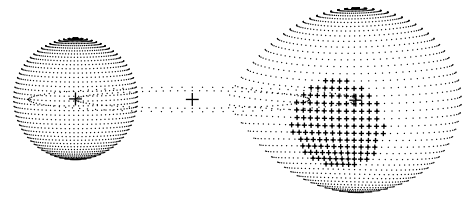


Figure 16: *Solution 2*: Configuration of the system (2010) at the phase $\varphi = 0.24$.

4. Results and Discussion

We analysed multicolor observations of the binary system WZ Crv, collected in 2012 and 2010. We noticed that the primary minimum has a flat bottom. We found differences in the shape of the light curve and in depth of the primary minimum. We assumed that magnetic activity, manifesting by the presence of a dark

spot, is responsible for the observed changes. These light curve variations could be easily noticed also in the combined SuperWASP data and confirm a strong magnetic activity of one or both components of this system.

The light curves taken at the two seasons were modeled using the Wilson-Devinney code. Two alternative solutions were considered: (1) in the first one the temperature of the primary was assumed to be 6200 K as corresponding to the F7 spectral class; (2) in the second solution we determined the temperature of the secondary, the only component visible at the primary eclipse, from its $V - R$ color measured at flat bottom phases. We were able to obtain models within both solutions that have the same stellar parameters but differ only in these describing a cool spot on the surface of the secondary. Our solution indicated that the cool spot was located at longitude of about 80 degrees in 2010 while in 2012, its longitude position was about 180 degrees. We conclude, that the magnetically active component in WZ Crv is the secondary star.

Spectroscopic observations are needed to confirm the photometric mass ratio derived in this paper. Further photometric observations are required to monitor the magnetic activity of WZ Crv.

Acknowledgements.

Authors are thankful to Arne Henden. 2012 data was obtained by the AAVSONet robotic photometry telescope network: <http://www.aavso.org/aavsonet>.

Authors are also thankful to Prof. I. L. Andronov for helpful comments.

NV thanks Fabio Martinelli for hospitality during her stay in Italy, where the paper was written.

References

- Andronov I.L., Baklanov A.V.: 2004, *Astronomy School Reports*, **5**, 264, <http://uavso.pochta.ru/mcv>
- Bradstreet D.H., Steelman D.P.: 2004, *Binary Maker 3 Light Curve Synthesis Program*
- Claret A., Díaz-Cordovés J., and Gimenez, 1995, *A&AS*, **114**, 247
- Cox, A. N.: 2000, *Allens Astrophysical Quantities* (4th ed.; New York: Springer)
- Díaz-Cordovés J., Claret A., and Gimenez A., 1995, *A&AS*, **110**, 329
- Kilkenny D., O'Donoghue D., Koen C., Stobie R. S., Chen A.: 1997, *Mon. Not. R. Astron. Soc.*, **287**, 867.
- Lafler J., Kinman T.D.: 1965, *ApJ:Suppl*, **11**, 216
- Lucy, L. B.: 1967, *Z. Astrophys.*, **65**, 89
- Luyten W. J.: 1937 *Astron. Nachr.*, **261**, 451.
- Rucinski S. M.: 1973, *Acta Astron.*, **23**, 79
- Terrell D., Wilson, R.E.: 2005, *Ap&SS*, **296**, 221
- van Hamme W.: 1993, *AJ*, **106**, 2096
- Vanmunster, T. 2010, PERANSO, period analysis software, <http://www.peranso.com>
- Virnina N.A., Andronov I.L., Mogorean M.V.: 2011, *Journal of Physical studies*, **15**, 2910
- Wilson R.E., Devinney, E.J.: 1971, *ApJ*, **166**, 605
- Wilson R.E.: 1979, *ApJ*, **234**, 1054
- Wilson R.E.: 1993, *Documentation of Eclipsing Binary Computer Model*, University of Florida
- Zola S., Kolonko M., Szczech M.: 1997, *A&A*, **324**, 1010
- Zola S., Gazeas K., Kreiner J.M. et al.: 2010, *Mon. Not. R. Astron. Soc.*, **408**, 464

DISCOVERY OF THE FIRST SUPER-LITHIUM RICH BEAT CEPHEID: V371 PER

V. V. Kovtyukh¹, N. I. Gorlova², M. Hillen²

- ¹ Astronomical observatory Odessa National University,
T.G. Shevchenko Park, Odessa 65014 Ukraine, *val@deneb1.odessa.ua*
² Institute of Astronomy, Celestijnenlaan 200D, 3001, Leuven, Belgium

ABSTRACT. Four high-resolution spectra of the double-mode Cepheid V371 Per, obtained for the first time, showed the presence of the abnormally strong Li I 6707.76 Å line. Our analysis of the light element abundances indicates that the star did not go through the evolutionary dredge-up stage. Large distance from the galactic plane and the low metallicity suggest that V371 Per may belong to the thick disc (or to the halo) of the Galaxy, which is consistent with its low metallicity $[Fe/H]=-0.42$ and the enhancement of the α - and s-elements relative to iron. Line splitting is observed in one of the spectra, which can be due to the non-radial pulsations.

Key words: Classical Cepheids – stars: individual: V371 Per

1. Introduction

Beat Cepheids are classical Cepheid variable stars that simultaneously pulsate in two radial modes. They are sometimes referred to as double-mode Cepheids. A beat Cepheid pulsates either in the first overtone and the fundamental modes (P1/P0), or in the second and the first overtone modes (P2/P1). Previous studies clearly established that the period ratio (higher to lower mode) of the P1/P0 pulsators is around 0.72, while that of P2/P0 is closer to 0.80. The period ratios can be measured very accurately and have been found to correlate with the Cepheid masses, luminosities, T_{eff} , and the abundances of the heavy elements. For example, from the OGLE photometry and the stellar atmosphere models, Kovács (2009) showed that in both Magellanic Clouds the average metallicity of the P1 Cepheids is lower than those pulsating in the fundamental mode.

Extensive photometry of V371 Per (=BD+41 563 = 2MASS J02553118+4235197) over a number of years has clearly shown it to be a Galactic beat Cepheid, with the shortest period known so far (P0=1.738 d). The high value of the period ratio (P1/P0 = 0.731)

suggests low metallicity: $[Fe/H]$ should be between -1.0 and -0.7 according to Wils et al. (2010). Its distance, which is derived from the empirical period-luminosity (PL) relation, places it in the Galactic thick disk or the halo, 0.8 kpc above the Galactic plane. The amplitude of the first overtone mode is larger than that of the fundamental mode, which is quite rare for the Galactic beat Cepheids (Wils et al. 2010). Only in AX Vel (with a fundamental period of 3.67 d) and V458 Sct (4.84 d) the first overtone has a larger amplitude than the fundamental mode.

In the present paper we report on the detection of the Li I 6707.8 Å line in V371 Per.

2. The spectral material

Four spectra were obtained on three nights in September 2011 with the fiber echelle-type spectrograph HERMES, mounted on the 1.2m Belgian telescope on La Palma. A high-resolution configuration with $R=85\,000$ and the wavelength coverage 3800–9000 Å was used. The spectra were reduced using the Python-based pipe-line, that performs the order extraction, wavelength calibration using the Thr-Ne-Ar arcs, division by the flat field, cosmic-ray clipping, and the order merging. For more details on the spectrograph and the pipe-line, see Raskin et al (2011).

We chose to derive abundances from two spectra observed on the same night of September 29, because of their superior signal to noise ratio (S/N). The rest two spectra were used for the determination of the radial velocity and the effective temperature (T_{eff} , see Table 1).

We used the DECH 20 software package (Galazutdinov 1992) to normalize the individual spectra to the local continuum, to identify the lines of different chemical elements, and to measure the equivalent widths of the individual lines.

Table 1: Observations of V371 Per, radial velocity measurements and photospheric parameters determined in this work.

Spectrum	HJD 2455800+	RV (km s^{-1})	σ (km s^{-1})	T_{eff} (K)	σ (K)	N	$\log g$ (km s^{-1})	V_t	[Fe/H]	Remark
374513	31.6483530	-17.094	0.112	6213	320	8	
374659	33.6369571	-2.649	0.073	5984	378	15	
374737	34.6177909	-14.455	0.040	5950	148	48	2.20	3.70	-0.42	+
374738	34.6461523	-12.859	0.042	5996	145	40	2.20	3.70	-0.42	+

Remark: +: spectra used for the abundance analysis.

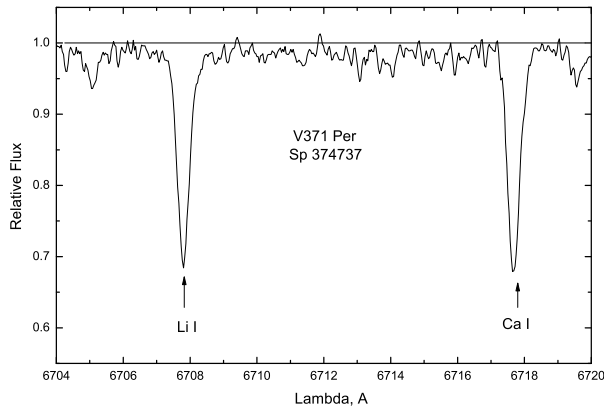


Figure 1: The Li region in V371 Per spectrum number 374737.

3. Fundamental parameters and the chemical composition

To determine the effective temperature for our star we employed the method of Kovtyukh (2007) which is based on the line depth ratios. This technique allows the determination of T_{eff} with an exceptional precision. It relies on the ratio of the central depths of two lines that have very different functional dependences on T_{eff} (and there are several tens of line pairs that are used in this analysis). The method is independent of the interstellar reddening and only marginally dependent on individual characteristics of stars, such as rotation, microturbulence, metallicity and others. The use of ~ 50 calibrations per spectrum results in the uncertainty of 10–20 K for spectrum with S/N greater than 100, and 30–50 K for S/N less than 100.

To determine the microturbulent velocities (V_t) and gravities ($\log g$), we used a modified version of the standard analysis as proposed by Kovtyukh & Andrievsky (1999). In this method the microturbulence is determined from FeII lines (instead of FeI lines used in the classic abundance analysis). The gravity is determined by forcing the equality of the total iron abundance derived from FeI and FeII. Normally, this method results in the iron abundance determined from FeI to show a

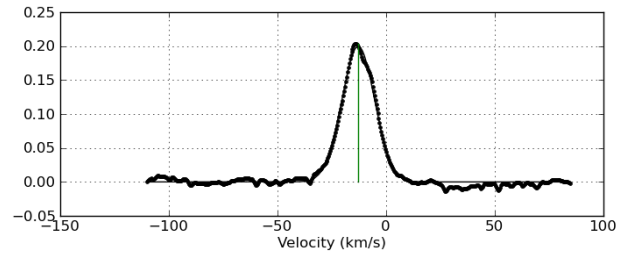


Figure 2: Cross-correlation function of the spectrum 374738 with a G2 template. One can see that the average line profile in this spectrum consists of at least two absorption components, which could be due to the non-radial pulsations.

strong dependence on the equivalent width (due to the non-LTE effects). In this case we take as the proper iron abundance the abundance extrapolated to the zero equivalent width.

The resulting T_{eff} , $\log g$ and V_t are presented in Table 1.

The elemental abundances were calculated with the help of the Kurucz's WIDTH9 code. The resulting averaged values are listed in Table 2. As usual, they are given relative to the solar abundances, which were adopted from Grevesse et al. (1996).

Our oscillator strengths have been obtained by means of the inverse spectroscopic analysis of the solar spectrum, namely, by requiring the adopted solar abundance for each line with the measured equivalent width (EW). The benefit of these "solar" oscillator strengths is that the relative abundances (CNO, in particular) deduced for a given object will not change if the the currently adopted solar abundances were to be modified.

4. The lithium abundance in V371 Per

For a long time no classical Cepheids or supergiants were known to show the Li I 6707.8 Å line. Luck (1982) was the first to identify two lithium supergiants in the Galaxy – HD 172365 and HD 174104. Later on, Luck & Lambert (1992, 2011) discovered lithium in the LMC

Table 2: Elemental abundances in V371 Per

Ion	[El/H]	σ	NL	(El/H)
Li I	2.19	...	1	3.35
C I	-0.32	0.11	9	8.23
N I	-0.21	0.04	2	7.76
O I	-0.18	...	1	8.69
Na I	-0.45	0.17	3	5.88
Mg I	-0.43	0.00	2	7.15
Al I	-0.28	0.15	4	6.19
Si I	-0.28	0.05	15	7.27
Si II	-0.30	0.16	2	7.25
S I	-0.13	0.13	6	7.08
Ca I	-0.25	0.09	11	6.11
Sc II	-0.17	0.07	9	3.00
Ti I	-0.04	0.12	32	4.98
Ti II	-0.16	0.08	9	4.86
V I	-0.24	0.09	3	3.76
V II	-0.14	0.10	4	3.86
Cr I	-0.46	0.13	14	5.21
Cr II	-0.38	0.12	13	5.29
Mn I	-0.41	0.07	3	4.98
Fe I	-0.42	0.10	235	7.08
Fe II	-0.43	0.12	43	7.07
Co I	-0.27	0.14	4	4.65
Ni I	-0.34	0.09	56	5.91
Cu I	-0.35	0.17	5	3.86
Zn I	-0.08	...	1	4.52
Y II	0.03	0.11	8	2.27
Zr II	-0.05	0.06	3	2.55
La II	-0.02	0.38	2	1.20
Ce II	0.03	0.06	6	1.58
Pr II	-0.24	...	1	0.47
Nd II	-0.22	0.10	6	1.28
Eu II	0.01	0.05	2	0.52

NL – number of lines

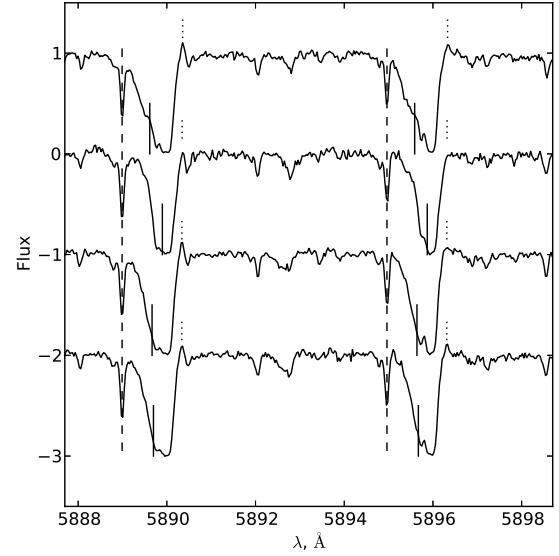


Figure 3: Complicated profiles of the sodium D12 lines in our spectra of V371 Per. Solid lines: photospheric component; dashed: likely interstellar stationary component; dotted: telluric emission.

Cepheid HV 5497 and in Galactic Cepheid V1033 Cyg. Every lithium supergiant thus presents a great interest, as it may indicate a recent creation or a unique evolutionary path of the object. In this paper we present the first detection of the lithium line in all four spectra of V371 Per. In Fig. 1 we show the Li region in the spectrum number 374737.

According to the theory (see de Laverny et al. 2003), when a star of about $3 M_{\odot}$ reaches $T_{\text{eff}} = 6400$ K, lithium starts to be depleted in the photosphere, dropping to $\log N(\text{Li}) = 1.0$ at about $T_{\text{eff}} = 5500$ K (assuming the original abundance to be equal to the Solar system meteoritic abundance of 3.3 [Lodders 2003]). This agrees with our estimate of the upper limit on $\log N(\text{Li}) = 1.0$ for the great majority of Cepheids, which follows from the non-detection of the lithium line. In contrast, for V371 Per we derive a large overabundance of lithium: $\log N(\text{Li}) = 3.35 \pm 0.09$.

Beside lithium enrichment, V371 Per shows non-symmetrical line profiles due to the presence of the additional absorption component (Fig. 2). Kovtyukh et al. (2003) proposed that the observed bumps in the line profiles in some Cepheid spectra could result from a combination of the large broadening (either due to rotation or macroturbulence) and the resonant interaction between the radial modes responsible for the non-radial oscillations.

Sodium lines show complicated profiles (Fig. 3): photospheric component is overlaid on the saturated, likely circumstellar absorption; in addition, there is

a narrow stationary component at the velocity ~ -49 km/s, which can be of the interstellar origin.

4. Discussion and conclusions

In an evolved intermediate-mass star one expects the lithium abundance to be severely diluted due to the combined effects of the mass-loss on the Main Sequence and the subsequent first dredge-up. The sensitivity to mass-loss stems from the fact that in B stars (the progenitors of Cepheids) Li remains in only the outer 2% of the star at the end of the Main Sequence. Even without the mass loss, the standard stellar evolution predicts a dilution about a factor of 60 relative to the initial value. Assuming an initial lithium content of $\log A(\text{Li}) = 3.3$ dex, this means that Cepheids should have lithium abundances $\log A(\text{Li}) < 1.5$ dex. In contrast, V371 Per has a strong lithium line with the deduced LTE lithium abundance of $\log A(\text{Li}) = 3.35$ dex. How could V371 Per maintain such a high abundance of lithium in its photosphere?

The simplest answer is that V371 Per is crossing the HR diagram towards the giant branch for the first time. The photospheric composition then has not been altered by the dredge-up, and we are observing an unaltered abundance of lithium. For this to be the case, the CNO, Na content should also be in its original state. Indeed, this appears to be true: the [C/Fe], [N/Fe], and [Na/Fe] ratios are +0.1, +0.2 and 0.0, respectively, while the C/O ratio is 0.72. The [N/Fe] ratio is a bit high, but could have been overestimated by up to 0.2–0.3 dex due to the non-LTE effects (Lyubimkov et al. 2011). The [C/Fe] and C/O ratios in V371 Per are significantly larger than the typical ratios of –0.21 and 0.25, respectively, found in Cepheids. They, however, are typical of those found in young, unevolved stars.

Another way to potentially ascertain the evolutionary status of a Cepheid is to look for the systematic period change over the time. For example, Turner et al. (2010) found four first overtone or double mode Cepheids with the period changes: Polaris, DX Gem, BY Cas, and HDE 344787. They argued that this is a manifestation of these stars evolving across the Hertzsprung gap. A similar monitoring could help clarify the nature of V371 Per.

Summarizing, with its peculiar abundances of lithium, carbon, nitrogen and sodium (compared with ordinary Cepheids) V371 Per can be considered as the Cepheid which is presently crossing the instability strip for the first time.

Acknowledgements. The spectra were collected with the Mercator Telescope, operated on the island of La Palma by the Flemish Community, at the Spanish Observatorio del Roque de los Muchachos of the Instituto de Astrofísica de Canarias.

References

- Galazutdinov G.A.: 1992, *Preprint SAO RAS*, **92**, 2.
 Grevesse N., Noels A., Sauval J.: 1996, *ASP Conf. Ser.*, **99**, 117.
 Kovács G.: 2009, *EAS Publ. Ser.*, **38**, 91.
 Kovtyukh V.V.: 2007, *MNRAS*, **378**, 617.
 Kovtyukh V.V. & Andrievsky S.M.: 1999, *A&A*, **351**, 597.
 Kovtyukh V.V., Andrievsky S.M., Luck R.E., Gorlova N.I.: 2003, *A&A*, **401**, 661.
 de Laverny P., do Nascimento J. D. Jr., Lebre A., De Medeiros J. R.: 2003 *A&A*, **410**, 937.
 Lodders K.: 2003, *ApJ*, **591**, 1220.
 Luck R.E.: 1982, *PASP*, **94**, 811.
 Luck R.E. & Lambert D.L.: 1992, *ApJSS*, **79**, 303.
 Lyubimkov L.S., Lambert D.L., Korotin S.A., Poklad D.B., Rachkovskaya T.M., Rostopchin S.I.: 2011, *MNRAS*, **410**, 1774.
 Raskin G., van Winckel H., Hensberge H. et al.: 2011, *A&A*, **526**, 69.
 Turner D.G., Majaess D.J., Lane D.J., Percy J.R., English D.A., Huziak R.: 2010, *Odessa Astr. Publ.*, **23**, 125.
 Wils P., Henden A.A., Kleidis S., Schmidt E.G., Welch D.L.: 2010, *MNRAS*, **402**, 1156.

ARE THE s-CEPHEIDS CROSSING THE INSTABILITY STRIP FOR THE FIRST TIME?

S.M. Andrievsky^{1,2}, G.A. Garbuzov¹, D.N. Doikov³

¹ Department of Astronomy and Astronomical Observatory, Odessa National University, Shevchenko Park, 65014 Odessa, Ukraine, *scan@deneb1.odessa.ua*

² GEPI, Observatoire de Paris-Meudon, F-92125 Meudon Cedex, France

³ Odessa National Maritime University

ABSTRACT. Using the literature data on secular period changes reported for the small-amplitude Cepheids (s-Cepheids) it is shown that these stars are not crossing the instability strip for the first time. After correction of the observed pulsational characteristics of s-Cepheids, in the diagram " $\log\left(\frac{dP}{P}\right)_{100} - \log P$ " they become indistinguishable from usual classic Cepheids, which are supposed to have already crossed the instability strip more than (or at least) once.

Key words: Stars: Cepheids.

1. Introduction

More than forty years ago Efremov (Efremov, 1968) supposed that the small-amplitude Cepheids (or so-called s-Cepheids) having the sinusoidal curves of the light and radial velocity may be the stars which are crossing the instability strip for the first time. Since that time this hypothesis was not doubted. Efremov's argumentation was the following. The large-amplitude pulsators (usual Cepheids) should likely have an increased atmospheric helium abundance (but this could not be checked observationally because of the lack of photospheric helium lines in the yellow supergiant spectra), which can appear just after the star becomes the red giant and experiences the large-scale mixing which may bring an additional helium from the central parts of the star into the upper layers. If so, then the weak pulsational activity of s-Cepheids (i.e. small amplitudes of the light and radial velocity) can be explained by the relatively "low" (i.e. primordial) atmospheric helium content.

Kovtyukh et al. (Kovtyukh et al., 1996) performed the detailed spectroscopic analysis of some s-Cepheids and also summarized the results of previous investigations. The authors showed that carbon abundance is decreased in these stars. This is an obvious sign that s-Cepheids with decreased carbon abundance have already passed the evolutionary stage of the red super-

giant (where the large-scale mixing event and the subsequent alteration of the atmospheric abundances of carbon and nitrogen should appear), and thus they are crossing the instability strip not for the first time. One can speculate that CN-anomalies may appear even earlier, i.e. at the main-sequence phase. It is very likely that a large fraction of Cepheids were rapid rotators on the main-sequence, with meridional mixing bringing CNO-processed material to the stellar surface. This theoretical prediction is made, e.g., by (Przybilla et al., 2010; see also references therein for the earlier papers about rotationally-induced mixing). Nevertheless, we have to note that some observational data contradict this theoretical conclusion. Fast rotation of B star could be the favouring factor for the turbulent mixing, but not necessarily. For instance, (Mathys et al., 2002, their Table 3) derived the NLTE CNO abundance for O-B I-V type stars in several open clusters. The CNO abundances in those stars show quite large differences from star to star. The mean values for C and O are slightly lower than the corresponding solar values, but the mean nitrogen abundance is the same as the solar one, while incomplete CNO cycle together with dredge-up episode require that carbon should be deficient and nitrogen remarkably abundant.

Another illustrative example can be found in (Luck et al., 2000), where IC 4725 open cluster was investigated. It contains, in particular, several B stars and one Cepheid U Sgr. What we can learn from the Table 6 and 7 of that paper? B stars show a variety of the abundance values for each investigated elements, and this is different from what we see in Cepheid, although all of these stars are from the same cloud. For instance, carbon in B stars is lower than in U Sgr. The main reason for this strange situation could be the following. B stars show their superficial abundance anomalies, they are not yet mixed stars. These superficial anomalies can arise, e.g. due to an atomic diffusion process in their rather dynamically stable atmospheres (despite they could be even fast rotators with meridional circu-

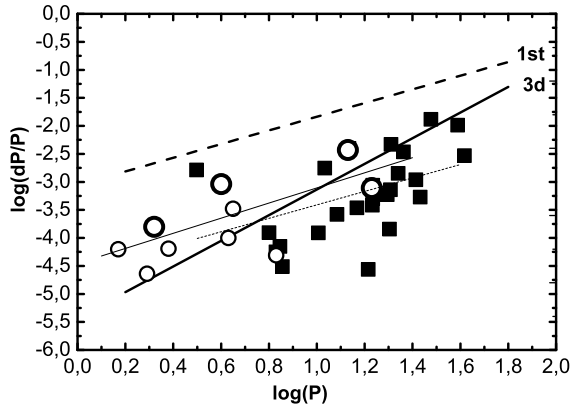


Figure 1: Secular period change $\log\left(\frac{dP}{P}\right)_{100}$ vs. observed pulsational period $\log(P)$. The shown are: a) position of the s-Cepheids as determined by Berdnikov et al. (Berdnikov et al., 1997): *large circles* - the stars with reliably determined evolutionary period change (assigned weight is 2), *small circles* - those having the less reliable determination (assigned weight is 1), b) *filled squares* - ordinary Cepheids from Saitou (Saitou, 1989), c) *thick long-dashed line* represents the theoretical relation for the first crossing, d) *thick solid line* - the same for the third crossing), e) *thin short-dashed line* gives the fit for ordinary Cepheids, f) *thin solid line* is the best fit for s-Cepheids.

lation).

After the main-sequence phase, all superficial anomalies will be erased due to a global convective mixing, and we may observe yellow supergiant star with a normal chemical composition of all the elements, with an exception for C, N and Na.

However, Berdnikov et al. (Berdnikov et al., 1997) provided some observational argumentation in favour of the hypothesis that s-Cepheids are crossing the instability strip for the first time. Those authors determined the secular changes in the pulsational periods among the s-Cepheids and compared obtained values with theoretically predicted period changes. The latter ones come from Saitou (Saitou, 1989). In Fig. 1 we reproduced the original Fig. 6 from Berdnikov et al. (Berdnikov et al., 1997), but with more detailed representation of the data for ordinary galactic Cepheids, as listed by Saitou (Saitou, 1989). Shown in Fig. 1 is the fractional pulsational period change during 100 yrs (i.e., $\log\left(\frac{dP}{P}\right)_{100}$) vs. observed pulsational period $\log(P)$. Observed period changes for studied s-Cepheids and for ordinary Cepheids are compared with theoretically expected values for the stars performing their first and third passages across the instability strip (from all ordinary Cepheids listed by Saitou (Saitou, 1989) only the stars showing the positive increments

of period were selected, which are appropriate for the 1st or 3d crossing). It should be noted that Saitou (Saitou, 1989) gives the derived period change also as a function of the helium content and overall metallicity. Taking into account that 1) the helium content cannot be directly estimated for yellow supergiants, and 2) the metallicity of the classical Cepheids within the errors of spectroscopic analysis is close to the solar one, we adopted for *theoretical* dependencies shown in Fig. 1 the normal mass fractions of helium and other metals (i.e., $Y=0.28$ and $Z=0.02$).

Although, as it might be concluded from Fig. 1, the secular changes for s-Cepheids are quite similar to what is theoretically expected for the third crossing, Berdnikov et al. (Berdnikov et al., 1997) argued that a) there is an offset between the theoretical relation for the third crossing and the fitting line for ordinary Cepheids (supposedly crossing the instability strip not for the first time, for example, more likely for the third time, if only positive increments are selected), b) some offset also takes place between the locus of s-Cepheids and theoretical relation for the third crossing. As one can guess from above mentioned assumption, this should mean that by a formal shift of the theoretical dependencies "period change-period" to a best agreement between the fitting line for ordinary Cepheids and theoretical relation for the third crossing, one can also reach a marginal agreement between the observed position of the s-Cepheids and the theoretical line for the first crossing. Thus, those authors make a conclusion that within the " $\log\left(\frac{dP}{P}\right)_{100} - \log(P)$ " diagram the small-amplitude s-Cepheids deviate from the ordinary Cepheids, and that these stars therefore are crossing the instability strip for the first time (while ordinary Cepheids with positive increments do cross for the third time). This conclusion appears to be in some contradiction with our previous results based on spectroscopic investigation of the s-Cepheids, and it deserves a special consideration.

2. Solution of the problem

During the last years it became clear that many properties of the s-Cepheids can be understood and explained by supposing that they are not fundamental pulsators, but instead are the first overtone ones (see, e.g. Antonello et al., 1990). Thus, their observed pulsational periods should be considered as overtone ones P_1 , and they have to be converted into periods of the fundamental mode $P_0 \approx P_1/0.71$ (Christensen-Dalsgaard & Petersen, 1995), if we are particularly interested in the further comparison with the fundamental pulsators.

With recalculated periods ($\log(P)$), the position of s-Cepheids within the discussed diagram has been revisited. For unique galactic s-Cepheid V473 Lyr the

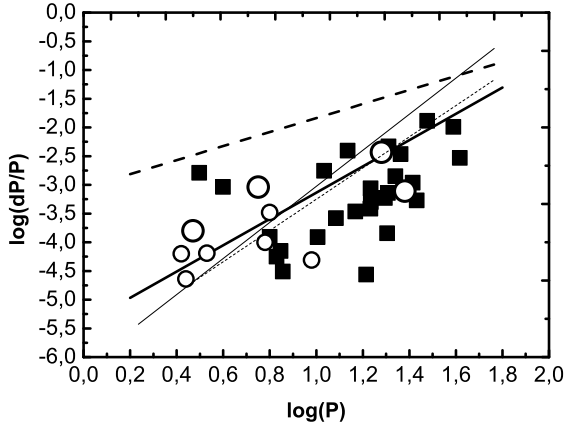


Figure 2: Same as Fig.1, but with corrected periods for s-Cepheids (case A).

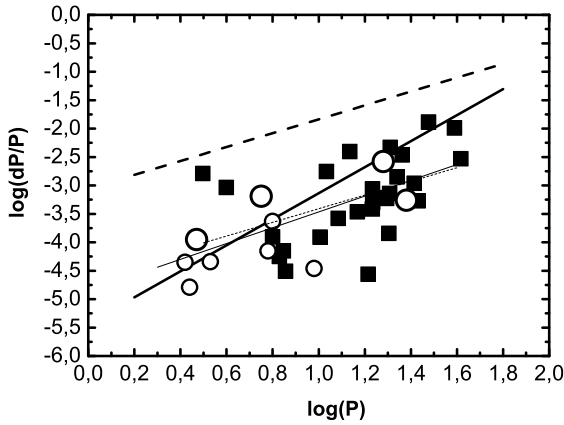


Figure 3: Same as Fig.2, but for the case B.

pulsations in the second overtone were supposed (see, Burki et al. Burki et al., 1986; Andrievsky et al., 1998), and its true fundamental period was found as $P_0 \approx P_2/0.57$. The term $\log\left(\frac{dP}{P}\right)_{100}$ (the ratio between the experimentally determined period change dP and observed period) may also require some correction. Let us consider two cases.

Case A. Period changes dP for s-Cepheids are smaller than those observed in usual Cepheids of the comparable periods P_0 of a fundamental mode (i.e., $dP \equiv dP_1 = \text{const} \times dP_0$, where $\text{const} = 0.71$). In this case one gets $\frac{dP}{P} = \frac{dP_1}{P_1} = \frac{dP_0}{P_0}$, therefore we have to leave observed ratio $\frac{dP}{P}$ unchanged. This means that comparably to Fig. 1, the corrected positions of the s-Cepheids are conditioned by the horizontal rightward shift due to transformation of the observed period P_1 into P_0 . The corrected positions are shown in Fig. 2.

Case B. Although s-Cepheids are overtone pulsators,

Table 1: Initial and redetermined characteristics for s-Cepheids

Star	1	2	3	4	5
V473 Lyr	0.17	0.42	-4.20	-4.35	+
SU Cas	0.29	0.44	-4.64	-4.79	+
EU Tau	0.32	0.47	-3.80	-3.95	++
UY Mon	0.38	0.53	-4.19	-4.34	+
α UMi	0.60	0.75	-3.04	-3.19	++
V1726 Gyg	0.63	0.78	-4.00	-4.15	+
GI Car	0.65	0.80	-3.48	-3.63	+
V496 Aql	0.83	0.98	-4.31	-4.46	+
SZ Cas	1.13	1.28	-2.43	-2.58	++
Y Oph	1.23	1.38	-3.11	-3.26	++

1 – $\log(P)$, where P is observed period,

2 – $\log(P_0)$, where P_0 is fundamental period,

3 – $\log\left(\frac{dP}{P}\right)_{100}$ – original value of the secular period change determined by Berdnikov et al. (Berdnikov et al., 1997),

4 – $\log\left(\frac{dP}{P_0}\right)_{100}$ – with corrected period (case B, see text),

5 – Remarks: stars denoted by "++" have the reliably determined value of the secular period change, while for the stars denoted by "+" these values are less reliable.

We use an usual classification for SU Cas as s-Cepheid (General Catalogue of Variable Stars).

their actual (observed) period changes may correspond to the unexcited fundamental pulsations. In other words, the period change in a given s-Cepheid may be larger than that in the fundamental pulsator of a similar observed period. This assumption implies that the evolutionary period change (which should, of course, depend upon the stellar radius and luminosity, and their variation with a time) $dP \equiv dP_0$, and thus observed ratio $\frac{dP}{P}$ should be substituted with $\frac{dP_0}{P_1/0.71} = \frac{dP_0}{P_0}$. In this case, an additional vertical downward shift (≈ 0.15 dex) should be taken into account. The corrected positions of the s-Cepheids are shown in Fig. 3 (the necessary numerical values for s-Cepheids are also presented in Table 1).

3. Discussion and conclusion

Figs. 2-3 (and even Fig. 1) leave practically no doubt that observed period changes in s-Cepheids are close to those in classical Cepheids, and being taken together, the observed changes in both stellar groups are close to those which are expected for the 3d crossing Cepheids,

It is interesting to note that (Neilson et al., 2012) have shown that mass loss during the Cepheid stage can result in a positive period changes if large enough. Thus one can imagine that it is not necessary to advocate overtone pulsation (first or second) to explain the displacement of points in the "period - period change" diagram away from that expected for a third crossing using overtone pulsation.

Nevertheless, we cannot rely only on this hypothesis simply because Neilson et al. considering the case of Cepheid Polaris were forced to tune their model using a quite large mass loss rate for this star (10^{-6} solar masses per year). We think that there is no reason to believe in a such large ratio taking into account that Polaris has a quite high gravity value and a very small pulsational activity - two factors that can hardly enlarge the mass loss.

Summarizing, one can conclude that there is no firm ground to consider all the small-amplitude s-Cepheids as the stars which are performing their crossing the instability strip only for the first time. It is, of course, not completely excepted that some of them can really be the first crossers (for example, Luck, Kovtyukh & Andrievsky (Luck et al., 2001) detected and described Cepheids with solar-like carbon abundance: SV Vul).

Acknowledgements. We thank anonymous referee for his criticism and valuable comments.

References

- Antonello E., Poretti E., Reduzzi L.: 1990, *A&A*, **236**, 138.
- Berdnikov L.N., Ignatova V.V., Pastukhova E.N., Turner D.G.: 1997, *SvA Lett*, **23**, 204.
- Burki G., Schmidt E.G., Arellano Ferro A., Fernie J.D., Sasselov D., Simon N.R., Percy J.R., Szabados L.: 1986, *A&A*, **168**, 139.
- Christensen-Dalsgaard, Petersen J.O.: 1995, *A&A*, **299**, 17.
- Efremov Yu.N.: 1968, *Per. Zv.*, **16**, 365.
- Kovtyukh V.V., Andrievsky S.M., Usenko I.A., Klochkova V.G.: 1996, *A&A*, **316**, 155.
- Luck R.E., Lambert D.L.: 1992, *ApJS*, **79**, 303.
- Luck R.E., Andrievsky S.M., Kovtyukh V.V., Korotin S.A., Beletsky Yu.V.: 2000, *A&A*, **361**, 189.
- Luck R.E., Kovtyukh V.V., Andrievsky S.M.: 2001, *A&A*, **373**, 589.
- Mathys G., Andrievsky S.M., Barbuy B., Cunha K., Korotin S.A.: 2002, *A&A*, **387**, 890.
- Neilson H.R., Engle S.G., Guinan E., Langer N., Wasatonic R.P., Williams D.B.: 2012, *ApJ*, **745**, 32.
- Przybilla N., Firnstein M., Nieva M.F., Meynet G., Maeder A.: 2010, *A&A*, **517**, 38.
- Saitou M.: 1989, *Ap&SS*, **162**, 47.

MIRAS OR SRA'S – THE TRANSIENT TYPE VARIABLES

V.I. Marsakova¹, I.L. Andronov²

¹Department of Astronomy, Odessa National University, Odessa, Ukraine
vmarsakova@mail.ru

²Department “High and Applied Mathematics”, Odessa National Maritime University,
 Odessa, Ukraine, *tt_ari@ukr.net*

ABSTRACT. The variability of several stars shows “Mira-type” and “semiregular” behavior during long-time data ranges. Such data are available due to amateur visual observations from AAVSO and AFOEV databases. We have studied these properties by using different methods of time-series analysis, such as the periodogram analysis using trigonometric polynomial fit, wavelet analysis and individual cycle characteristics analysis using the running parabola fit. As the result, very similar multiperiodicities were detected.

Key words: Stars: LPVs, Mira-type, semiregular, individual: S Aql, S Tri, Y Per.

Three variables: S Aql, S Tri, Y Per drew our attention due to similar properties of their photometric behavior: intervals of periodical (Mira-type) variability with relatively high amplitudes turns to “semi-regular” (SR-type) small-amplitude oscillations with not so prominent periodicity on their light curves (Fig. 4, see also Fig 5 in Marsakova (1999)). Such transitions were mentioned also in R Dor (Bedding et al., 1998). Another similarity is their main and secondary periods that are close too. The fourth star RU And with similar periods was analyzed by (Chinarova, 2010) so we also refer to it here.

We have analyzed light curves of these stars obtained by amateur astronomers from the AFOEV and AAVSO databases of visual observations, which cover the interval J.D. 2418000–2455600 (only for S Tri the interval is shorter - since J.D. 2439000).

Traditional classification in the “General Catalogue of Variable Stars” (GCVS, Kholopov et al, 1985; Samus’ et al., 2012) separates Miras from SR’s is related with the 2^m level of visual amplitude. Thus in the Table 1 we represent main characteristics of these variables from the GCVS as well as our own results – the values of the mean periods and amplitudes calculated using trigonometric polynomial fit (Andronov, 1994) and the amplitudes determined by fitting individual cycles using the method of “running parabola” (Andronov, 1997). A review on long-period variables was presented by Kudashkina (2003).

One may see that during individual cycles, the amplitude reaches Mira-like values, but not all the time.

1. Periodogram analysis. Multiperiodicity.

The periodogram analysis was made using the program MCV described by Andronov and Baklanov (2004).

S Aql. Kiss et al. (1999) have analyzed the variability of this star, but haven’t found multiperiodicity. The periods of it were also discussed by Chinarova and Andronov (2000). We have obtained very similar values: $P_1=146.7^d$, $P_2=245.2^d$, $P_3=104.6^d$, $P_4=746.3^d$ (See Fig. 1). But one may see that, in the “semiregular” interval J.D. 2449800–2453800, the main peak at the periodogram became relatively smaller and appears peak of 133.2^d instead 104.6^d that come very small.

S Tri. In the case of this star we deal with smaller time range and the percentage of the “semiregular” variability is higher. From the periodogram (Fig. 2), we have obtained periods $P_1=249.5^d$, $P_2=148.1^d$, $P_3=129.1^d$, $P_4=792.6^d$.

Y Per. Kiss et al. (1999) have found changes from mono-periodicity with $P=253^d$ to bi-periodicity with $P_1=245^d$, $P_2=127^d$. Our Fig. 3. shows peaks at both $P=253^d$ and $P=245.3^d$ in whole interval followed by small peaks $P_2=149.4^d$, $P_4=768.9^d$, and more clear $P_1=247.3$, $P_2=776.4^d$, $P_3=147.6^d$, $P_4=129.0^d$ in the “semiregular” interval J.D. 2447000–2453800.

Two periods (147.6 (4 harmonics), 247.3 (2 harmonics)) trigonometric polynomial fit of “semiregular” interval S Aql is shown at Fig. 5.

Three periods (247.3, 129, 147.6.) trigonometric polynomial fit of “semiregular” interval Y Per is shown at Fig. 6.

RU And – the variability analysis was discussed by Chinarova (2010). The wavelet analysis was made there and periods $P_1=247^d$, $P_2=260^d$, $P_3=125.1^d$, $P_4=735.8^d$ have been detected. It was also pointed that the semi-amplitude of RU And varies drastically from 0.027^m (“nearly constant star”) to 1.204^m (“Mira”- type pulsating variable).

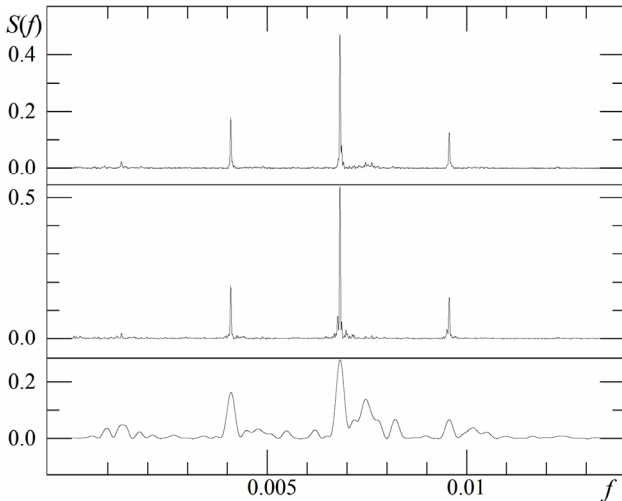


Fig. 1. Periodograms for S Aql (from up to bottom: whole interval, interval without J.D. 2449900–2453800, interval J.D. 2449800–2453800)

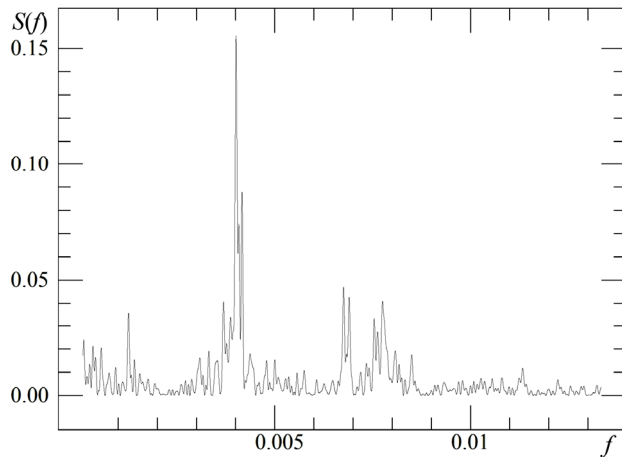


Fig. 2. Periodogram for S Tri

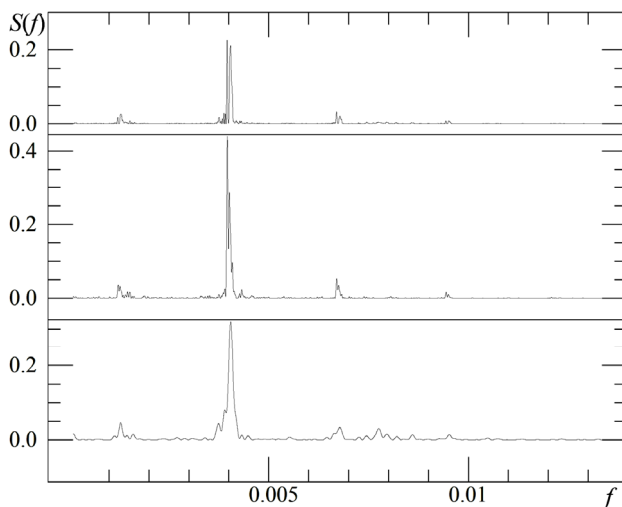


Fig. 3. Periodograms for Y Per (from up to bottom: whole interval, interval without J.D. 2447000–2455800, interval J.D. 2447000–2455800)

It's remarkable, that the periods 245–250^d are represented by all these stars and the periods 145–150^d and 125–130^d we meet very often. The period of about 750^d may be interpreted as 3×250^d or 5×150^d. 125^d is a half of 250^d and may be a harmonic of the main period. But what is the sense of 245–250^d and 145–150^d periods and its ratio (near 1.7)? Is this evidence of close evolutionary stages? Is this stage long-lasting, if we observe many variables with these periods?

2. Wavelet analysis

The wavelet analysis was performed using the program WWZ (Andronov, 1998). Using the wavelet analysis, we have determined best fit values of the period as a function of trial time. The corresponding plots are shown in Fig. 4.

It seems that Y Per has more stable period than other two variables. Before the date J.D. 2447000, it looks like a typical carbon Mira-type variable (Marsakova, 1999). Long periodicity, which sometimes appears in S Tri, may be caused by a small amount of data points in these time intervals.

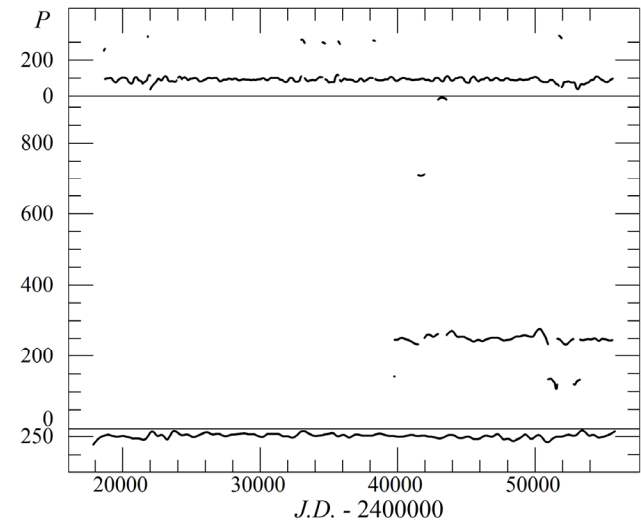


Fig. 4. The best fit values of the period as function of trial time determined using wavelet analysis

3. Individual cycle variability analysis

Classification criteria based on individual cycle variability of Miras were discussed by Marsakova and Andronov, 2006). Let's compare Fig. 2, 5, 7 there with our Table 2. (Where ΔAm , ΔT_{\min} , ΔM are the ranges of individual amplitudes, times between successive minima and mean brightness in the sense of (Marsakova & Andronov, 2006). The denominators are mean values (see Table 1)). According to Marsakova and Andronov (2006), typical Miras lie under values 1.5, 0.3, 1, respectively. One may see that one or several parameters are not in the Miras' range.

Table 2. Individual cycle variability parameters.

Star	$\Delta Am / \langle Am \rangle$	$\Delta T_{\min} / \langle P \rangle$	$\Delta M / \langle Am \rangle$
S Aql	1.6	0.8	0.8
S Tri	3.2	0.8	2.3
Y Per	1.2	0.6	0.4

Table 1: Some mean characteristics of the variables

Star	GCVS			Our calculations			
	Type	Sp.	P	P	AM	AM_{max}	AM_{min}
S Aql	SRa	M3e–M5,5e	146.45 ^d	146.6 ^d	1.82 ^m	3.04 ^m	0.12 ^m
S Tri	M	M2e	241.6 ^d	249.3 ^d	0.52 ^m	2.06 ^m	0.35 ^m
Y Per	M	C4,3e	248 ^d	252.69 ^d	1.55 ^m	2.20 ^m	0.41 ^m

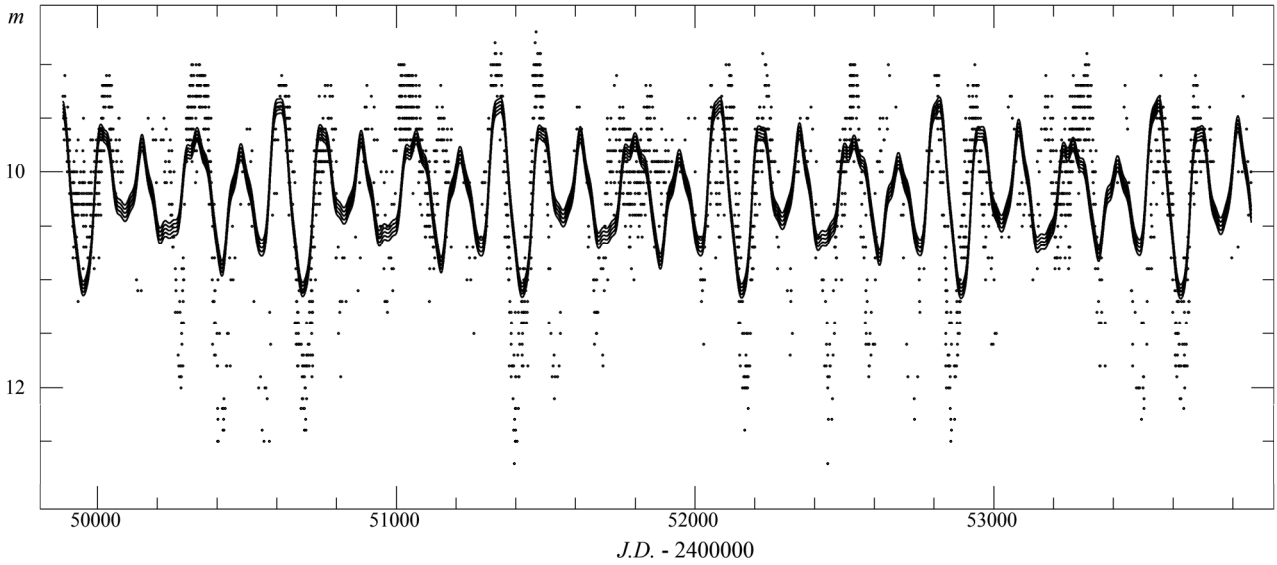


Fig. 5. Variability of S Aql: with trigonometric polynomial fit (with two periods 146.7^d (4 harmonics), 245.2^d (2 harmonics)) in the interval J.D. 2449900–2453800.

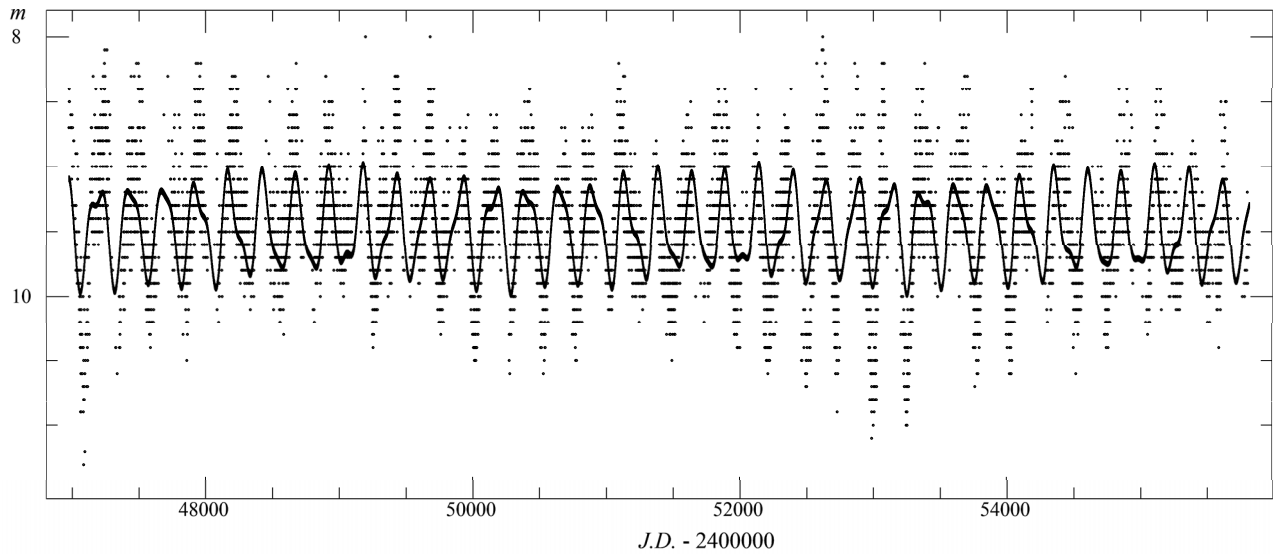


Fig. 6. Three periods (247.3^d, 129^d, 147.6^d) trigonometric polynomial fit of Y Per variability in the interval J.D. 2447000–2453800.

The amplitude and mean brightness changes are shown in Fig. 7 for a sample star Y Per.

So these variables may be classified as “Miras” only in short time intervals. Generally such classification is unacceptable for them. But among SRa’s, they may form the separate group of “transient” variables.

Acknowledgements. We sincerely thank variable star observers of AFOEV and AAVSO (and other association of variable stars observers) for their work which made such researches possible.

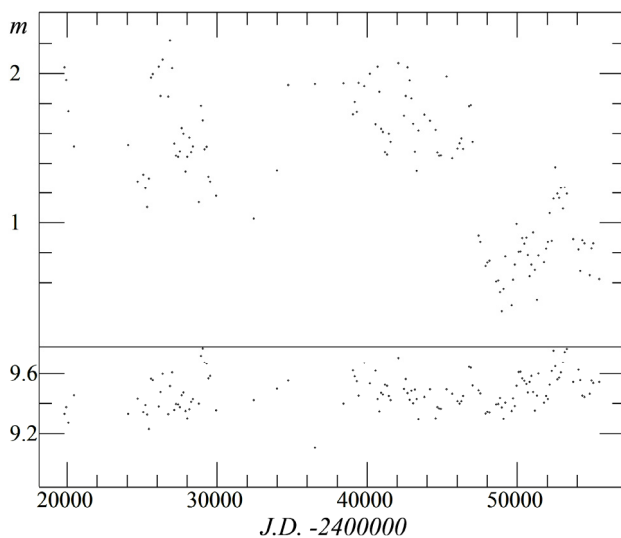


Fig. 7. Y Per: amplitudes and mean brightness for ascending and descending branches of each individual cycle.

Also we are grateful to L.S. Kudashkina for helpful discussions and ideas.

References

- Andronov I.L.: 1994, *Odessa Astron. Publ.*, **7**, 49
 Andronov I.L.: 1997, *Astron. Astrophys. Suppl.*, **125**, 207
 Andronov I.L.: 1998, *Kinem. Phys. Celest. Bodies*, **14**, 490
 Andronov I.L., Baklanov A.V.: 2004, *Astronomy School Reports*, **5**, 264, <http://uavso.pochta.ru/mcv>
 Andronov I.L., Chinarova L.L.: 2001, *Odessa Astron. Publ.*, **13**, 113
 Bedding T.R., Zijlstra A.A., Jones A., Foster G.: 1998, *Mon. Not. Roy. Astr. Soc.*, **301**, 1073
 Chinarova L.L.: 2010, *Odessa Astron. Publ.*, **23**, 25
 Chinarova L.L., Andronov I.L.: 2000, *Odessa Astron. Publ.*, **13**, 116
 Kiss L.L., Szatmáry K., Cadmus Jr R.R., Mattei J.A.: 1999, *Astron. Astrophys.*, **346**, 542
 Kholopov P.N. et al: 1985, *General Catalogue of Variable Stars*, 4-th edition. Moscow: Nauka
 Kudashkina L.S.: 2003, *Kinem. Phys. Celest. Bodies*, **19**, 193
 Marsakova V.I.: 1999, *Odessa Astron. Publ.*, **12**, 205
 Marsakova V.I., Andronov I.L.: 2006, *Astrophysics*, **49**, 506
 Samus N.N., Durlевич O.V., Kazarovets E V., Kireeva N.N., Pastukhova E.N., Zharova A.V., et al. *General Catalog of Variable Stars* (GCVS database, Version 2012Jan), <http://www.sai.msu.su/gcvs/gcvs/>

PRELIMINARY STUDY OF RED SUPERGIANT RM_1-667 IN THE LARGE MAGELLANIC CLOUD

V.Gopka¹, A.Shavrina², S.Vasilyeva¹, A.Yushchenko^{1,3}, S.Andrievsky¹, V.Yushchenko¹

¹ Astronomical observatory, Odessa National University, T.G. Shevchenko Park, Odessa 65014, Ukraine, *gopkavera@mail.ru*

² Main Astronomical observatory, NAS of Ukraine, Kyiv, 03680, Ukrai

³ Department of Astronomy & Space Sciences, Sejong University, Gunja-dong, Seoul, 143-747, Korea

ABSTRACT. The observed lines of hydrogen and another strong lines in the spectrum of RM_1-667 (red region of spectra, 5900-7100 Å, spectral type is K7 I) are discussed. Analysis of these lines indicates the presence of mass outflow from the star at a significant velocity. Using the iron lines and the model atmospheres of supergiants (Teff = 3750 K – 4300 K) of the Kurucz' grid, we obtained the iron abundance $\lg \epsilon(\text{Fe}) = 6.75-7.08$, which is equivalent to $[\text{Fe}/\text{H}]$ equal -0.75 to -0.42.

1. Introduction

Red supergiants are short evolutionary phase of the He-burning of moderately massive stars from 10 to 25 solar masses [1]. Large size of the stars, very cool effective temperature, the dusty circumstellar environments, the mass loss of those stars, the huge number of atomic and molecular lines in their spectra – all these facts made the investigation of those objects be very complicated. Supergiant RM_1-667 from the Large Magellanic Cloud is an example of such object.

2. Observations

The observation of this K-supergiant was carried out by Hill [2] at the European Southern Observatory (ESO) at La Silla. The spectral resolution of the spectra is near 30 000, the range of wavelengths is 5900-7100 Å. According to study [3], RM_1-667 has the following photometric data: $V=13.126$, $B=14.634$, $U=14.933$.

3. Choice of the model atmosphere and the specific characteristics of the H α 6563 Å line and Na I lines 5890 and 5896 Å.

The atmospheric parameters of supergiant RM_1-667 were determined by the method of modeling of equivalent widths of lines of neutral and ionized iron. On the basis of preliminary calculations of iron lines equivalent widths, and Kurucz' models with effective temperatures in the range of 4300-3750 K, we found the iron abundance of RM_1-667 $[\text{Fe}/\text{H}]$ from -0.4 to -0.8 dex. We should note the wide spread of iron abundances, determined with the "solar" oscillator strengths [4] and the Kurucz' atmosphere models [5]. One of the reasons of the indicated spread is the actual difficulties in the constructing of extended supergiant atmospheres. Strong lines in the spectrum of supergiant RM_1-667 indicate the difference of observed temperatures and element abundance distribution with depth in the atmosphere from modeled ones. The H α line and the strong lines of sodium doublet profiles indicate the significant evidence of that stratification. Comparing the H α line profiles in the spectra of two supergiants of the Large Magellanic Cloud, namely RM_1-390 and RM_1-667, we can see that RM_1-390 has a symmetric strong line profiles in contrast to the line profiles in the spectrum of RM_1-667. Note, that RM_1-390 was studied previously as PMMR39 [6]. In RM_1-390 (Teff =4250 K, $\lg g=0.16$, $v_{\text{micro}}=3.1$ km/s) all 20 studied chemical elements are underabundant with respect to solar values. An emission component is obvious in the center of H α profile of RM_1-667. It can be interpreted as the possible hydrogen outflow both towards us (blue part of the line profile) and from us (red component). Also the emission in the central part of H α line profile (Fig. 1, Fig. 3) could be explained by the temperature inversion in the layers of H α formation. The sodium lines 5890 and 5896 Å are very strong and show a blue shift of profile central parts of

0.32 Å, that corresponds to the outflow from star with velocity 16 km/sec (Fig. 2). Strong iron lines could also have distorted profiles that results in iron abundances spreading. The temperature, determined from the modeling of the H α profile, is higher than that determined using the iron lines. Figures 2 and 3 show the synthetic spectra

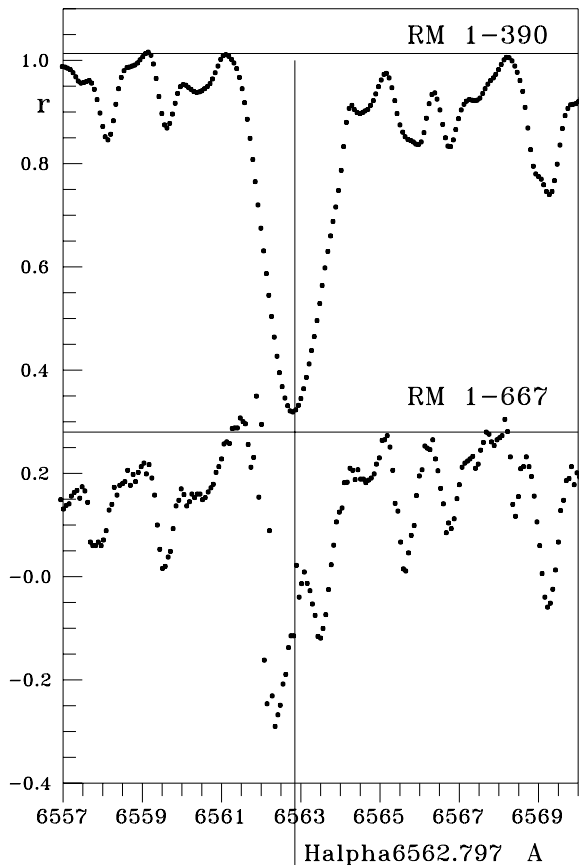


Fig.1. The H α profiles of two supergiants of the Large Magellanic Cloud: RM_1-667 and RM_1-390

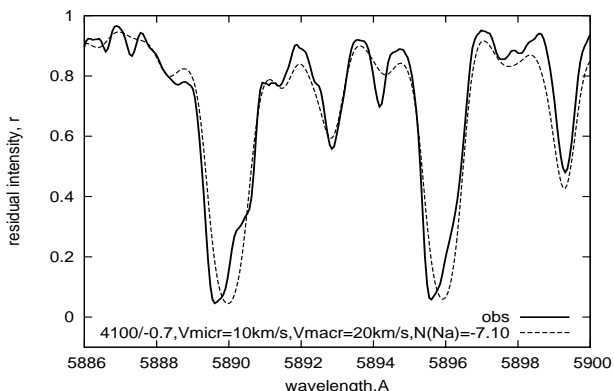


Fig.2. Observed and modeled sodium lines 5890 and 5896 Å in the spectrum of RM_1-667

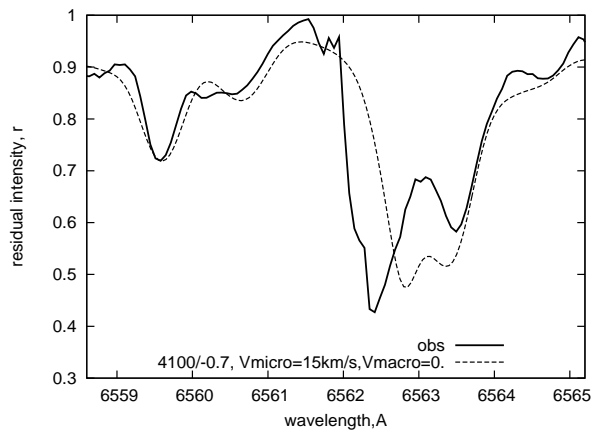


Fig.3. Observed and modeled H α line in the spectrum of RM_1-667.

near the sodium and hydrogen lines (5890, 5896, and 6563 Å), calculated with the effective temperature $T_{\text{eff}}=4100$ K and the surface gravity $\lg g=-0.7$. The observed spectrum is blue-shifted from the calculated line profiles by 0.4 Å or 18 km/sec. The emission component in the observed H α profile is fitted with the temperature inversion in the upper layers of stellar atmosphere.

3. Conclusions

The analysis of the hydrogen H α (6563 Å) line and the sodium lines (5890, 5896 Å) detects the evidence, first of all, of the specific conditions of the upper atmospheric layers of supergiant star RM_1-667. The preliminary analysis of iron abundances shows the metallicity in the range of $[\text{Fe}/\text{H}]=-0.8$ to -0.4 dex being determined with different models.

Acknowledgments. This work was partly supported by Mid-career and General Researcher Programs, and Science and Technology grant 2011-0028001 and 2011-00106996 respectively, through the National Research Foundation (NRF) funded by the Ministry of Education of Korea. Two of the authors were granted by the Swiss National Science Foundation (SCOPEs project No. IZ73Z0-128180/1).

References

1. Levesque E.: 2010, *NewAR*, **54**, 1.
2. Hill V.: 1999, *A&A*, **324**, 435.
3. Bonanos A.Z., Messa D.L., Sewilo M., et al.: 2009, *Astron. J.*, **138**, 1003.
4. Gurtovenko E.A., Kostik R.I.: 1981, *A&AS*, **46**, 239.
5. Kurucz R.: 1993, CD-ROMs 1-23.
6. Gopka V.F., Yushchenko A.V., Goriely S., et al.: 1995, *IAUS*, **228**, 535.

RESULTS OF OBSERVATIONS OF SELECTED ASTEROIDS AT THE NEW TELESCOPE MOBITEL OF NAO IN 2011-12

A. Ivantsov, A. Pomazan, V. Kryuchkosriy, L. Gudkova

Research Institute "Nikolaev Astronomical Observatory"
54030, Observatornaya, 1, Nikolaev, Ukraine
anton@nao.nikolaev.ua

ABSTRACT. The results of position observations of selected asteroids with the new telescope Mobitel of NAO are presented. The possibility of using them for contemporary problems is discussed.

Key words: astrometry, asteroid, positional observations.

In 2011 regular observations of selected bright asteroids were begun with Mobitel telescope set up in Nikolaev Observatory. The asteroids were chosen from the compiled observational program for Russian-Turkish telescope RTT150 (Shulga et al., 2010; Shulga et al., 2012). The first list consists of the objects for determination masses of some large asteroids, the second one consists of small asteroids, less than tens kilometers for detection of Yarkovsky effect which changes orbits of small bodies due to re-emission by them in the infrared wavelength. The peculiarity of the selected asteroids is their small size which requires high aperture telescopes and makes difficulty for measuring positions with high accuracy. Namely the high accuracy of astrometric measurements, better than 0.1", is necessary for successful detection of perturbation effects in the motion of smaller asteroids having encounters with bigger ones and thus determination of their masses.

The results of the past observations under these programs with the RTT150 have demonstrated very good results. The mean internal precision of a single position was 0.10" in right ascension and 0.08" in declination in the UCAC2, UCAC3, UCAC4 reference catalogs for objects of 15-19 magnitudes (Ivantsov, 2011). The first observations of near-Earth asteroids at the Mobitel telescope were made in 2010 (Shulga et al., 2011). That results appeared to be promising for improving orbits.

The telescope Mobitel (D=0.5 m, F=3.0m) is equipped with the CCD camera Alta U9000 (3056x3056, 12x12 mkm²) of Apogee Imaging Systems, which allows to get imaging with 42'x42' field of view and 1.6"/pix of scale.

The observations were made in R Johnson-Cousins-Bessel band. That system allows to get number of reference stars enough for reduction in the UCAC catalogs. The peculiarity of the telescope consists in using time delay and integration mode solely for observations. The length of exposure was not greater than 85s there.

Since June 2011 there were measured 705 positions of 26 program asteroids and 82 positions of 6 asteroids appeared to be present in the same images from the observations at the Mobitel telescope. The reduction was made using "Astrometrica" with the UCAC4 reference catalog. For estimating accuracy of the observations, there was made comparison with the ephemerides provided with the online service "HORIZONS" of Jet Propulsion Laboratory, USA (<http://ssd.jpl.nasa.gov/?horizons>). The comparison of observed (O) and calculated (C) positions is given by distribution of mean values of (O-C) on Fig. 1. Each point represents the mean of the series of measurements of each asteroid per night. So, one can find points there which correspond to the same asteroid, but obtained in different observational periods. The error bars correspond to one-sigma interval. The weighted mean value of (O-C) for two years gives zeros, while there are significant both negative values in right ascension and declination in 2011, and significant both positive values in 2012.

The distribution of internal errors for a single position with respect to magnitudes are presented on Fig. 2, 3. The errors are 0.1" for the observed asteroids up to 14 magnitude. The weighted standard error of a single position was 0.2" in each coordinate for asteroids to 16 magnitudes and it was calculated using standard deviations of (O-C) in positions for each series of observations.

The great values of (O-C) and errors can have explanation in insufficient exposure for faint objects, which is limited by time delay and integration mode of observation.

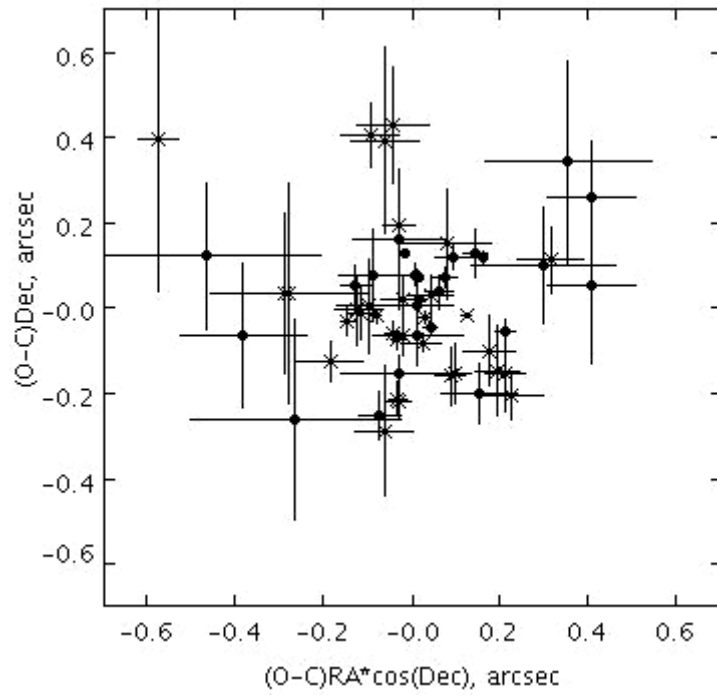


Figure 1: The distribution of (O-C) in positions of asteroids: crosses correspond to the positions observed in 2011, points correspond to the positions of 2012.

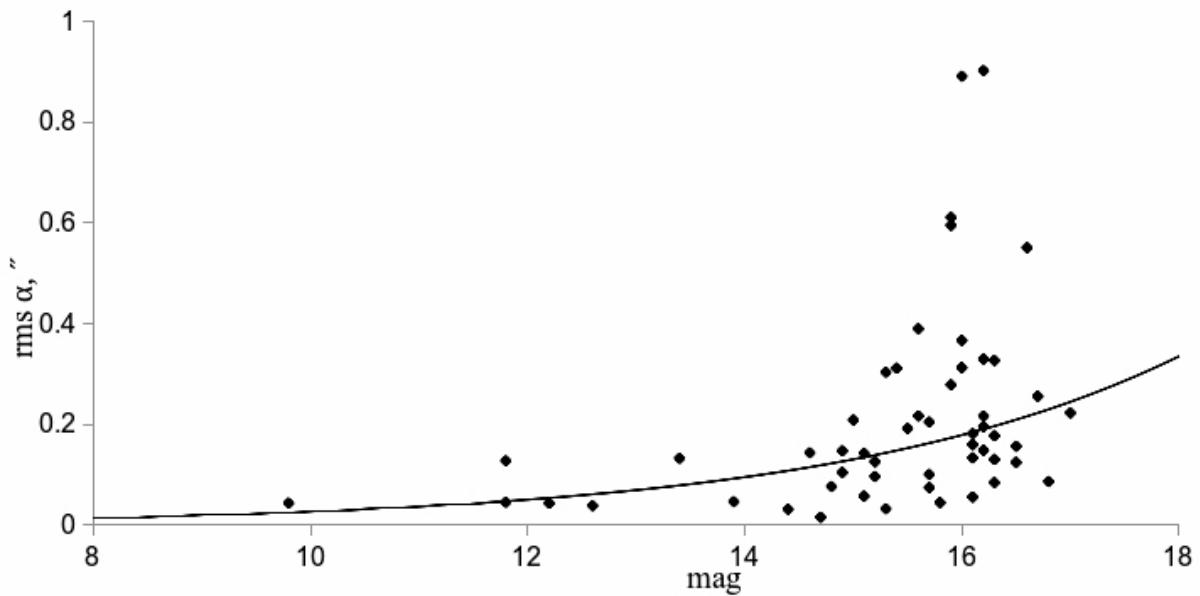


Figure 2: The standard error of position of asteroid in right ascension with respect to magnitude

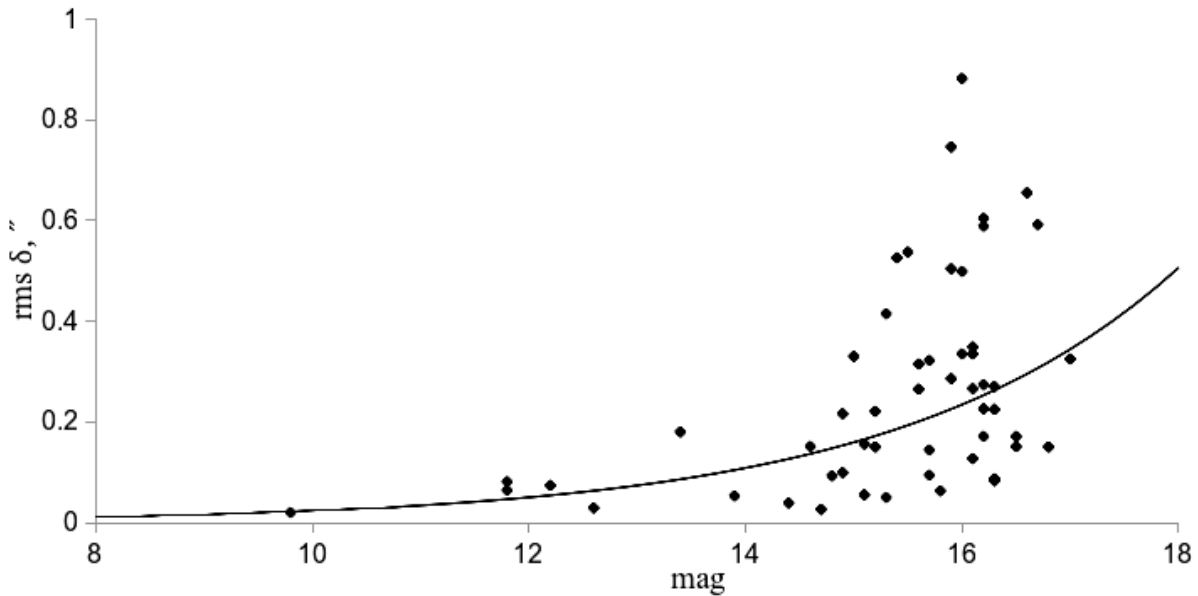


Figure 3: The standard error of position of asteroid in declination with respect to magnitude

Conclusions

At present astrometric observations of selected asteroids at the Mobitel telescope have accidental error of 0.1" in each coordinate for asteroids brighter 14 magnitude and weighted 0.2" for objects up to 16 magnitudes.

For improving systematic and accidental errors of astrometric observations of asteroids, it is necessary to study the field corrections and improve techniques of observations, which will allow to use this telescope for research small effects in the motion of small bodies of the Solar system.

Acknowledgments. This research was supported by the State Agency of Science, Innovations and Information of Ukraine (contracts No. M/415-2011 and No. M/331-2012).

The authors are also thankful to Prof. G. I. Pinigin and N.V.Maigurova for discussion and assistance in the article preparation to print.

References

- Shulga A.V., Kozyrev Ye.S., Kovalchuk A.N., Chernozub V.M., Sibiryakova Ye.S., Bochkarev A.B., Lopachenko V.V., Ryhalsky V.V.: 2010, in *Proc. NAO2010 Conf., Mykolaiv*, 62.
- Shulga A.V., Kozyrev Ye.S., Sibiryakova Ye.S., Khalolei M.I., Chernozub V.M.: 2012, *Kosmichna nauka i tekhnologiya*, **18**, № 4, 70.
- Ivantsov A., Gumerov R., Khamitov I., Aslan Z., Thuillot W., Pinigin G., Hestroffer D., Mouret S.: 2011, in *Proc. of Gaia follow-up network for Solar system objects workshop held at IMCCE - Paris observatory, France*, 93.
- Shulga O., Kozyryev Ye., Sybiryakova Ye.: 2011, in *Proc. of Gaia follow-up network for Solar system objects workshop held at IMCCE - Paris observatory, France*, 97–100.